Dune geometry and the associated hydraulic roughness at the transition from a fluvial to tidal regime at low river discharge

Sjoukje Irene de Lange[1], Ryan Bradley[2], Reinier Schrijvershof[3], Daniel Murphy[4], Kryss Waldschlager[3], Ray Kostaschuk[2], Jeremy G. Venditti[2], and A.J.F. (Ton) Hoitink[1]

[1]Wageningen University
[2]Simon Fraser University
[3]Wageningen University and Research
[4]School of Environmental Science, Simon Fraser University

July 20, 2023

Abstract

In deltas and estuaries throughout the world, a fluvial-to-tidal transition zone (FTTZ) exists where both the river discharge and the tidal motion drive the flow. It is unclear how bedform characteristics are impacted by changes in tidal flow strength, and how this is reflected in the hydraulic roughness. To understand bedform geometry and variability in the FTTZ and possible impacts on hydraulic roughness, we assess dune variability from multibeam bathymetric surveys, and we use a calibrated 2D hydrodynamic model (Delft3D-FM) of a sand-bedded lowland river (Fraser River, Canada). We focus on a period of low river discharge during which tidal impact is strong. We find that the fluvial-tidal to tidal regime change is not directly reflected in dune height, but local patterns of increasing and decreasing dune height are present. The calibrated model is able to predict local patterns of dune heights using tidally-averaged values of bed shear stress. However, the spatially variable dune morphology hampers local dune height predictions. The fluvial-to-tidal regime change is reflected in dune shape, where dunes have lower leeside angles and are more symmetrical in the tidal regime. Those tidal effects do not significantly impact the reach-scale roughness, and predicted dune roughness using dune height and length is similar to the dune roughness inferred from model calibration. Hydraulic model performance with a calibrated, constant roughness is not improved by implementing dune-derived bed roughness. Instead, large-scale river morphology may explain differences in model roughness and corresponding estimates from dune predictors.

Dune geometry and the associated hydraulic roughness at the transition from a fluvial to tidal regime at low river discharge

S.I. de Lange[1], R. Bradley[2,3], R.A. Schrijvershof [1], D. Murphy[3], K. Waldschläger[1], R. Kostaschuk[3], J.G. Venditti[3], A.J.F. Hoitink[1]

[1]Wageningen University, Department of Environmental Sciences, Hydrology and Quantitative Water Management, Wageningen, the Netherlands
[2]Northwest Hydraulic Consultants Ltd., North Vancouver, British Columbia, Canada
[3]School of Environmental Science, Simon Fraser University, Burnaby, British Columbia, Canada

Key Points:

- Hydraulic roughness in the fluvial-to-tidal transition zone can be predicted from dune geometry and agrees with calibrated model roughness.
- Variation in dune symmetry and leeside angle across a fluvial-to-tidal transition zone has little impact on reach-scale hydraulic roughness.
- Predicted spatial bedform patterns from modelled shear stress match measured bedform patterns, but absolute dune heights do not.

Corresponding author: Sjoukje de Lange, sjoukje.delange@wur.nl

Abstract

In deltas and estuaries throughout the world, a fluvial-to-tidal transition zone (FTTZ) exists where both the river discharge and the tidal motion drive the flow. It is unclear how bedform characteristics are impacted by changes in tidal flow strength, and how this is reflected in the hydraulic roughness. To understand bedform geometry and variability in the FTTZ and possible impacts on hydraulic roughness, we assess dune variability from multibeam bathymetric surveys, and we use a calibrated 2D hydrodynamic model (Delft3D-FM) of a sand-bedded lowland river (Fraser River, Canada). We focus on a period of low river discharge during which tidal impact is strong. We find that the fluvial-tidal to tidal regime change is not directly reflected in dune height, but local patterns of increasing and decreasing dune height are present. The calibrated model is able to predict local patterns of dune heights using tidally-averaged values of bed shear stress. However, the spatially variable dune morphology hampers local dune height predictions. The fluvial-to-tidal regime change is reflected in dune shape, where dunes have lower leeside angles and are more symmetrical in the tidal regime. Those tidal effects do not significantly impact the reach-scale roughness, and predicted dune roughness using dune height and length is similar to the dune roughness inferred from model calibration. Hydraulic model performance with a calibrated, constant roughness is not improved by implementing dune-derived bed roughness. Instead, large-scale river morphology may explain differences in model roughness and corresponding estimates from dune predictors.

Plain Language Summary

Where rivers meet the sea, the flow will be driven by tides from the sea and by river flow, resulting in a fluvial-to-tidal transition zone. The transition can be abrupt or gradual, which might influence the bed of the river, which is covered by bedforms (dunes and ripples). Bedform geometry is important in understanding the degree of friction in the river, which in turn determines water levels. It is unclear how bedform characteristics and the related friction are impacted by change in tidal flow strength. This study of the Fraser River in Canada used survey data of the river bed and a computer model of the river flow to study the geometry of dunes and the corresponding friction in this transitional region. We find that dune height and length vary considerably, but that it was unrelated to this regime change. Instead, only the dune leeside, i.e. the downstream facing side, was impacted. The difference in leeside angle before and after the regime change, did not result in a different friction produced by the dunes. Using the friction produced by dunes in the model, instead of a constant friction, does not improve model performance. Instead, large-scale river morphology determines roughness variations.

1 Introduction

Rivers debouching into a water body subject to tides have a fluvial-to-tidal transition zone (FTTZ). The FTTZ can be defined as the part of the river that is fully dominated by fluvial processes at its upstream end, and dominated by tidal and coastal processes at the downstream boundary (Phillips, 2022). The transition from fluvial to tidal can be gradual, but is often impacted by processes that modify the character of this transition by altering the channel bathymetry and adding friction (Godin, 1999; Horrevoets et al., 2004), such as an irregular underlying channel geology, bifurcations or confluences (Kästner et al., 2017), or dredging works (Gisen and Savenije, 2015). These changes can cause the gradual transition to become more abrupt, and a sudden change in tidal flow strength can lead to a change in hydraulic regime from a more fluvial to a more tidally dominated system. It is unclear how bedforms and their corresponding roughness respond to a change in hydraulic regime, while dune geometry and roughness prediction is essential for river management (ASCE Task Force, 2002; Best, 2005; Warmink et al., 2013), interpreting sedimentary rock records (Das et al., 2022), and understanding sediment fluxes (Venditti and Bradley, 2022).

Bedforms adjust to changes in the hydraulic regime, but not in a consistent manner. Until recently, it was often assumed that any spatial variability in dune geometry was caused by dunes that are not in equilibrium (Carling et al., 2000; Bridge, 2003; Holmes and Garcia, 2008), and the primary geometry (dune height and length) of equilibrium dunes was assumed to scale with water depth (Yalin, 1964). However, recent research has shown significant local spatial variation in dune height (Bradley and Venditti, 2017; Murphy, 2023; Venditti and Bradley, 2022) in riverine systems, independent of the water depth. In the FTTZ, this variability is expected to be even more pronounced, since tidally-influenced currents impose spatially-varying water level fluctuations (and therefore bed shear stress changes) on diurnal and semi-diurnal time scales (Sassi et al., 2011; Hoitink et al., 2003). The resulting spatial longitudinal variability of dune geometry in the FTTZ is understudied, but two key studies exist.

Prokocki et al. (2022) studied dunes in the lower 90 km of the Lower Columbia River (USA), and recognized differences in shape and 3D planform of dune geometry across the study reach. They related the changing dune morphology to downstream variations in grain size and spatiotemporal changes in tidal and fluvial flow. In the thalweg, they observed small-scale upstream-oriented dunes downstream, and larger scale downstream-oriented dunes upstream. Unfortunately, they did not report on flow conditions in those distinct regions, or on the resulting hydraulic roughness differences. Lefebvre et al. (2021) studied 4-year long bathymetric data of the downstream 160 km of the Weser Estuary in Germany. They did not observe a clear trend in dune geometry in the longitudinal direction, but found dunes that are generally smaller than predicted based on the water depth. They did not provide information on the flow conditions or resulting roughness. Beyond these recent studies, the response of dune geometry in the FTTZ to shear-stress variation at the change from a fluvial to tidal regime is unknown, and it is uncertain if dune geometry predictors apply here.

To date, it remains unclear to what extent variability in dune geometry is relevant for the large-scale roughness needed to model the FTTZ. Bedforms, especially dunes, are known to be a major source of roughness in lowland rivers (Gates and Al-Zahrani, 1996; Julien et al., 2002), and dune variability can impact roughness parametrizations. When modelling the FTTZ hydraulically, a roughness value must be chosen. Roughness is often represented by a single constant coefficient (Paarlberg et al., 2010), found by calibration, and is therefore a conceptualized and simplified representation of the physical process. To better include spatial variation in roughness in the FTTZ, De Brye et al. (2011) used a linearly decreasing roughness coefficient from a delta apex to the coast, to include the gradual transition from the riverine to the marine environment. However, proof for the validity of this approach is lacking. There is a need to improve hydraulic roughness parametrization in the FTTZ, since the output of hydrodynamic models strongly depends on an accurate specification of roughness (Lesser et al., 2004; Morvan et al., 2008; Wright and Crosato, 2011).

In this research, we aim to increase understanding of bedform variability and related roughness that occurs at the transition from a shallow mixed tidal-fluvial regime to a tidal regime. To do so, we assess the bedform characteristics and the resulting hydraulic roughness of the FTTZ of the Lower Fraser River. The lower Fraser River is a sand-bedded lowland river in British Columbia, Canada, with a significant decrease in tidal energy 40 kilometer landward of the river mouth (Wu et al., 2022). We aim to answer three research questions. 1) How are bedform characteristics impacted by the sudden change in tidal flow strength? 2) How can dune variability in the fluvial-to-tidal transition zone be explained and predicted? 3) To what extent does dune geometry and variability exert an impact on reach-scale hydraulic roughness, and which other factors can play a role in determining this bed roughness? Bathymetric field data from base flow conditions were used, allowing us to focus on the impact of the tides, which penetrate further upstream during base flow. A 2D hydrodynamic model is created to assess hydraulic roughness, and to explore the impacts of spatial variation in river and tidal flow.

2 Field site

The Fraser River (Figure 1) is located in British Columbia, Canada, and drains 228,000 km^2 of mountainous terrain. The Fraser exits a series of bedrock canyons approximately 185 km upstream of the river mouth at Sandheads, where it enters the gently-sloping Fraser Valley, past the towns of Hope (river kilometer (RK) 165) and Mission (RK 85). The Fraser River has an annual river discharge of 3,410 m^3 s^{-1} at Mission (Water Survey of Canada (WSC) Station 08MH024), but flow rates vary between a mean low discharge of 1,000 m^3 s^{-1} in winter time (November - April) and a mean high discharge of 9,790 m^3 s^{-1} during the snow melt-dominated freshet in May, June and early July (Attard et al., 2014; McLean et al., 1999). At New Westminster, 34 km upstream from the river mouth, the river bifurcates, forming the Fraser Delta where the Main Channel splits into two tributaries: the North Arm and the Main Channel. The Main Channel carries 88% of the flow, until it bifurcates into Canoe Pass (RK 13), which conveys approximately 18% of the total flow (Dashtgard et al., 2012; WCHL, 1977; NHC, 2008). The fluvial-to-tidal transition zone of the river is influenced by a predominantly semi-diurnal tide (Wu et al., 2022), with a mean tidal range at the mouth of approximately 3 m (Kostaschuk and Atwood, 1990). The tidal motion influences water levels up to Mission during high flow, but can penetrate up to Chilliwack (RK 120) during low flow creating a strong backwater effect (Kostaschuk and Atwood, 1990). It is an undammed, unregulated flow, which reflects climatic conditions. Human-made influences include dikes (90% of the reach), pipelines and bridge constructions, and dredging of the Main Channel occurs.

The Port of Vancouver dredges from the river mouth (RK 0) to the Port Mann Pumping Station (RK 42), with the most significant dredging in the deltaic reach from RK 35 to the river mouth (Nelson, 2017) to maintain a constant fairway depth (McLean and Tassone, 1989; Stewart and Tassone, 1989). The depth is larger in the tidal region, and has been made deeper by dredging. This results in a large decrease in momentum flux (Wu et al., 2022) at the upstream limit of the dredging works. Additionally, Wu et al. (2022) related this decrease in momentum flux to the influence of the Pitt River. They identified the junction of the Pitt River as the transition from a tidally-dominated to a river-dominated regime, and they noted the importance of this system for tidal attenuation. Therefore, two different regimes can be identified in the study area. The first regime, hereafter called the tidally-dominated regime, is characterized by a strong influence of tides and a large tidally-averaged water depth, and occurs seaward of RK 40. The second regime is the mixed tidal-fluvial regime, in which tides are less strong and the water depth is shallower, which occurs landward of RK 40. This roughly coincides with the upstream end of the modern Fraser Delta (RK 35) (Venditti et al., 2015; Venditti and Church, 2014), where the Fraser River bifurcates into the North Arm and the Main Channel.

The difference in tidal strength in the two regimes does not impact grain sizes of bed sediments in the thalweg. The main transition of grain size characteristics occurs around RK 100. Upstream of RK 100, the bed of the Fraser River consists of gravel, and downstream of a gravel-sand-transition near Mission, the main bed material is sand (Venditti and Church, 2014) (median grain size (D_{50}) 351 μm, mean 415 μm; Figure 2). There is a minor trend of downstream fining in the thalweg of the lower 50 km of the river, (1.14 μm per kilometer, Figure 5c), resulting on average in a decrease in D_{50} of approximately 100 μm over this reach, although there is a lot of scatter which can be related to gravel and mud deposits along the banks. The data underlying this figure is a compilation of multiple sources. The samples up until RK 48.5 were collected by McLaren and Ren (1995), who sampled bed material in the Main Channel and delta front at 0.5 km increments with a Shipek sampler. Although this grain size data is decades old, broad patterns are likely to be consistent with present conditions (Venditti and Church, 2014), and grain size shows little seasonal or year-to-year variation (Kostaschuk et al., 1989; McLean et al., 1999; Pretious, 1956). Venditti and Church (2014) measured 33 samples of RK 48.5 - 80, with a dredge sample in 2009, and Murphy (2023) collected 115 additional samples in this same reach using a pipe dredge.

They did not perform analysis on the fraction smaller than 63 μm. The Pitt system does not impact the sediment composition of the Fraser, since the net bedload transport is directed upstream toward Pitt lake (Ashley, 1980). In the delta, the river deposits its sand load in the channel and its banks, and its silt load on the distal margins and tidal flats (Venditti and Church, 2014) (Figure 2a, c, d). Seaward of the river mouth, the grain size decreases dramatically to a D_{50} of 22 μm. Locally, the river interacts with its bank and bed substrate. Gravel and clay patches are present at the outer banks on the north and south sides of the river. These patches are either modern deposits, such as gravel bars, or older Pleistocene glacial deposits (fine outwash deposits and coarse glacial till) (Nelson, 2017) (Supplementary Figures S1), constraining the river's course.

This study focuses on the Main Channel of the Fraser River, from the confined part of delta mouth at Steveston Harbor at RK 10, to Mission at RK 85 (Figure 1). The area is located in the FTTZ, and low-angled dunes (Bradley et al., 2013; Kostaschuk and Best, 2005; Kostaschuk and Villard, 1996), with no or intermittent flow separation, cover the river bed. When assessing local scale processes, we focus on three zones in the FTTZ (Figure 2, and Supplementary Figure S7).The zones are located at RK 21.5-23 (zone 1; tidal regime), 50-52.5 (zone 2; fluvial-tidal regime) and 57-59.5 (zone 3; fluvial-tidal regime). The selection of zones is based on three criteria. Firstly, a decreasing amount of tidal energy from zone 1 to 3. Secondly, a simple geometry, without bifurcations or confluences, to limit the influence of complex currents on dune geometry. Thirdly, a limited amount of human influence on the river bed. Zone 1 is 1 km shorter than the other zones due to dredging along the downstream side and an engineering structure on the upstream side.

3 Methods

3.1 Hydraulic model setup

A 2DH (two dimensional horizontal) hydraulic model was set up in the Delft3D Flexible Mesh (FM) model suite (Kernkamp et al., 2011). The model simulates depth-averaged flow quantities based on the two-dimensional shallow water equations. The numerical domain covers the Fraser River from river kilometer 85, to the offshore region of the Strait of Georgia reaches where depth exceeds >200 m. Bathymetry for the Main Channel is interpolated on an unstructured curvilinear grid with a median cell size of 30 m, and varies between 5 m in the river and 1000 m offshore. The bathymetry of the model of Wu et al. (2022) was taken as a basis, and the higher resolution MBES data described above were used for the bathymetry of the channels in the estuary. Bars that do not get submerged during an average yearly freshet (flood) were not well-represented in the bathymetry data, and its elevation in the model was manually increased till 10 m above mean sea level to prevent flooding.

The main imposed upstream boundary condition is the discharge at Mission (RK 85) for the time period of November 2017 till October 2018. The discharge at Mission is estimated using a rating curve if the discharge exceeds 5,000 m^3 s^{-1}. At lower discharge conditions, tidal influences make the rating curve at Mission inaccurate, and therefore the discharge was calculated using the discharge at Hope (RK 165) and two smaller tributaries (Chilliwack River and Harrison River). Using this calculation method, discharges measured at Mission (larger than 5,000 m^3 s^{-1}), were on average underestimated by 3%, and no significant temporal delay was observed. Additionally, at two downstream confluences, a constant discharge of 315 m^3 s^{-1} at Stave River (RK 74) and 130 m^3 s^{-1} at Pitt River (RK 45) were added to the Fraser flow. Stave River is dammed at 3 km upstream, therefore having a controlled flow. The Pitt River drains a lake and has therefore a nearly constant outflow. At the downstream boundary, water levels influenced by tides are imposed. Eight primary tidal constituents, the most important overtide (M4) and compound tides are determined via the Delft Dashboard toolbox (Van Ormondt et al., 2020), using the TPXO8.0 database (Egbert and Erofeeva, 2002).

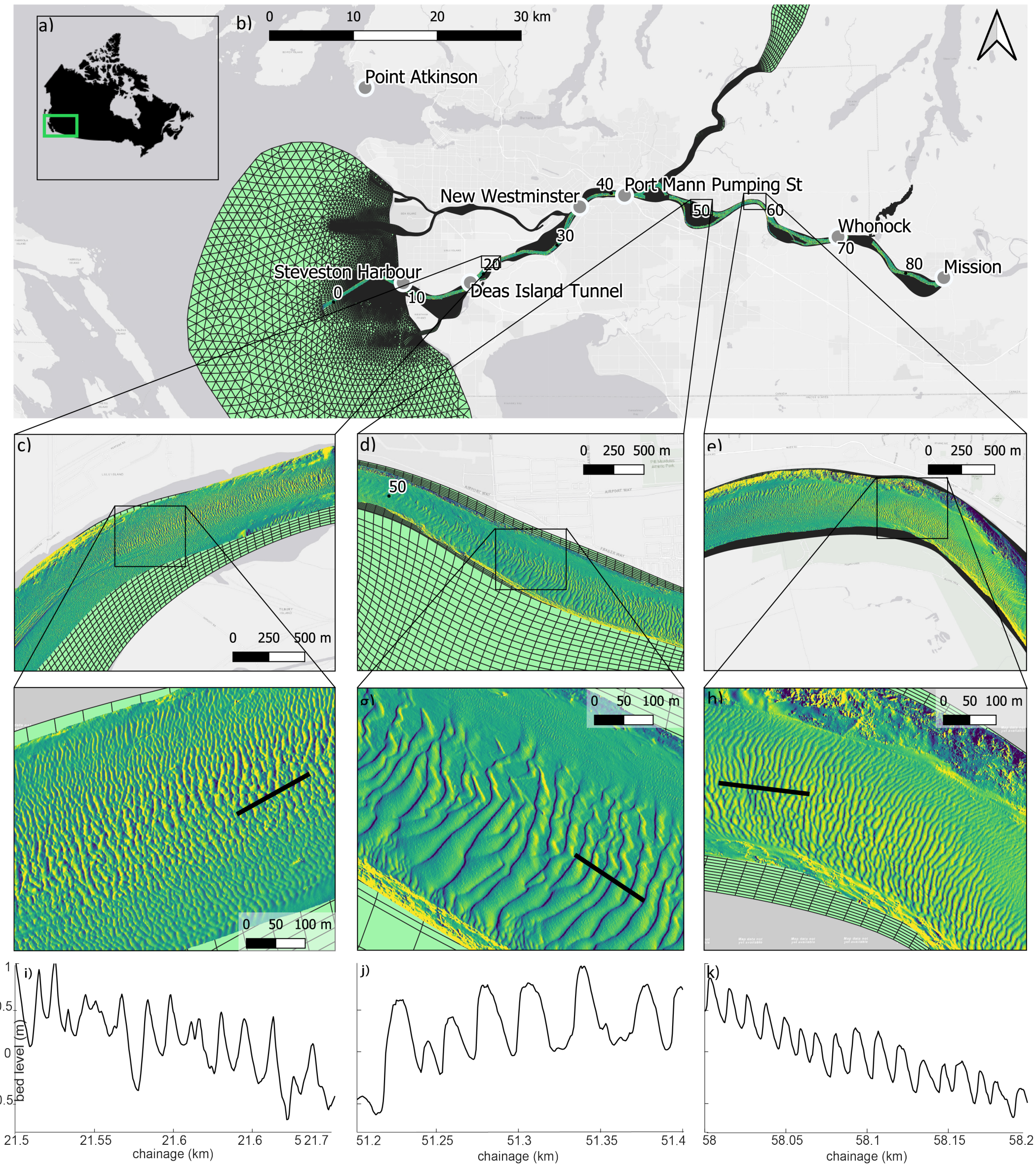

Figure 1. Study area of the Fraser River in British Columbia, Canada (a). b) The Fraser River from river kilometer 10 (Steveston Harbor) to 85 (Mission). Green shaded area indicates the model domain. Grey markers indicate gauging stations. c-e) three focus zones examined in this study, f-h) example zoom ins of the dune fields. i-k) example profiles of the dune fields.

The amplitudes and phases at the downstream boundary were corrected to minimize the error in the model-data comparison at the Point Atkinson tidal gauging station. This correction was on average 0.8% of the tidal amplitude and 20° for the tidal phases, for the 13 tidal components. The model was calibrated for low discharge (<1600 m^3 s^{-1}; Figure 3b), to simulate flow conditions that correspond to the low-discharge bathymetry. The calibration was performed by varying the Manning's roughness coefficients and evaluating the resulting water levels and tidal amplitudes of the three most important tidal constituents at 7 gauging stations (RK 0, 9, 18.5, 35, 42, 70, 85) (Figure 2). The principal tidal constituent M_2 is used for calibration, together with M_4 and K_1. Relative phase differences between M_2 and M_4 (the first overtide of M_2) influence tidal duration asymmetry, the main mechanism for

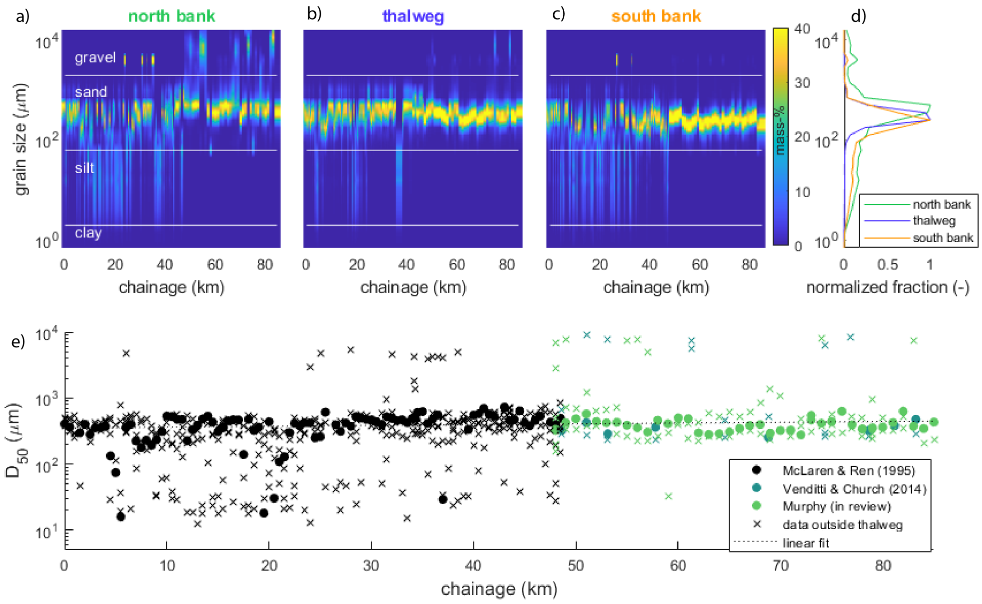

Figure 2. Grain size distributions of bed sediment in the Fraser River. a, b, c) grain size distribution along the north bank, thalweg and south bank. d) cumulative distribution at the north bank, thalweg and south bank. e) median grain size (D_{50}) in and outside of the thalweg. Markers differentiate between samples taken in the thalweg (solid marker) or outside along the river banks (indicated with 'x'). The data is from a data compilation by Venditti and Church (2014), which includes reanalyzed observations from McLaren and Ren (1995), and recent observations by Murphy (2023).

driving residual bed-load transport in estuaries (Van De Kreeke and Robaczewska, 1993). The diurnal tide K_1 is relatively large at the west coast of North America, and interaction between diurnal and semi-diurnal frequencies can produce asymmetric tides as well (Hoitink et al., 2003).

The tidal amplitudes were derived from harmonic analysis using t_tide (Pawlowicz et al., 2002). The best performing model had a uniform Manning's coefficient (roughness) of 0.026 s $m^{-1/3}$ (Figure 3). Disconnecting the hydraulic roughness at the regime transition at RK 40, thereby allowing for two different roughness values, did not improve the calibration (Supplementary materials Figure S3a). The uniform Manning's coefficient (roughness) of 0.026 s $m^{-1/3}$ is slightly higher than the calibrated Manning's coefficient of Wu et al. (2022), who used a uniform roughness of 0.015 s $m^{-1/3}$. The difference in roughness value is attributed to the difference in grid resolution. Our model grid in the river domain is overall coarser than the model of Wu et al. (2022) who used a 10 m resolution, so that the schematization of the bathymetric data on our grid results into slightly wider channels. Our value for roughness is considered to be more appropriate for natural sand-bedded rivers (Chow, 1959).

3.2 Field data and preprocessing

Raw multibeam echosounder (MBES) riverbed data were provided by the Public Works and Government Services, Canada. The measured bathymetry comprises data of the Main Channel between river kilometer -1 to 85 and covers the navigation, but does not provide full bank-to-bank spatial coverage. Data were collected during base flow conditions in January,

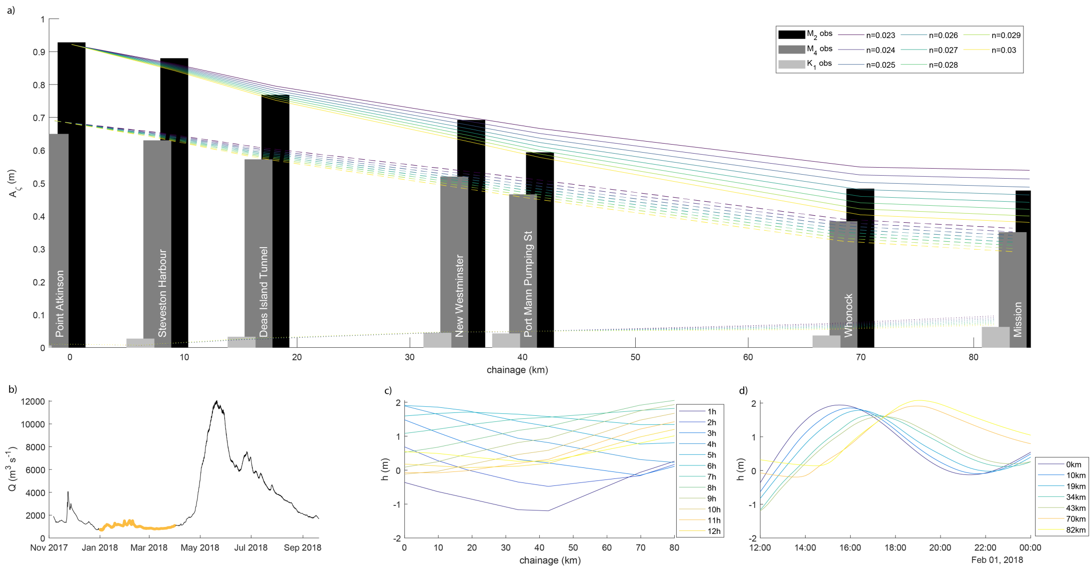

Figure 3. a) Calibration of the model with uniform roughness. The observed tidal amplitude of the tidal constituents M2 (black bars), K1 (dark grey bars), and M4 (light grey bars), and the corresponding modelled tidal amplitudes are indicated. b) Discharge at Mission. Highlighted part of the discharge curve indicates the timeframe of MBES data collection. c) Modelled water surface slope over time, simulated with the model with $n_{man} = 0.026$ s m$^{-1/3}$. d) Modelled propagation of the tidal wave per station, simulated with the model with $n_{man} = 0.026$ s m$^{-1/3}$.

February and March of 2021. This period is characterized by relatively constant discharge and little change to the bed surface (Bradley and Venditti, 2021). During the survey period, the measured discharge (at an hourly interval) was relatively constant, with monthly mean values of 1416 $m^3\ s^{-1}$ (SD 184 $m^3\ s^{-1}$), 1051 $m^3\ s^{-1}$ (SD 140 $m^3\ s^{-1}$) and 1074 $m^3\ s^{-1}$ (SD 35 $m^3\ s^{-1}$) at Hope (RK 165) for the three months, respectively (Water Survey of Canada, Station 08MF005).

The MBES data is gridded onto a 1x1 m^2 grid, and the resulting MBES datasets contain x, y and z coordinates. Next, all bed level data is converted from Cartesian (x, y) coordinates to curvilinear coordinates (s, n) with the same spatial resolution (Vermeulen et al., 2014a). Herein, s is the longitudinal direction, parallel to the river, and corresponds with river kilometers (RK) and n is the cross-sectional direction, wherein n = 0 m is defined as the central river axis, which roughly coincides with the thalweg.

3.3 Data analysis

3.3.1 Analysis of river bathymetry: dune detection

Bathymetry was analyzed to derive dune characteristics. Three longitudinal profiles were taken, along the centerline and at approximately 80 m from the north and south bank. In three focus areas (Figure 1), a longitudinal profile was taken every 10 meters, resulting in 27, 41, 23 profiles for zones 1, 2 and 3 respectively, depending on the river width. To ensure that bedforms in all profiles were primarily caused by natural mobile bed conditions, we excluded bathymetry that showed extensive scour, human-made structures and dredging marks (Figure Supplementary Figures S2).

From the filtered profiles, bedform characteristics were determined by using a standard Bedform Tracking Tool (Mark et al., 2008). In the tool, the default filter span (c = 1/6) was suitable to filter out small features such as measurement errors or outliers. Three span values (P0), corresponding with bedforms with a length of 20 m ±10, 50 m ±20 and 100 m ±30, were used as input to detrend and smooth the profile. The span values in the tool are based on a spectral analysis yielding the dominant bedform wave lengths in each section.

Based on the detrended and smoothed profile, a zero-crossings profile was defined, based on which individual dunes were identified, and dune characteristics were calculated. Dune characteristics include dune height Δ (m), the vertical distance between the crest and downstream trough, dune length λ (m), the horizontal distance between two subsequent crests, leeside angle LSA (°), the slope from a linear fit of the dune's leeside, excluding the upper and lower 1/6 of the dune height, and the stoss side angle SSA (°) calculated in the same maner as the leeside angle. The bedform slipface angle SFA (°), the steepest part of the leeside angle, and is defined as the 95-percentile of the leeside angle. Finally, bedform asymmetry is calculated as the ratio between the length of the (seaward) leeside and the total bedform length (Lefebvre et al., 2021).

Bedforms with heights smaller than 0.1 m are not distinguishable from the error of the survey, and are excluded from the analysis. Bedform lengths smaller than 3 m are excluded as well, since the resolution of the bathymetric data (1 m) is too small to detect small bedform features. Features with a height greater than 2.5 m (2% of all detected bedforms) or a length greater than 200 m (0.08% of all detected bedforms) are considered another type of bed fluctuation unrelated to dunes such as scour holes or wake deposits downstream of human-made structures. These had a different geometry than mobile dunes, which was confirmed by visual inspection of the batymetric data. Large dunes (>2.5 m) as found in previous studies (Kostaschuk and Luternauer, 1989; Venditti et al., 2019; Pretious and Blench, 1951) were not observed in the low-discharge bathymetry used in this study.

3.3.2 Analysis of river geometry

River geometry was parametrized by river width, curvature, transverse bed slope and excess depth. River width W (m) was determined from a polygon following the longitudinal low water line, which is considered to be the discharge carrying section of the river under low discharge conditions. Cross-sectional area A (m^2) was subsequently approximated from the tidally-averaged water depth and river width, assuming a trapezoidal shape of the cross-sectional area, where the river bank has a 60° slope. Curvature r (km^{-1}) was defined as the inverse of bend radius following the approach of de Ruijsscher et al. (2020). Local transverse bed slope ξ (-) was defined as the slope between the two sides of the main river channel, longitudinally discretized at intervals of 100 m. Finally, an excess depth parameter D_e (-) was used as a measure to identify pools and scour holes (Vermeulen et al., 2014b), and was defined as:

$$D_e = \text{sign}(r)\left(\frac{D_{max}}{D_r} - 1\right) \tag{1}$$

where D_r is the regional mean depth of a discretized section of 500 m long, and D_{max} the local maximum depth in this section. Sign indicates the signum function, which returns the sign of a real number.

3.3.3 Analysis of river hydrodynamics

To assess local flow conditions and tidal attenuation, the hydrodynamic model was evaluated during low flow conditions in March 2018 (Figure 3b). The flow magnitude and direction, water depth and bed shear stress magnitude and direction per grid cell were saved every ten minutes in the simulation. The calculation of bed shear stresses in Delft3D is based on a logarithmic approximation of the near bed velocity and is explicitly solved. All output data were tidally-averaged using a Godin filter (Godin, 1972). The Godin filter removes the tidal and higher frequency variance to obtain a low-passed signal primarily caused by the river flow.

Besides transforming the data into along and across-channel coordinates (s,n) (Vermeulen et al., 2014a), the flow and shear stress vectors were rotated, to transform their orientation to along-channel direction (s-direction). This allowed differentiation between the in- and outgoing currents, which are in -s and s-direction, respectively. The percentage of time that the flow reverses and flows upstream (reversal time t_{rev} (%) was then calculated.

3.3.4 Dune geometry prediction

Flow data from the model was used to predict dune height Δ (m), using dune height predictors that include some measure of flow strength (Van Rijn, 1984; Yalin, 1964; Karim, 1995; Venditti and Bradley, 2022). Firstly, dune height was predicted using the widely applied dune geometry predictor of Van Rijn (1984). This predictor is based on 84 laboratory experiments, with grain sizes ranging from 190 - 2300 μm, and 22 field data sets (490 - 3600 μm) of relatively wide rivers (width / depth > 0.3) with unidirectional flow. This corresponds well with conditions found in the Fraser River, except that the Fraser experiences bidirectional currents. To account for this, values of water height and shear stress are tidally averaged, since bed-material sediment transport in the Lower Fraser River generally follows the pattern of mean velocity over the tidal cycle (Kostaschuk and Best, 2005). The tidal averaging is described in section 3.3.3. Dune height is thus:

$$\Delta_{vRijn} = 0.11h\left(\frac{D_{50}}{h}\right)^{0.3}(1 - e^{-0.5T})(25 - T) \tag{2}$$

in which D_{50} is median grain size (m), h is the water dept (m) and transport stage T is:

$$T = \frac{(u^*)^2 - (u_c^*)^2}{(u_c^*)^2} \tag{3}$$

where u^* is the shear velocity (m s^{-1}), and u_c^* is the critical shear velocity (m s^{-1}). Shear stress (τ, N m^{-2}) relates to shear velocity and can be expressed non-dimentionally as the Shields number (θ) as in:

$$\tau = u^{*2} * \rho_w \tag{4}$$

$$\theta = \frac{\tau}{(\rho_s - \rho_w) g D_{50}} \tag{5}$$

in which g is the gravitational acceleration (9.81 m s^{-2}), ρ_s is the sediment density (2,650 kg m^{-3} for quartz) and ρ_w is the water density (1,000 kg m^{-3} for fresh water). Therefore, equation 3 can be rewritten as:

$$T = \frac{\tau - \tau_c}{\tau_c} = \frac{\theta - \theta_c}{\theta_c} \tag{6}$$

When 50 μm < D_{50} < 5,000 μm, the critical shields number θ_c (-) can be approximated as (Zanke, 2003). The resulting values of θ_c are approximately 0.03 (medium sand).

$$\theta_c = 0.145 Re_p^{-0.333} + 0.045 * 10^{-1100 Re_p^{-1.5}} \tag{7}$$

in which the particle Reynolds number Re$_p$ is:

$$Re_p = D_{50}^{3/2} \frac{\sqrt{Rg}}{\nu} \tag{8}$$

where the relative submerged density R = $(\rho_s - \rho_w)/\rho_w$ (-) and ν is the kinematic viscosity (m^2 s^{-1}), which is slightly dependent on water temperature as $\nu = 4 * 10^{-5}/(20 + t)$ in which t = temperature (°C). Here, ν = 1.3 * 10^{-6} is used for 10 °C.

We also predict dune height using the predictor of Yalin (1964):

$$\Delta_{Yalin} = \frac{h}{6}\left(1 - \frac{\tau_c}{\tau}\right) \tag{9}$$

The predictor of Karim (1995) builds on that of Van Rijn (1984) and Allen (1978), and is based on the suspension criterion which utilizes the shear velocity and the particle fall velocity (w$_s$). The predictor of Allen (1978) is not included in this research, since it is mostly based on laboratory experiments.

$$\Delta_{Karim} = h\left(0.04 + 0.294(\frac{u^*}{w_s}) + 0.00316(\frac{u^*}{w_s})^2 - 0.0319(\frac{u^*}{w_s})^3 + 0.00272(\frac{u^*}{w_s})^4\right) \tag{10}$$

where w$_s$ can be defined as (Ferguson and Church, 2004):

$$w_s = \frac{RgD_{50}^2}{C_1\nu + (0.75 C_2 R g D_{50}^3)^{0.5}} \tag{11}$$

in which C_1 and C_2 are constants with values of 18 and 1.0, respectively, for slightly irregular particles.

Finally, we test the equation of Venditti and Bradley (2022).

$$\Delta_{VB} = h\left(10^{\left(-0.397(log\frac{\theta}{\theta_c}-1.14)^2-0.503\right)}\right) \tag{12}$$

3.3.5 Hydraulic roughness estimation

To estimate the impact of dunes on the water levels in the study reach, the hydraulic roughness was determined. The total predicted hydraulic roughness, expressed as a friction factor $\hat{f}$, results from form friction and grain friction (Einstein, 1950). Assuming dunes are the dominant structures causing form resistance, the total hydraulic roughness was predicted as in Van Rijn (1984):

$$\hat{f} = \frac{8g}{(18\log(\frac{12d}{k_s}))^2} \tag{13}$$

Herein, k_s consists of form roughness height k_{sf} and grain roughness height k_{sg}:

$$k_s = k_{sg} + k_{sf} \tag{14}$$

$$k_{sg} = 3D_{90} \tag{15}$$

where D_{90} is the 90^{th} percentile of the grain size distribution, and

$$k_{sf} = 1.1\gamma_d\Delta(1-e^{\frac{-25\Delta}{\lambda}}) \tag{16}$$

where the calibration constant γ_d is taken as 0.7 in field conditions (Van Rijn, 1984).

In the modelling suite of Delft3D, roughness values of Manning's n, n_{man} (s $m^{-1/3}$), are converted to a Chézy coefficient C ($m^{1/2}s^{-1}$) via (Manning, 1891):

$$C = \frac{R_h^{1/6}}{n_{man}} \tag{17}$$

in which R_h is the hydraulic radius, which can be simplified to the water depth h (m) for rivers that satisfy W $\gg$ h.

The Chézy coefficient is converted to the dimensionless Darcy-Weisbach friction factor f_m according to Silberman et al. (1963):

$$f_m = \frac{8g}{C^2} \tag{18}$$

4 Results

4.1 Hydraulics and morphology of the fluvial-to-tidal transition zone

The tidally-averaged water depth in the study area fluctuates between 3 and 18 m (Figure 4a). In the mixed-fluvial tidal regime of the river (RK > 40), it increases gradually in seaward direction, and in the tidal regime (RK < 40) it remains constant. The local increase in water depth is reflected in the tidally averaged and instantaneous shear stress profiles (Figure 4b). The downstream-directed maximum shear stress increases from 0.4 N m^{-2} in the upstream area to 10 N m^{-2} at the river mouth. Similarly, the upstream-directed maximum shear stress in relation to flow reversal (indicated by a minus sign in Figure 4c) increases to 6 N m^{-2}. In contrast, the tidally-averaged shear stresses remain relatively constant over distance (fitting a linear model gives a slope of 10^{-5} N m^{-2} km^{-1}). The tidally averaged shear stress is on average 0.64 N m^{-2} and fluctuates between -1.0 N m^{-2} (indicating an upstream directed shear stress at the most downstream area, RK 0) and 2.2 N m^{-2} (at RK 67).

The tidal effect on the water levels and flow direction weakens in the upstream direction, and the amplitude of the tidal constituents M_2 and K_1 decreases as the tides attenuate (Figure 4d). The M_2 tidal constituent shows a particularly strong decrease from RK 10 to 40, while landwards the tidal attenuation is minimal. In the most upstream reach, bidirectional currents can still be observed (Figure 4c). During low flow conditions, upstream (flood) flow occurs for 45% of the time at the river mouth (about RK 10), and decreases to 25% at the most upstream location of the study reach.

The morphology of the Fraser River does not show consistent trends in the stream-wise direction. The river width fluctuates between 500 and 1100 m (Figure 5a). The cross-sectional area of the river remains relatively constant in the more upstream part of the river (RK > 40), since river depth varies inversely with river width. The more downstream part experiences larger fluctuations in cross-sectional area, since water depth remains relatively constant (Figure 5a). The bed level (Figure 5b) shows large variations, but remains relatively constant in the downstream part. River curvature, transverse bed slope and depth excess are strongly related ($R^2 = 0.15$ - 0.61, $p < 0.005$, Figure 5c), which reflects the low-sinuosity meandering morphology.

4.2 Morphological response of dunes to tidal hydraulics

Dune geometry in the study reach varies considerably (Figure 6), with dune heights up to 2.4 m (mean: 0.46, median: 0.39 m, SD: 0.28 m) and dune lengths up to 194 m (mean: 24 m, median: 16, SD: 22 m). Multiple scales of superimposed bedforms co-exist, although most of the bed is covered by only primary dunes. Patterns in dune geometry are apparent, with some areas of relatively low and short dunes, and others with increasing or decreasing dune heights and lengths. For example, the thalweg has large dunes around RK 68, 77 and 85, with increasing and decreasing dune heights upstream and downstream of those local maxima. Such patterns are not consistent over whole river width however, and where relatively large dunes prevail on one part of the river (e.g. north side), dunes can be small on the other parts (see for example around RK 68). This variation in dune height and length, along the cross-section and longitudinally, is expressed as the standard deviation of all dunes present in one unit of channel width. This allows for comparison between longitudinal and cross-sectional variability. The mean standard deviation in dune height and dune length in cross-sectional direction (0.20 m and 13.0 m, respectively) is twice as high as the variation along the longitudinal direction (on average 0.11 m and 6.8 m, respectively) (Figure 6).

Local patterns in dune height and length are difficult to explain, and do not reflect the regime change around RK 40 or trends in grain size in the thalweg. However, visual inspection reveals dune occurrence is primarily determined by grain size along the outer banks – when the grain size is too large (gravel) or too small (clay), dunes will be absent (Supplementary Figure S2e and f). When the river cuts into a clay or gravel layer on the north or south sides of the channel, abrupt changes in dune geometry can result.

The gradual increase in strength and duration of tidal currents in the seaward direction influences dune shape. Firstly, the dune crests become sharper (Figure 1 i-k). Secondly, the leeside and slipface angle of the dunes decrease in downstream direction (Figure 7a, b). In particular the slipface angle decreases faster in the tidal regime than in the fluvial-tidal regime. Since the stoss side angle remains relatively constant (with a slight increase in the tidal regime), dunes become more symmetrical in seaward direction (Figure 7c). When the asymmetry is equal to 0.5, dunes are perfectly symmetric. This is possible at nearly every

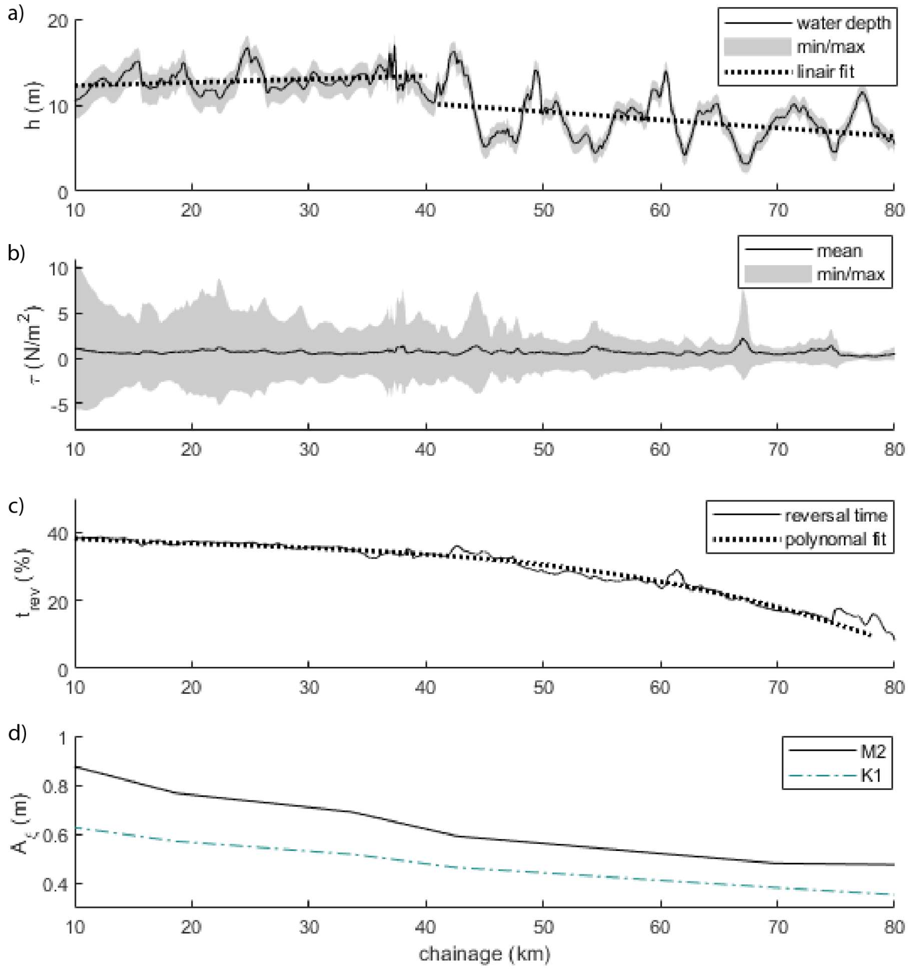

Figure 4. Hydraulic characteristics of the Lower Fraser River. a) water depth (h), b) tidally-averaged, maximum and minimum shear stress (τ), c) reversal time (t_{rev}), d) tidal amplitude (A_ξ) of the M_2 and K_1 tide.

location up to a distance of 75 km from the river mouth, and becomes consistent at around 40 km from the river mouth, indicating the impact of the regime change. Results from a two-paired student t-test shows that the leeside angle, slip face angle and asymmetry is significantly different (at a 95% confidence level) in the tidal and the fluvial-tidal regime, while stoss side angle is not. The leeside angle directly correlates with flow-reversal time (Figure 7d) and maximum shear stress (Figure 7e), showing lower leeside angles and more symmetric dunes in seaward direction, however large variation is observed.

4.3 Dune geometry prediction from model output

Dune height predictors whre applied to the FTTZ of the Fraer River at both small and large scales. The models were not specifically developed for tidal rivers with bidirectional currents, so input values were tidally-averaged.

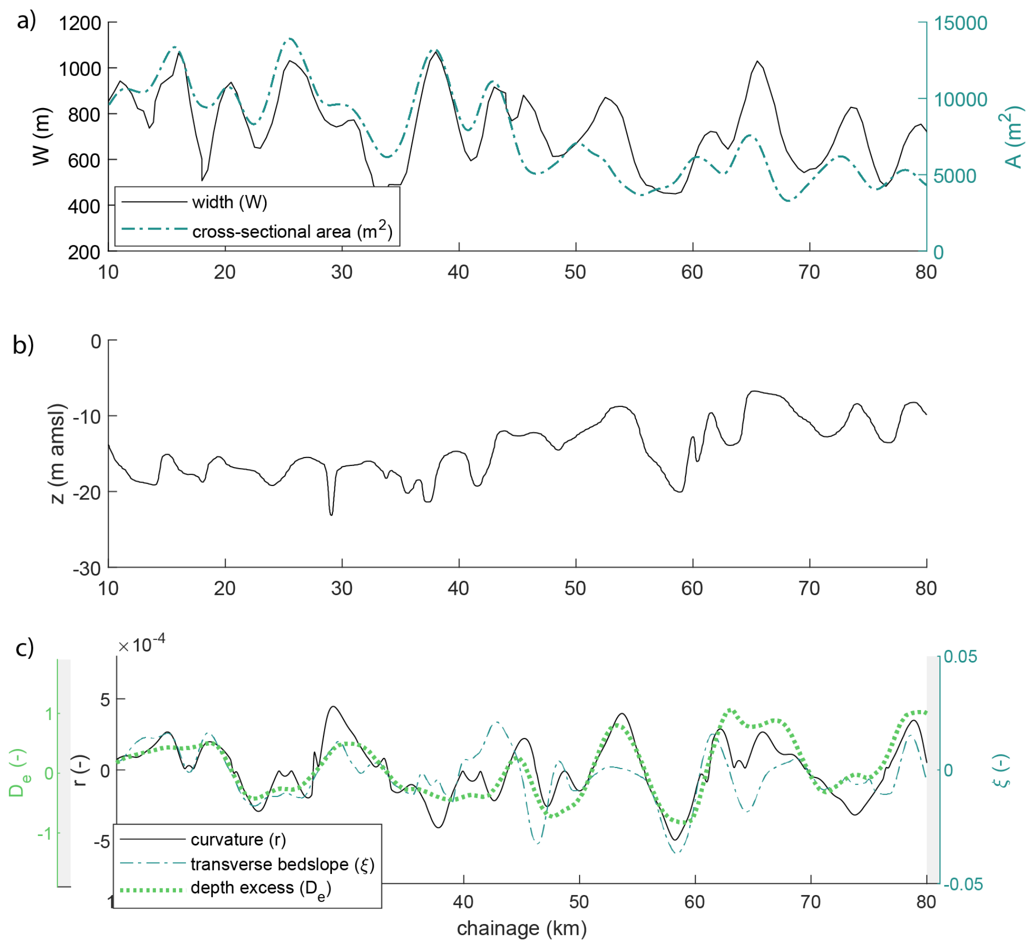

Figure 5. Morphological characteristics of the Lower Fraser River. a) smoothed channel width (W) and smoothed cross-sectional area (A), b) bed level z in meters above sea level, c) channel shape, expressed in depth excess (D_e), transverse bed slope (ξ) and curvature (r)

The predictor of Van Rijn (1984) works well when all data is reach-averaged (predicted Δ_{vRijn} = 0.52 m, compared to measured Δ = 0.50 m; Figure 8 a). However, it underestimates dune height in the mixed fluvial-tidal regime (by about 20 cm at RK 80), and overestimates it in the tidally-dominated regime (by about 24 cm at RK 10). All other predictors are inaccurate and overestimate the dune height significantly, with an increasing error in the downstream direction (Figure 8 b-d). For example, the reach-averaged predicted dune heights are 0.87 m, 1.27 m and 1.83 m for the predictors of Yalin (1964), Karim (1995) and Venditti and Bradley (2022), respectively.

Local variability in dune height in the study area is not captured in dune geometry predictors because of the considerable spatial variability in the measured dune geometry. To establish the degree to which local variability in dune properties relates to flow properties obtained with the 2DH hydraulic model assuming a constant roughness, we focus on three zones in the FTTZ (Figure 2). In those zones, flow characteristics are modelled (see Supplementary Figures S7-S11) and the dune height predictor of (Van Rijn, 1984) (equation

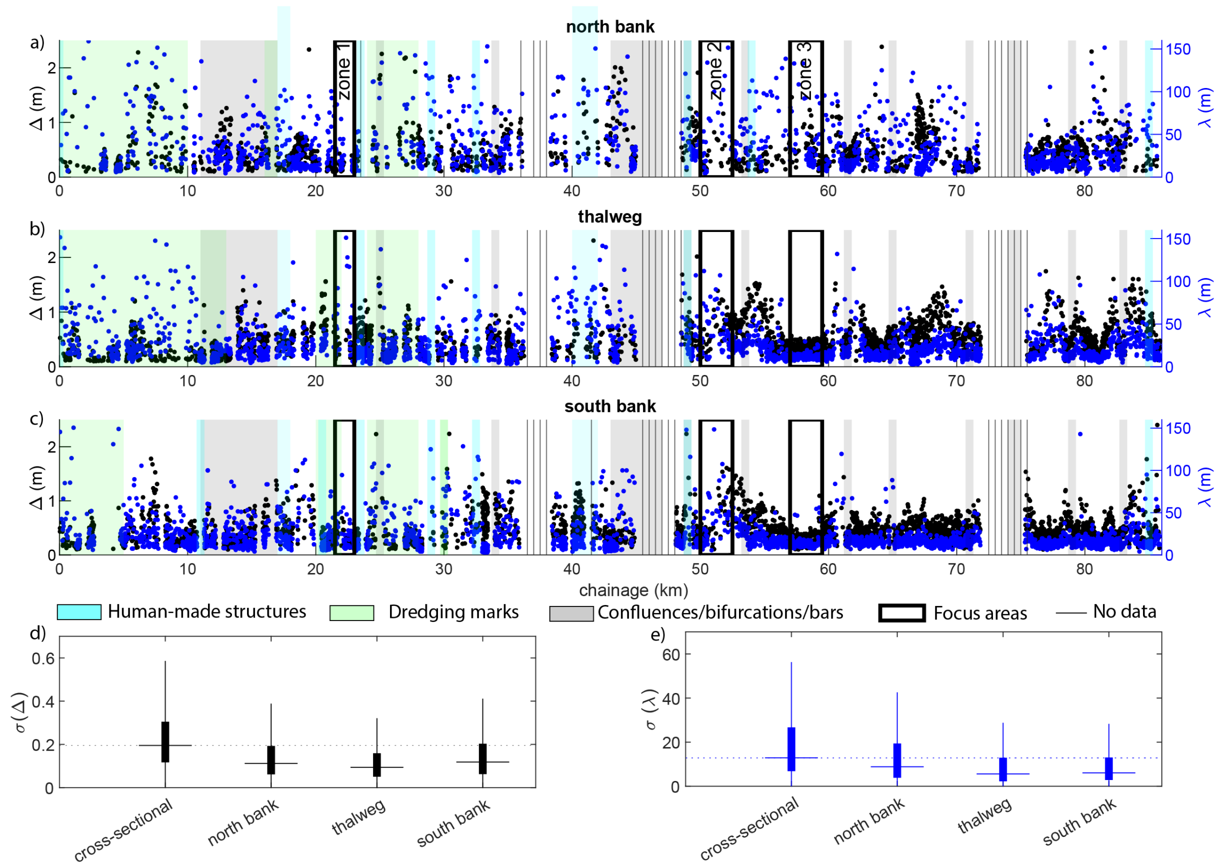

Figure 6. Dune geometry. a, b, c) Dune height (Δ; black) and dune length (λ; blue) throughout the research area. Human-made structures, dredging marks, confluences, bifurcations and bars, focus areas, and zones with no data are indicated (see legend). d, e) Standard deviation (σ) within the mean multibeam echosounder coverage width (230 m) of dune height and dune length over the cross-section, north bank, thalweg and south bank. In each bar, the central mark indicates the median, and the bottom and top edges of the box indicate the 25^{th} and 75^{th} percentiles, respectively. The whiskers extend to the most extreme data points, and outliers are not shown.

2) is applied to each zone using model output per grid cell. The dune height predictor of Van Rijn (1984) performs reasonably well in predicting the local spatial pattern of dune height in the three zones (Figure 9 a-c), but the mean dune height is overestimated for zone 1 and 3, and underestimated for zone 2. To assess the performance of the van Rijn model in predicting dune patterns, a bias correction is performed. Numerical values were added to or subtracted from the predicted dune height in order to minimize the RMSE, and assess the overall patterns in the dune field rather than the actual value (Supplementary Figure S5). The bias-corrected RMSE values of dune height average 0.13 m, which indicates that the spatial pattern of dune heights is relatively well captured by the predictor. The van Rijn dune height predictor captures the main processes that determine dune height in tidal environments, but does not reliably predict absolute values. The dune height predictors of Yalin (1964), Karim (1995) and Venditti and Bradley (2022) perform worse on the local scale pattern (Figure 9 d-l). Notably, the bias correction improves their performance, (Supplementary Figure S6), but they capture the pattern less than well than the predictor of Van Rijn (1984).

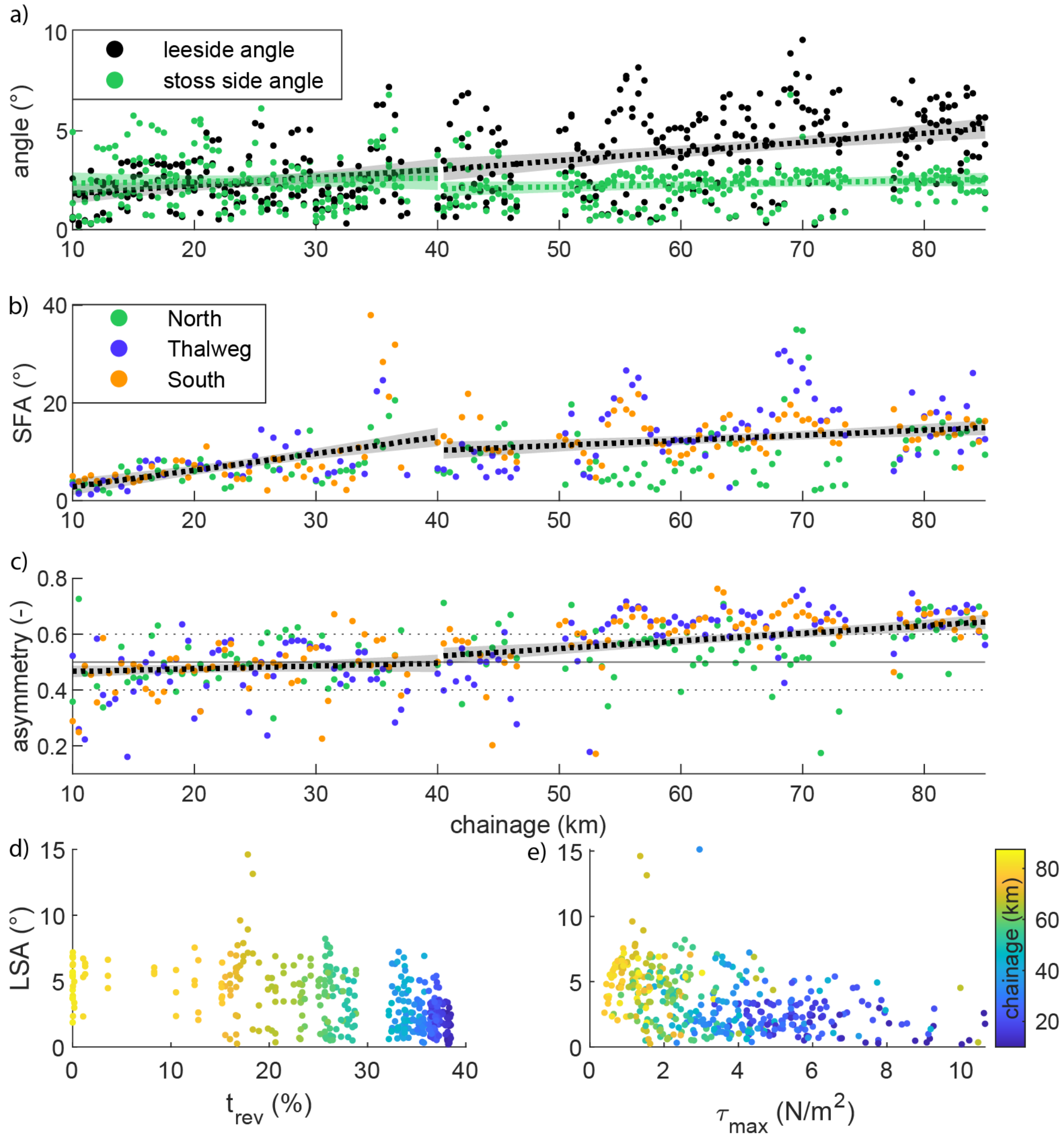

Figure 7. Dune shape in the study area. a) leeside angle (LSA) and stoss side angle (SSA), b) dune slipface angle (SFA), c) dune asymmetry, expressed as the ratio between the length of the (seaward) leeside and the total bedform length. A value of 0.5 indicates symmetric dunes, values of asymmetry smaller than 0.4 are defined as flood-asymmetric, while values larger than 0.6 are ebb-asymmetric. Confidence intervals of linear regressions are shown. Subfigure d) and e) show dune leeside angle against against reversal time (t_{rev}) and against maximum shear stress (τ_{max}), respectively.

4.4 Comparison of observed dune roughness and model roughness

The variability in dune geometry is reflected in the hydraulic roughness generated by the dunes, which ultimately can be used in the hydraulic model to assess the importance of dunes for the large-scale hydraulic roughness.

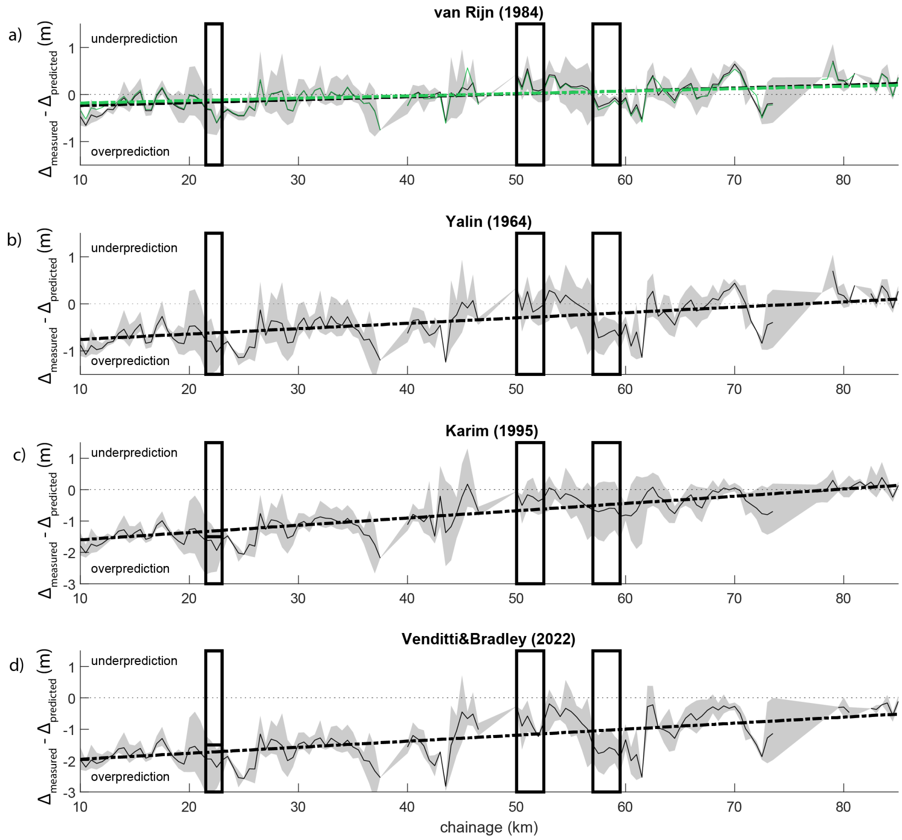

Figure 8. Residual dune height (measured minus predicted) to assess dune height predictor performance of the predictor of a) Van Rijn (1984), b) Yalin (1964), c) Karim (1995) and d) Venditti and Bradley (2022). The measured data is based on the average of three longitudinal transects, and includes the minimum and maximum values in a grey shading. The modelled data is based on the model with a constant roughness of n_{man} = 0.026 s m$^{-1/3}$. In subfigure a) predicted dune height with dune-adjusted roughness (varying between 0.024 and 0.028 s m$^{-1/3}$) is displayed in green.

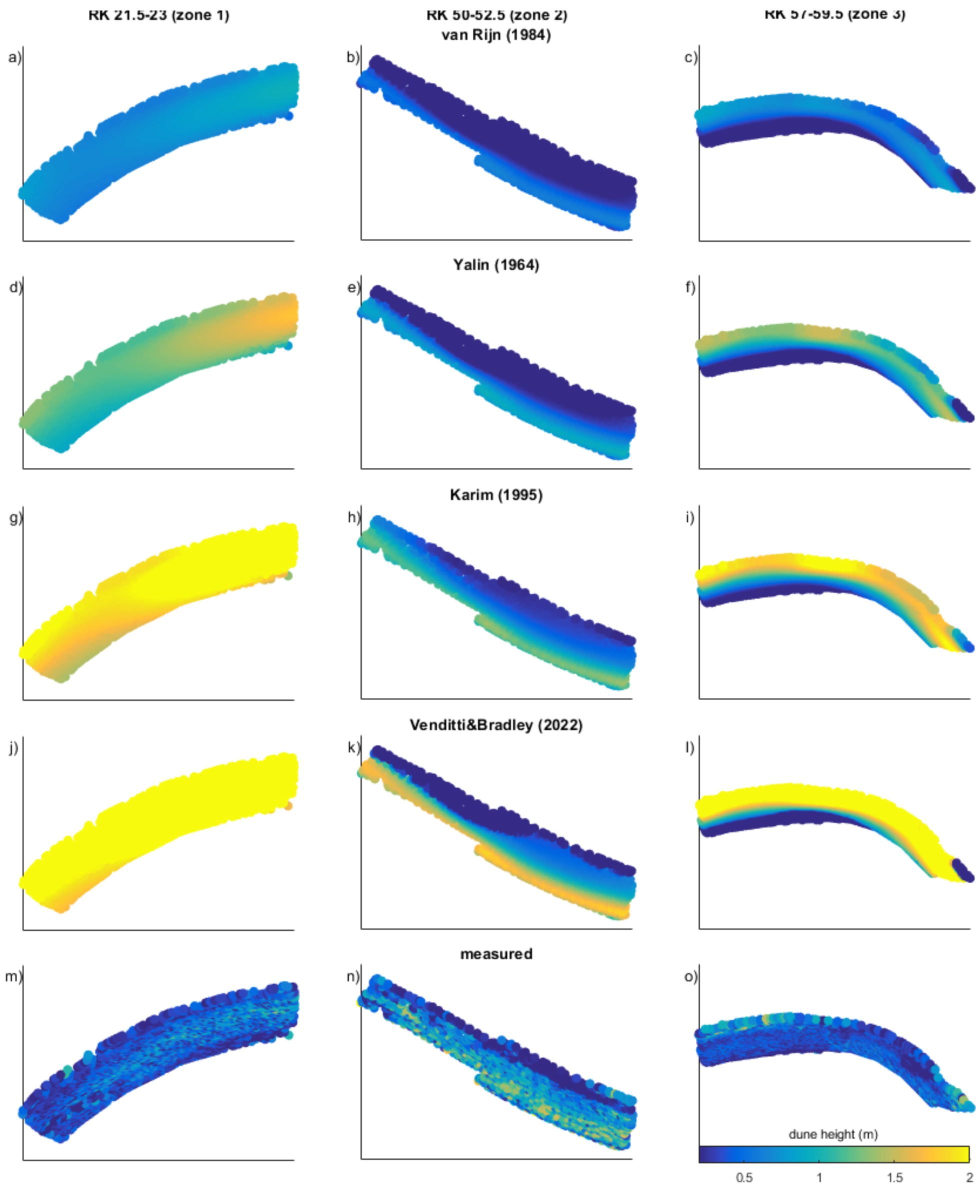

Figure 9. Dune height predictor performance of the predictor of Van Rijn (1984) (a,b,c), Yalin (1964) (d,e,f), Karim (1995) (g,h,i) and Venditti and Bradley (2022) (j,k,l), compared to the measured dune height (m,n,o).

Hydraulic roughness generated by dunes was calculated using equation 13, which includes dune height and length, but does not include the leeside or stoss side angles. The predicted roughness decreases in the downstream direction (Figure 10), which is mainly caused by an increase in water depth. The main variability in roughness is due to variability in water depth, which is most pronounced in the upstream part (RK $>$ 40) of the river (Figure 4). Additionally, local fluctuations in roughness correspond to the local patches of higher dunes, for example at RK ∼54, 63 and 68. The decrease in grain roughness due to a subtle degree of downstream fining has a small impact on overall roughness, because grain roughness values are only around 3% of typical form roughness values. In the downstream reach (RK $<$ 40), smoothed roughness shows a persistent out-of-phase relation with the gradient in smoothed bed elevation (moving average filter of 8 km) (Figure 10a) that is absent in the upstream part of the river.

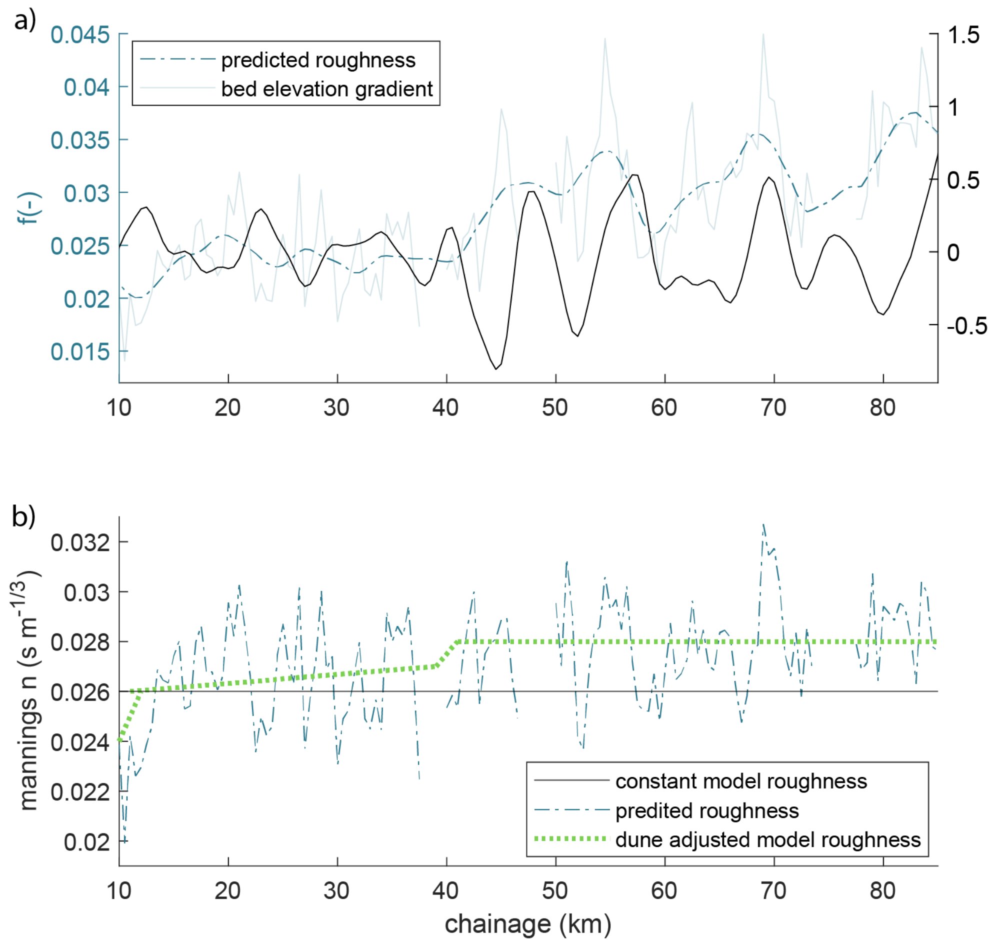

Figure 10. Hydraulic roughness in the study area. a) smoothed roughness (f) (and original roughness in grey) calculated from dune geometry (equation 13)(blue) and the gradient of the smoothed bed level (∂z/∂s; black). b) roughness expressed in Mannings' roughness coefficient n_{man}. Model roughness with a constant n_{man} of 0.026 s m$^{-1/3}$ (black), roughness calculated from dune geometry (equation 13 and 17)(blue), and dune-adjusted model roughness (green).

.

The calculated dune roughness differs slightly from the uniform roughness used in the from model (Manning's roughness of $n_{man} = 0.026$ s $m^{-1/3}$). The derived friction coefficient f_m from the model's roughness (equation 17 and 18) displays the expected decrease in seaward direction, reflecting the increase in water depth. Dune roughness agrees reasonably well to the uniform model roughness (Figure 10b), but local fluctuations are not well-represented. In the upstream region (RK > 40), the model roughness is slightly lower than the dune roughness, while they are similar in the downstream region.

To represent the effect of dune height variation on roughness in the hydrodynamic model, and to investigate if this can improve the calibration, the dune roughness as calculated by equation 13 is divided into three linear components: a uniform roughness of $n_{man} = 0.024$ s $m^{-1/3}$ from RK 0 - 10, a linearly increasing roughness of $n_{man} = 0.026$ to 0.027 s $m^{-1/3}$ in the tidally dominated regime (RK 10 - 40), and a constant roughness of $n_{man} = 0.028$ s $m^{-1/3}$ in the mixed fluvial-tidal regime (RK > 40). A small transition area between the breaks is implemented to ensure a smooth transition to the new roughness regime. These roughness transitions correspond with the transition from the fluvial regime to the deltaic regime around RK 40, and the downstream change from a confined to a less confined channel at around RK 10 (Figure 1).

The dune-derived roughness has little impact on the calibration of water levels and tidal amplitude of the M_2, K_1 and M_4 tidal components (Supplementary Figure S3b). On average, the RMSE value of the modelled water height decreases from 0.36 m to 0.35 m, and the difference between the modelled and observed M_2 amplitude increases from 3% to 4% and K1 from 4% to 6%. Additionally, using the dune-derived roughness for dune height prediction with the Van Rijn predictor only slightly improves the predicted values (17 cm at RK 80 and RK 10) (Figure 8).

5 Discussion

5.1 How are bedform characteristics impacted by the sudden change in tidal flow strength during periods of low river discharge?

During low river discharge conditions like studied in this research, the increase in water depth around RK 40 results into two different hydrodynamic regimes (Figure 11). The tidally-dominated regime is characterized by a large maximum absolute shear stresses, a large tidally-averaged water depth, relatively symmetrical dunes, low leeside and slipface angles and low hydraulic roughness. The mixed tidal-fluvial regime is characterized by a weaker tidal influence, a shallower and more variable water depth, lower maximum absolute shear stresses, asymmetric dunes, higher leeside and slipface angles, and a rougher hydraulically regime. The increase in depth is the main reason that hydraulic roughness is lower in the tidal regime (Equation 13), since the sources of roughness in the Main Channel, sediment composition and dune height, are relatively constant.

Contrasting flow conditions in the two regimes are not reflected in dune height or length. In other systems, dune height is sometimes found to decrease in tidally-influenced regions (Prokocki et al., 2022). Rapid local deposition of the sediment in the deltaic part of the Fraser might result in tidal dunes that are larger than expected (Villard and Church, 2005), leading to a relatively constant dune height. The change in flow regime is reflected in the leeside angle, slip face angle, dune symmetry and dune crest shape. In particular slipface angles are significantly larger in the fluvial-tidal regime, on average 13° compared to 7° in the tidal regime. Dunes are on average asymmetric upstream of the bifurcation at RK 40 (Figure 7), and symmetric downstream of RK 40. This agrees with the findings of Kostaschuk and Villard (1996), who relate the symmetric dunes to high sediment transport rates due to the tides. Indeed, high maximum shear stresses (Figure 11b) are observed in the tidal regime, although tidally-averaged shear stresses remain relatively constant (Figure 4b).

The reversal of the current switches the leeside and stoss side every tidal cycle, steepening both sides in a similar manner (Lefebvre and Winter, 2016). This could be one of the reasons for the large observed variability in angles, since the MBES data is simply a snapshot of the riverbed. Bidirectional currents cause crest orientation to be time-dependent (Hendershot et al., 2016). Both the duration (t_{rev}) and the strength of the flow reversal (τ or Q) determine the dune shape. During low river discharge conditions, the maximum upstream-oriented discharge at RK 22 varies between 4000 and 6000 m^3 s^{-1}, depending on the spring-neap tide cycle. Only 30 km further upstream this has decreased by 66-75%, although the reversal time has only dropped by 9%.

These observations partially agree with the findings of Lefebvre et al. (2021) and Prokocki et al. (2022). Prokocki et al. (2022) observed two different regimes in the Lower Columbia River, USA, based on dune geometry: (fluvial-)tidal dunes, and fluvial dunes. The former were restricted to the most downstream reach (RK < 30 km), and were upstream oriented, predominately low-angled (based on maximum LSA), 2D dunes. Fluvial dunes were downstream oriented, and were higher and longer than the tidal dunes. The division of the regimes in the Columbia is clearer than in the Fraser, most likely because the division in the Columbia coincides with a change in grain size. In addition, the division between the two regimes in the Columbia shifts downstream with an increased discharge. During low discharge, the division is located slightly more downstream (RK 30) than in the Fraser (RK ∼40), which could be attributed to the Columbia's lower tidal range.

Lefebvre et al. (2021) also found an increase in dune symmetry in the downstream direction in the Weser Estuary, Germany, but they did not distinguish between two different regimes. However, their data shows that around 60 km from the river mouth, upstream of the estuarine turbidity maximum, the leeside angle of dunes decreases, and dunes become more symmetric. This transition seems to be slightly more gradual than in this study or in the study of Prokocki et al. (2022). The gradual transition is almost twice as far upstream as in the Fraser River, which is likely because the tidal effect in the Weser extends much further upstream than in the Fraser. In this study, and in those of Prokocki et al. (2022) and Lefebvre et al. (2021), the transition in dune morphology coincides with an increase in channel cross-sectional area, either by widening, deepening or both. The deeper regimes are more tidally-dominated, and the constriction upstream of the cross-sectional area leads to a rapid dissipation of tidal energy, that is reflected in the dune leeside angle and symmetry.

5.2 How can dune variability in the fluvial-to-tidal transition zone during low river discharge be predicted and explained?

Tidally-averaged bed shear stresses from the hydrodynamic model can be used to reliably predict reach-averaged dune height using the predictor of Van Rijn (1984). Furthermore, the shear stress distribution predicted by the hydrodynamic model with constant roughness can predict local dune patterns (Figure 8b-g), thereby capturing the cross-sectional variability in dune heights as observed in Figure 6. Cross-sectional shear-stress variation, which is one of the input parameters of the dune predictor of Van Rijn (1984), largely explains the observed patterns. For example, in zone 1, dune height decreases downstream, becasue river width increases and vflow velocity decreases, resulting in lower shear stresses (Supplementary Figure S10). In zone 2, dunes are the highest on the south side of the channel where the river is deepest and the flow velocity and shear stresses are highest. Finally, in zone 3, centrifugal acceleration generates higher flow velocity and larger dunes on the outside of the bend, whereas upstream the dunes are the largest on the inner bend because flow is accelerated by the momentum inherited from the bend upstream (Jackson, 1975).

Van Rijn (1984) and other dune height predictors tested did not accurately predict absolute magnitude of local dune height using tidally-averaged bed shear stresses from the hydrodynamic model. However, they do a good job of predicting the overall patterns of

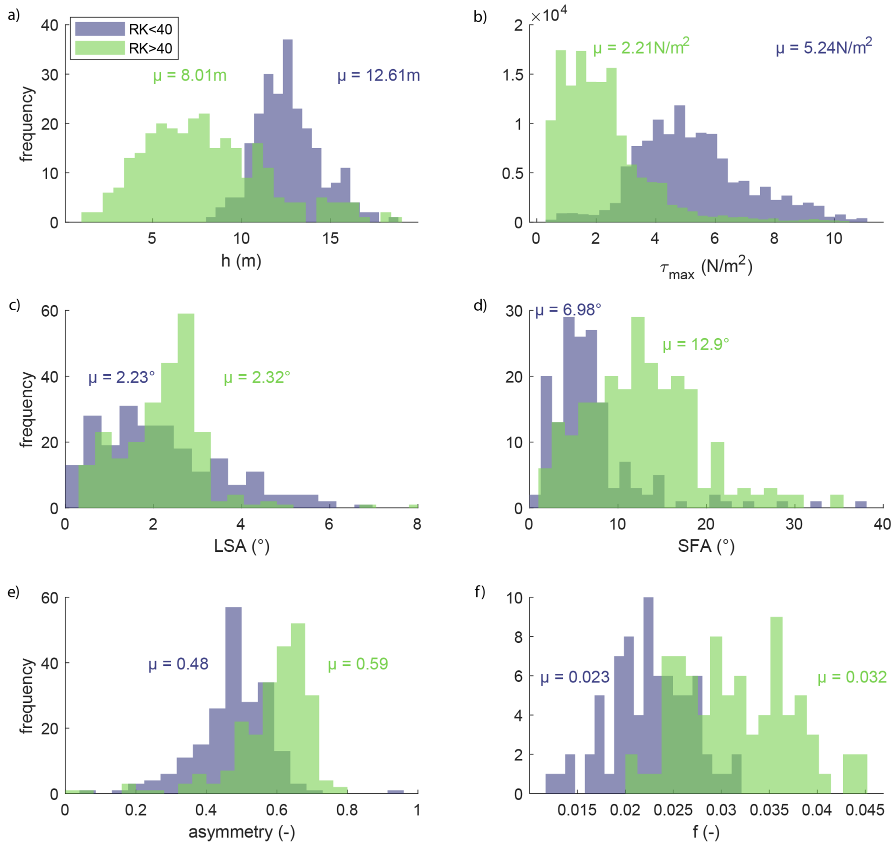

Figure 11. Characteristics of the tidally-dominated regime, seaward of river kilometer (RK) 40, and the mixed tidal-fluvial regime, landward of RK 40. a) water depth (h), b) maximum absolute shear stress (τ_{max}), c) leeside angle (LSA), d) slipface angle (SFA), e) asymmetry, f) friction coefficient (f) derived from dune geometry with equation 13. Mean values are indicated in the figure.

dune height, suggesting that the right processes are captured by the predictors. The poor prediction of absolute values is likely related to number of factors that are not included in the predictors, including self-organization dunes in a shear stress field (Bradley and Venditti, 2019) (such as merging and splitting (Hendershot et al., 2018; Gabel, 1993), crest line deformation (Venditti et al., 2005)), local sediment dynamics not captured by low resolution bed sediment sampling such as local scour (Leclair, 2002), discharge fluctuations and associated hysteresis (Bradley and Venditti, 2021; Julien et al., 2002) and the potential presence of remnant dunes from earlier high-flow conditions. The influence of local factors can be seen in our three focus zones. The larger dunes observed in zone 2 may be related to the local sediment supply being higher here, so dunes develop to a maximum equilibrium size compared to zones 1 and 3. The dunes in zone 2 become longer in the downstream direction until they disappear, even though flow velocity and grain size do not change significantly. The disappearance of dunes in this area could be because the surface of the bed consists of a thin layer of medium sand overlying a deposit of Pleistocene or early Holocene sediment, such as cohesive clay (Clague et al., 1983) (see Supplementary Figure S1), that is not conducive to dune formation. Similarly, in zones 1 and 3, dunes do not develop where the outer bank cuts into a clay layer (Supplementary Figure S9). Additionally, the dunes could be reworked remnants from the previous freshet (Bradley and Venditti, 2021) and their geometry could be related to the much stronger and predominantly downstream currents associated with high river discharge. However, Kostaschuk et al. (1989) found that dunes near Steveston (RK 10) adjusted to the post-freshet decline in discharge over a period of weeks, supporting our contention that the dunes observed herein (more than 6 months after the last freshet) are at least in quasi-equilibrium with low-flow conditions. Additionally, Bradley and Venditti (2021) interpreted low-amplitude bed undulations at RK $\sim$35 as relics from higher flow conditions with smaller dunes superimposed, the latter formed by the low-flow conditions. Kostaschuk et al. (1989) interpreted similar features as 'washed-out' dunes that represented a transition from large, freshet bedforms to small dunes adjusted to low river discharge. In this study we detrended the bed level prior to measuring dune geometry, thereby ensuring that the dunes that we analyzed were representative of low flows.

The poor prediction of local dune geometry in the FTTZ and the observed variability in dune morphology has practical implications for scientists and engineers. Firstly, fairway depth cannot be maintained solely on the basis of on an average dune height, because height varies unpredictably over the river bed. Secondly, measurements of dune height from rock records cannot be reliably used to estimate paleo-hydraulic conditions (Das et al., 2022). Thirdly, models based on reach-averaged dune geometry may result in inaccurate estimates of form roughness and water levels and local values should be used instead. Finally, because the variability in dune height across the channel is twice that of dune height variation along the channel, the grid cell size in hydraulic models should be twice as large in the longitudinal direction than in the cross-river direction.

5.3 To what extent does dune geometry and variability exert an impact on reach-scale hydraulic roughness?

Hydraulic roughness is traditionally predicted using dune height and length (Bartholdy et al., 2010; Lefebvre and Winter, 2016; Soulsby, 1997; Van Rijn, 1984). However, recent research shows that the leeside angle of dunes might be important for roughness prediction (Lefebvre and Winter, 2016) and is poorly represented by dune height and length. Characteristics of the leeside angle determine the strength of flow separation zone (Lefebvre et al., 2014) which impacts form roughness (Lefebvre et al., 2013) induced by dunes. Large rivers are covered by low-angled dunes (LAD) with slip face angles (SFA) $< 30°$ (Cisneros et al., 2020; Kostaschuk and Venditti, 2019) that generate less flow separation than high-angled dunes that have steeper slip face angles (Kwoll et al., 2016). However, weak or intermittent flow separation, with mean leeside angles (LSA) of only $10°$ still generate flow resistance (Kwoll et al., 2016). Lefebvre and Cisneros (2023) show that not only the leeside angle itself, but also the shape of the leeside impacts flow properties and turbulence. Based on numerical experiments, they found that LADs with a mean LSA of $<10°$ and a SFA of $<20°$ are not capable of permanent flow separation. LADs are still able to generate turbulence (Kostaschuk and Villard, 1996; McLean and Smith, 1979) however, because the decelerated downstream flow generates a shear layer that causes eddy generation (Kostaschuk and Villard, 1999; Best and Kostaschuk, 2002), sand resuspension and roughness.

In this study, the transition from a fluvial-tidal to a tidal regime and the corresponding change in dune leeside and slipface angle are not reflected in the reach-scale hydraulic roughness needed to attenuate the tidal motion in the model. Implementing a roughness change at the depth break at RK 40 could be used to parameterize the change in dune leeside angle at the regime transition. However, models with a higher roughness downstream than upstream performed slightly better than models with the highest roughness upstream (Supplementary Materials Text S3). This is contrary to the expectations based on the leeside angle observations and suggests a different source of roughness in the tidal regime (see below). Additionally, the dune roughness predictor (equation 2), based on dune height and dune length, yields very similar values to the calibrated model roughness (RMSE $f = 0.0053$).

This supports the application of the dune roughness predictor in a tidal environment and also indicates that dune leeside angle might not be important in determining reach-scale model roughness. Finally, local values of dune height and length are not required to accurately predict reach-scale model roughness, because hydraulic model performance is not improved by using local dune geometry. This in turn suggests that variable dune roughness might not be needed to simulate large-scale (tidal) flow. Similar conclusions were drawn from a fluvial system where dune roughness calculated from dune geometry explained only 31% of the variance of the roughness inferred from the water surface slope (deLange et al., 2021) and the remaining variance could not be explained by leeside angle statistics.

The limited impact of local dune height, length and leeside angle on the hydraulic model could be due to several factors. Firstly, 3-dimensional dune fields such as those in our study area, generate less roughness than 2-dimensional dune fields (Venditti, 2007), which could explain the lack of model improvement when implementing dune-related roughness. Secondly, a complex leeside shape might have an effect on flow separation (Lefebvre and Cisneros, 2023) and form roughness. So even though the SFAs found in this study are large enough to generate flow separation, the shape of the leeside might prevent it. Thirdly, we evaluated the hydraulic model by assessing tidal attenuation and water level fluctuations and found minimal impact of local dune geometry. However, incorporating dune roughness could be important for prediction of residual sediment transport (Herrling et al., 2021), which is not implemented in our hydraulic model. Local values of shear stresses (for which detailed MBES data is needed) might be required for morphodynamic modelling, even if they are not needed for modelling tidal propagation in a hydrodynamic model. Finally, we evaluated the model on the reach-scale where other components of roughness dominate (see below). However these components are less relevant on the local scales, where dunes might be the main source of roughness. In addition, the prediction of hydraulic roughness generated by dunes deviates locally from the constant model roughness. As a result, in the mixed tidal-fluvial regime the dune-induced roughness is larger than needed for attenuation based on the calibrated roughness. For example, Davies and Robins (2017) found that the overall effective roughness of the bed is about half of the maximum local dune-induced roughness (expressed in k_s). Halving the k_s value in equation 13 results in a comparable dune roughness and calibrated roughness in the mixed fluvial-tidal regime (RMSE 0.0034 for RK > 40) (Supplementary Figure S4) but not in the tidally-dominated regime where dune roughness remains lower than calibrated roughness. This could be a result of the lower LSA in the tidal regime. However, including the LSA in roughness prediction using the equation developed by Lefebvre and Winter (2016) results in unrealistically low values of roughness. In general, evidence that the LSA impacts reach-scale model roughness is lacking.

In our research area there are several reach-scale sources of roughness. Firstly, large-scale river geometry, which is included in the hydraulic model by the bathymetry. We observed an out-of-phase relation between hydraulic roughness and the smoothed gradient of the bed level in the tidally-dominated regime of our study area (Figure 10). A similar relation was observed in the Rhine and Waal rivers in the Netherlands by deLange et al. (2021), and they hypothesised that multi-kilometer depth oscillations induce flow divergence associated with depth increase, which in turn causes energy loss. This in turn is reflected in an elevated hydraulic roughness. However, this out-of-phase relation is not observed in the mixed tidal-fluvial regime in the Fraser, where increases in depth coincide with decreases in width, keeping the cross-sectional area relatively constant. As a result, changes in depth do not result in flow divergence or convergence and the out-of-phase relation does not develop. Secondly, intertidal areas affect reach-scale roughness. The calibrated friction in our model is an indication of the friction required to attenuate the tide. The model calibrated with a uniform Manning's roughness ($n_{man} = 0.026$ s m$^{-1/3}$) performs reasonably well in modelling of water level and tidal amplitude, but regions with a significant decrease in tidal energy (between RK 9-18.5 and 35-42) are not well captured by the model (Figure 3). These regions possess intertidal areas (Supplementary Figure S11) which flood during high tide and are not properly represented in the model due to the lack of topographical data, resulting in a local tidal attenuation that is too low. Finally, engineering works, such as the tunnel at RK 18 and the bridge at RK 36, could be an extra source of roughness.

6 Conclusions

During low flow discharge, the Fraser River deepens downstream of 40 km from the river mouth, separating a fluvial-tidal regime landward and a tidal regime seaward. Bathymetric data and a hydraulic model of the lowermost 85 km of the river were used to explore the spatial variability and controls of dune morphology in this fluvial-to-tidal transition zone (FTTZ). Dune height was predicted using several semi-empirical equations to explore the potential for local and regional dune height prediction. Finally, the hydraulic model was used to assess the importance of dune generated roughness on model performance. From these investigations we conclude that:

- There are no significant spatial trends in dune height or length, even though the river deepens at 40 km. Local variability in dune height and length dominates, and variability in dune height and length is two times as large in the cross-sectional direction than in the longitudinal direction.
- Dune height predictors provide a good first approximation of regional dune height and local spatial patterns, but local shear stress predictions need to be improved to enable prediction of local dune heights. Using shear stresses from the hydraulic model calibrated with a constant roughness of $n_{man} = 0.026$ s $m^{-1/3}$, the dune height predictor of Van Rijn (1984) is able to predict local local patterns of dune heights using tidally-averaged values of bed shear stress. Other tested predictors of dune height do a worse job.
- Mean leeside angle and stoss side of dunes are lower in the tidal regime compared to the fluvial-tidal regime, and dunes become symmetric due to the stronger tidal influence. These changes in dune morphology however do not affect reach-scale hydraulic roughness, because the calibrated model roughness is similar to the dune-derived roughness based on dune height and dune length. As a result, hydraulic model performance using a calibrated, constant, roughness is not improved by implementing dune-derived bed roughness.
- Large-scale variations river morphology are more important than dune morphology in controlling variations in reach scale roughness. Reach-scale variations in depth can elevate hydraulic roughness in the tidal region, but this does not occur in the fluvial-tidal regime because changes in depth are compensated by changes in width, keeping the cross-sectional area of the channel relatively constant. Intertidal areas in the Fraser are likely a significant source of roughness, but are difficult to incorporate into hydraulic models because of limited topographic information.

Acknowledgments

SdL and RS were funded by the Netherlands Organisation for Scientific Research (NWO), within Vici project "Deltas out of shape: regime changes of sediment dynamics in tide-influenced deltas" (Grant NWO-TTW 17062). RB, DM, and JV were funded through a Natural Sciences and Engineering Research Council of Canada (NSERC) Discovery Grant and Accelerator Supplement. T. Cain and I. Darke at Public Service and Procurement Canada graciously provided the bathymetric data. Reviewers and editors will be thanked. Data is publicly available via DOIxxx

References

Allen, J. R.L. (1978). "Computational models for dune time-lag: calculations using Stein's rule for dune height". In: *Sedimentary Geology* 20.C, pp. 165–216. ISSN: 00370738. DOI: 10.1016/0037-0738(78)90054-4.

ASCE Task Force (2002). "Flow and transport over dunes". In: *Journal of Hydraulic Engineering* 127, pp. 726–728.

Ashley, G. M. (1980). "Channel morphology and sediment movement in a tidal river, Pitt River, British Columbia." In: *Earth Surface Processes* 5.4, pp. 347–368. ISSN: 03601269. DOI: 10.1002/esp.3760050406.

Attard, Maureen E., Jeremy G. Venditti, and Michael Church (2014). "Suspended sediment transport in Fraser River at Mission, British Columbia: New observations and comparison to historical records". In: *Canadian Water Resources Journal* 39.3, pp. 356–371. ISSN: 07011784. DOI: 10.1080/07011784.2014.942105. URL: http://dx.doi.org/10.1080/07011784.2014.942105.

Bartholdy, J. et al. (2010). "Hydraulic roughness over simple subaqueous dunes". In: *Geo-Marine Letters* 30.1, pp. 63–76. ISSN: 14321157. DOI: 10.1007/s00367-009-0153-7.

Best, Jim (2005). "The fluid dynamics of river dunes: A review and some future research directions". In: *Journal of Geophysical Research: Earth Surface* 110.4, pp. 1–21. ISSN: 21699011. DOI: 10.1029/2004JF000218.

Best, Jim and Ray Kostaschuk (2002). "An experimental study of turbulent flow over a low-angle dune". In: *Journal of Geophysical Research C: Oceans* 107.9, pp. 18–1. ISSN: 01480227. DOI: 10.1029/2000jc000294.

Bradley, R. W. et al. (2013). "Flow and sediment suspension events over low-angle dunes: Fraser Estuary, Canada". In: *Journal of Geophysical Research: Earth Surface* 118.3, pp. 1693–1709. ISSN: 21699011. DOI: 10.1002/jgrf.20118.

Bradley, Ryan W. and Jeremy G. Venditti (Feb. 2017). *Reevaluating dune scaling relations.* DOI: 10.1016/j.earscirev.2016.11.004.

— (2019). "Transport Scaling of Dune Dimensions in Shallow Flows". In: *Journal of Geophysical Research: Earth Surface* 124.2, pp. 526–547. ISSN: 21699011. DOI: 10.1029/2018JF004832.

— (2021). "Mechanisms of Dune Growth and Decay in Rivers". In: *Geophysical Research Letters* 48.20, pp. 1–10. ISSN: 19448007. DOI: 10.1029/2021GL094572.

Bridge, J.S. (2003). *Rivers and Floodplains: Forms, Processes, and Sedimentary Record.* Malden, Massachusetts: John Wiley & Sons, p. 491.

Carling, P. A. et al. (2000). "The morphodynamics of fluvial sand dunes in the River Rhine, near Mainz, Germany. I. Sedimentology and morphology". In: *Sedimentology* 47.1, pp. 227–252. ISSN: 00370746. DOI: 10.1046/j.1365-3091.2000.00290.x.

Chow, V.T. (1959). *Open-channel hydraulics.* McGraw-Hill Book Company, USA. ISBN: ISBN 0-07- 085906-X.

Cisneros, Julia et al. (2020). "Dunes in the world's big rivers are characterized by low-angle lee-side slopes and a complex shape". In: *Nature Geoscience* 13.2, pp. 156–162. ISSN: 17520908. DOI: 10.1038/s41561-019-0511-7.

Clague, John J., John L. Luternauer, and Richard J. Hebda (1983). "Sedimentary environments and postglacial history of the Fraser Delta and Lower Fraser Valley, British Columbia". In: *Canadian journal of earth sciences* 20.8, pp. 1314–1326. ISSN: 00084077. DOI: 10.1139/e83-116.

Das, Debsmita et al. (Sept. 2022). "The Influence of Transport Stage on Preserved Fluvial Cross Strata". In: *Geophysical Research Letters* 49.18. ISSN: 19448007. DOI: 10.1029/2022GL099808.

Dashtgard, Shahin E et al. (2012). "Sedimentation Across the Tidal-Fluvial Transition in the Lower Fraser River, Canada". In: *The Sedimentary Record* 10.4, pp. 4–9. ISSN: 15438740. DOI: 10.2110/sedred.2012.4.4. URL: http://www.wateroffice.ec.gc.ca/,.

Davies, A. G. and P. E. Robins (2017). "Residual flow, bedforms and sediment transport in a tidal channel modelled with variable bed roughness". In: *Geomorphology* 295, pp. 855–872. ISSN: 0169555X. DOI: 10.1016/j.geomorph.2017.08.029. URL: http://dx.doi.org/10.1016/j.geomorph.2017.08.029.

De Brye, Benjamin et al. (2011). “Preliminary results of a finite-element, multi-scale model of the Mahakam Delta (Indonesia)”. In: *Ocean Dynamics* 61.8, pp. 1107–1120. ISSN: 16167341. DOI: 10.1007/s10236-011-0410-y. URL: www.climate.be/slim.

de Ruijsscher, Naqshband, and Hoitink (2020). “Effect of non-migrating bars on dune dynamics in a lowland river”. In: *Earth Surface Processes and Landforms*.

deLange, S. I., S. Naqshband, and A. J.F. Hoitink (2021). “Quantifying Hydraulic Roughness From Field Data: Can Dune Morphology Tell the Whole Story?” In: *Water Resources Research* 57.12, pp. 1–22. ISSN: 19447973. DOI: 10.1029/2021WR030329.

Egbert, Gary D. and Svetlana Y. Erofeeva (2002). “Efficient inverse modeling of barotropic ocean tides”. In: *Journal of Atmospheric and Oceanic Technology* 19.2, pp. 183–204. ISSN: 07390572. DOI: 10.1175/1520-0426(2002)019<0183:EIMOBO>2.0.CO;2.

Einstein, H. A. (1950). “The bed-load function for sediment transportation in open channel flows”. In: *Technical Bulletins 156389, United States Department of Agriculture, Economic Research Service.*

Ferguson, R I and M Church (2004). *A simple universal equation for grain settling velocity.* Tech. rep. 6, pp. 933–937. URL: http://pubs.geoscienceworld.org/sepm/jsedres/article-pdf/74/6/933/2821499/933.pdf.

Gabel, Sharon L. (Apr. 1993). “Geometry and kinematics of dunes during steady and unsteady flows in the Calamus River, Nebraska, USA”. In: *Sedimentology* 40.2, pp. 237–269. ISSN: 0037-0746. DOI: 10.1111/j.1365-3091.1993.tb01763.x.

Gates, T. and M. Al-Zahrani (1996). “Spatiotemporal stochastic open-channel flow. II: simulation experiments.” In: *Journal of Hydraulic Engineering* 122.11, pp. 652–611. DOI: 10.1061/(ASCE)07339429(1996)122:11(652)..

Gisen, Jacqueline Isabella Anak and Hubert H.G. Savenije (Apr. 2015). “Estimating bankfull discharge and depth in ungauged estuaries”. In: *Water Resources Research* 51.4, pp. 2298–2316. ISSN: 0043-1397. DOI: 10.1002/2014WR016227.

Godin, G. (1972). *The analysis of tides.* University of Toronto Press, p. 264.

— (Mar. 1999). “The Propagation of Tides up Rivers With Special Considerations on the Upper Saint Lawrence River”. In: *Estuarine, Coastal and Shelf Science* 48.3, pp. 307–324. ISSN: 02727714. DOI: 10.1006/ecss.1998.0422.

Hendershot, Megan L. et al. (2016). “Response of low-angle dunes to variable flow”. In: *Sedimentology* 63.3, pp. 743–760. ISSN: 00370746. DOI: 10.1111/sed.12236.

Hendershot, Megan L. et al. (Dec. 2018). “Crestline bifurcation and dynamics in fluvially-dominated, tidally-influenced flow”. In: *Sedimentology* 65.7, pp. 2621–2636. ISSN: 13653091. DOI: 10.1111/sed.12480.

Herrling, Gerald et al. (Sept. 2021). “The effect of asymmetric dune roughness on tidal asymmetry in the Weser estuary”. In: *Earth Surface Processes and Landforms* 46.11, pp. 2211–2228. ISSN: 10969837. DOI: 10.1002/esp.5170.

Hoitink, A. J.F., P. Hoekstra, and D. S. Van Maren (Oct. 2003). “Flow asymmetry associated with astronomical tides: Implications for the residual transport of sediment”. In: *Journal of Geophysical Research: Oceans* 108.10. ISSN: 21699291. DOI: 10.1029/2002jc001539.

Holmes, Marcelo H. and Marcelo H. Garcia (2008). “Flow over bedforms in a large sand-bed river: A field investigation”. In: *Journal of Hydraulic Research* 46.3, pp. 322–333. ISSN: 00221686. DOI: 10.3826/jhr.2008.3040.

Horrevoets, A.C. et al. (July 2004). “The influence of river discharge on tidal damping in alluvial estuaries”. In: *Journal of Hydrology* 294.4, pp. 213–228. ISSN: 00221694. DOI: 10.1016/j.jhydrol.2004.02.012.

Jackson, Roscoe G. (1975). “Velocity-bed-form-texture patterns of meander bends in the lower Wabash River of Illinois and Indiana”. In: *Bulletin of the Geological Society of America* 86.11, pp. 1511–1522. ISSN: 19432674. DOI: 10.1130/0016-7606(1975)86<1511:VPOMBI>2.0.CO;2.

Julien, P. Y. et al. (2002). "Case study: Bed resistance of Rhine River during 1998 flood". In: *Journal of Hydraulic Engineering* 128.12, pp. 1042–1050. ISSN: 07339429. DOI: 10.1061/(ASCE)0733-9429(2002)128:12(1042).

Karim, F. (1995). "Bed configuration and hydraulic resistance in alluvial-channel flows". In: *Journal of Hydraulic Engineering* 121.1, pp. 15–25.

Kästner, K. et al. (Mar. 2017). "Distributary channels in the fluvial to tidal transition zone". In: *Journal of Geophysical Research: Earth Surface* 122.3, pp. 696–710. ISSN: 21699011. DOI: 10.1002/2016JF004075. URL: https://onlinelibrary.wiley.com/doi/abs/10.1002/2016JF004075.

Kernkamp, Herman W.J. et al. (Aug. 2011). "Efficient scheme for the shallow water equations on unstructured grids with application to the Continental Shelf". In: *Ocean Dynamics* 61.8, pp. 1175–1188. ISSN: 16167341. DOI: 10.1007/s10236-011-0423-6.

Kostaschuk, R.A. and L.A. Atwood (1990). "River discharge and tidal controls on salt-wedge position and implications for channel shoaling: Fraser River, British Columbia". In: *Canadian Journal of Civil Engineering* 17.3, pp. 452–459. ISSN: 03151468. DOI: 10.1139/l90-049.

Kostaschuk, R.A., M.A. Church, and J.L. Luternauer (1989). "Bedforms, bed material, and bedload transport in a salt-wedge estuary: Fraser River, British Columbia". In: *Canadian Journal of Earth Sciences* 26.7, pp. 1440–1452. DOI: https://doi.org/10.1139/e89-122.

Kostaschuk, R.A. and J.L. Luternauer (1989). "The role of the salt wedge in sediment resuspension and deposition: Fraser River Estuary, Canada". In: *J. Coastal Res.* 5, pp. 93–101.

Kostaschuk, R.A. and P.V. Villard (1999). "Turbulent sand suspension over dunes". In: *Proceedings of the 6th International Conference on Fluvial Sedimentology.* Ed. by N.D. Smith and Rogers. J. Blackwell Sci., Malden, Mass.

Kostaschuk, Ray A and Jeremy G Venditti (2019). "Why do large, deep rivers have low-angle dune beds?" In: *Geology* 47.10, pp. 919–922. ISSN: 19432682. DOI: 10.1130/G46460.1. URL: https://doi.org/10.1130/G46460.1.

Kostaschuk, Ray and Jim Best (Dec. 2005). "Response of sand dunes to variations in tidal flow: Fraser Estuary, Canada". In: *Journal of Geophysical Research: Earth Surface* 110.4. ISSN: 21699011. DOI: 10.1029/2004JF000176.

Kostaschuk, Ray and Paul Villard (Jan. 1996). "Flow and sediment transport over large subaqueous dunes: Fraser River, Canada". In: *Sedimentology* 45.1, pp. 849–863. ISSN: 00370746. DOI: 10.1111/j.1365-3091.1996.tb01506.x.

Kwoll, E. et al. (Mar. 2016). "Flow structure and resistance over subaquaeous high- and low-angle dunes". In: *Journal of Geophysical Research: Earth Surface* 121.3, pp. 545–564. ISSN: 21699011. DOI: 10.1002/2013JF002871.Received.

Leclair, Suzanne F. (2002). "Preservation of cross-strata due to the migration of subaqueous dunes: An experimental investigation". In: *Sedimentology* 49.6, pp. 1157–1180. ISSN: 00370746. DOI: 10.1046/j.1365-3091.2002.00482.x.

Lefebvre, A. and J Cisneros (2023). "The influence of dune lee side shape". In: *EGUsphere [preprint].*

Lefebvre, A. et al. (2014). "Flow separation and roughness lengths over large bedforms in a tidal environment: A numerical investigation". In: *Continental Shelf Research* 91, pp. 57–69. ISSN: 02784343. DOI: 10.1016/j.csr.2014.09.001. URL: http://dx.doi.org/10.1016/j.csr.2014.09.001.

Lefebvre, Alice, Verner B. Ernstsen, and Christian Winter (2013). "Estimation of roughness lengths and flow separation over compound bedforms in a natural-tidal inlet". In: *Continental Shelf Research* 61-62, pp. 98–111. ISSN: 02784343. DOI: 10.1016/j.csr.2013.04.030.

Lefebvre, Alice and Christian Winter (2016). "Predicting bed form roughness: the influence of lee side angle". In: *Geo-Marine Letters* 36.2, pp. 121–133. ISSN: 14321157. DOI: 10.1007/s00367-016-0436-8.

Lefebvre, Alice et al. (2021). "Morphology of estuarine bedforms, Weser Estuary, Germany". In: *Earth Surface Processes and Landforms* 47.1, pp. 242–256. ISSN: 10969837. DOI: 10.1002/esp.5243.

Lesser, Giles R et al. (2004). "Development and validation of a three-dimensional morphological model". In: *Coastal Engineering* 51.8-9, pp. 883–915. ISSN: 03783839. DOI: 10.1016/j.coastaleng.2004.07.014. URL: www.elsevier.com/locate/coastaleng.

Manning, R. (1891). "On the flow of water in open channels and pipes". In: *Transactions of the Institution of Civil engineers of Ireland*.

Mark, C. F. van der, Astrid Blom, and S. M.J.H. Hulscher (2008). "Quantification of variability in bedform geometry". In: *Journal of Geophysical Research: Earth Surface* 113.3, pp. 1–11. ISSN: 21699011. DOI: 10.1029/2007JF000940.

McLaren, Patrick and Ping Ren (1995). *Sediment transport patterns in the lower fraser river and fraser delta*. Tech. rep.

McLean, D.G and B.L. Tassone (1989). *Effects of Dredging on Fraser River Channel Regime*. Tech. rep. Public Works Canada and Environment Canada, Vancouver. Unpublished report 883-578, p. 25.

McLean, David G., Michael Church, and Bruno Tassone (1999). "Sediment transport along lower Fraser River 1. Measurements and hydraulic computations". In: *Water Resources Research* 35.8, pp. 2533–2548. ISSN: 00431397. DOI: 10.1029/1999WR900101.

McLean, Stephen R. and J. Dungan Smith (1979). "Turbulence measurements in the boundary layer over a sand wave field". In: *Journal of Geophysical Research* 84.C12, p. 7791. ISSN: 0148-0227. DOI: 10.1029/JC084iC12p07791.

Morvan, Hervé et al. (2008). "The concept of roughness in fluvial hydraulics and its formulation in 1D, 2D and 3D numerical simulation models". In: *Journal of Hydraulic Research* 46.2, pp. 191–208. ISSN: 00221686. DOI: 10.1080/00221686.2008.9521855.

Murphy, Dan (2023). "Sediment Delivery and Bedform Variability of the Lower Fraser River and Delta". PhD thesis. Simon Fraser University.

Nelson, Andrew (2017). *Effect of Longterm Navigation Channel Lowering on Scour and Degradation Processes on Lower Fraser River*. Tech. rep. URL: https://www.researchgate.net/publication/323413777.

NHC (2008). *Fraser River hydraulic model update final report*. Tech. rep.

Paarlberg, Andries J. et al. (2010). "Modelling the effect of time-dependent river dune evolution on bed roughness and stage". In: *Earth Surface Processes and Landforms* 35.15, pp. 1854–1866. ISSN: 10969837. DOI: 10.1002/esp.2074.

Pawlowicz, Rich, Bob Beardsley, and Steve Lentz (2002). "Classical tidal harmonic analysis including error estimates in MATLAB using TDE". In: *Computers and Geosciences* 28.8, pp. 929–937. ISSN: 00983004. DOI: 10.1016/S0098-3004(02)00013-4.

Phillips, Jonathan D. (2022). "Geomorphology of the fluvial–estuarine transition zone, lower Neuse River, North Carolina". In: *Earth Surface Processes and Landforms* 47.8, pp. 2044–2061. ISSN: 10969837. DOI: 10.1002/esp.5362. URL: https://doi.org/10.1002/esp.5362.

Pretious, E.S. (1956). *Bed-load Measurement in the Main Arm Fraser River Estuary*. Tech. rep., Canada Department of Public Works. Fraser River Mo.

Pretious, E.S. and T. Blench (1951). *Final Report on Special Observations of Bed Movement in the Lower Fraser River at Ladner Reach during 1950 Freshet*. Tech. rep. Vancouver: Natl. Res. Counc. Can.

Prokocki, Eric W. et al. (2022). "The morphology of fluvial-tidal dunes: Lower Columbia River, Oregon/Washington, USA". In: *Earth Surface Processes and Landforms* 47.8, pp. 2079–2106. ISSN: 10969837. DOI: 10.1002/esp.5364.

Sassi, Maximiliano G et al. (2011). "Tidal impact on the division of river discharge over distributary channels in the Mahakam Delta". In: *Ocean Dynamics* 61.12, pp. 2211–2228. ISSN: 16167341. DOI: 10.1007/s10236-011-0473-9.

Silberman, E. et al. (1963). "Friction factors in open channels". In: *J. Hydraul. Eng.* 89.HY2, pp. 97–143.

Soulsby, R. (1997). *Dynamics of marine sands*.

Stewart, I and B Tassone (1989). *The Fraser River delta: a Review of Historic Sounding Charts*. Tech. rep. Environment Canada, Conservation and Protection, Vancouver, B.C, p. 39.

Van De Kreeke, J and K Robaczewska (1993). *Tide-induced residual transport of coarse sediment: application to the Ems estuary*. Tech. rep. 3, pp. 209–220.

Van Ormondt, Maarten, Kees Nederhoff, and Ap Van Dongeren (2020). "Delft Dashboard: A quick set-up tool for hydrodynamic models". In: *Journal of Hydroinformatics* 22.3, pp. 510–527. ISSN: 14651734. DOI: 10.2166/hydro.2020.092.

Van Rijn, L.C. (1984). "Sediment transport, part III: Bedforms". In: *Journal of Hydraulic Engineering* 110.12, pp. 1733–1754.

Venditti, J.G. et al. (2019). "Supply-limited bedform patterns and scaling downstream of a gravel–sand transition". In: *Sedimentology* 66.6, pp. 2538–2556. ISSN: 13653091. DOI: 10.1111/sed.12604.

Venditti, Jeremy G. (Nov. 2007). "Turbulent flow and drag over fixed two- and three-dimensional dunes". In: *Journal of Geophysical Research* 112.F4, F04008. ISSN: 0148-0227. DOI: 10.1029/2006JF000650.

Venditti, Jeremy G. and Ryan W. Bradley (Jan. 2022). "Bedforms in Sand Bed Rivers". In: *Treatise on Geomorphology*. Elsevier, pp. 222–254. ISBN: 9780128182352. DOI: 10.1016/B978-0-12-409548-9.12519-9.

Venditti, Jeremy G. and Michael Church (2014). "Morphology and controls on the position of a gravel- sand transition: Fraser River, British Columbia". In: pp. 300–316. DOI: 10.1002/2013JF002871.Received.

Venditti, Jeremy G., Micheal Church, and Sean J. Bennett (Nov. 2005). "On the transition between 2D and 3D dunes". In: *Sedimentology* 52.6, pp. 1343–1359. ISSN: 00370746. DOI: 10.1111/j.1365-3091.2005.00748.x.

Venditti, Jeremy G. et al. (2015). "The gravel-sand transition: Sediment dynamics in a diffuse extension". In: *Journal of Geophysical Research: Earth Surface*, pp. 300–316. DOI: 10.1002/2013JF002871.Received.

Vermeulen, B., M. G. Sassi, and A. J. F. Hoitink (2014a). "Improved flow velocity estimates frommoving-boat ADCP measurements". In: *Journal of the American Water Resources Association* 50. ISSN: 1093-474X. DOI: 10.1111/j.1752-1688.1969.tb04897.x.

Vermeulen, B. et al. (2014b). "Sharp bends associated with deep scours in a tropical river: The river Mahakam (East Kalimantan, Indonesia)". In: *Journal of Geophysical Research: Earth Surface* 119.7, pp. 1441–1454. ISSN: 21699011. DOI: 10.1002/2013JF002923.

Villard, P. V. and M. Church (2005). "Bar and dune development during a freshet: Fraser River Estuary, British Columbia, Canada". In: *Sedimentology* 52.4, pp. 737–756. ISSN: 00370746. DOI: 10.1111/j.1365-3091.2005.00721.x.

Warmink, J. J. et al. (2013). "Quantification of uncertainty in design water levels due to uncertain bed form roughness in the Dutch river Waal". In: *Hydrological Processes* 27.11, pp. 1646–1663. ISSN: 08856087. DOI: 10.1002/hyp.9319.

WCHL (1977). *Feasibility Study, Development of a Forty-Foot Draft Navigation Channel, New Westminster to Sandheads: Vancouver, Western Canada*. Tech. rep., Hydraulic Laboratories, p. 107.

Wright, N and A Crosato (2011). "The Hydrodynamics and Morphodynamics of Rivers". In: *Treatise on Water Science*. Vol. 2, pp. 135–156. ISBN: 9780444531933. DOI: 10.1016/B978-0-444-53199-5.00033-6.

Wu, Yongsheng et al. (2022). "Tidal propagation in the Lower Fraser River, British Columbia, Canada". In: *Estuarine, Coastal and Shelf Science* 264.November 2021, p. 107695. ISSN: 02727714. DOI: 10.1016/j.ecss.2021.107695. URL: https://doi.org/10.1016/j.ecss.2021.107695.

Yalin, M.S. (1964). "Geometrical Properties of Sand Wave". In: *Journal of Hydraulic Engineering* 90, pp. 105–119.

Zanke, U.C.E. (2003). "On the influence of turbulence on the initiation of sediment motion". In: *International Journal of Sediment Research* 18.1, pp. 17–31. ISSN: 00298018. DOI: 10.1016/0029-8018(79)90021-0.

Dune geometry and the associated hydraulic roughness at the transition from a fluvial to tidal regime at low river discharge

S.I. de Lange[1], R. Bradley[2,3], R.A. Schrijvershof [1], D. Murphy[3], K. Waldschläger[1], R. Kostaschuk[3], J.G. Venditti[3], A.J.F. Hoitink[1]

[1]Wageningen University, Department of Environmental Sciences, Hydrology and Quantitative Water Management, Wageningen, the Netherlands
[2]Northwest Hydraulic Consultants Ltd., North Vancouver, British Columbia, Canada
[3]School of Environmental Science, Simon Fraser University, Burnaby, British Columbia, Canada

Key Points:

- Hydraulic roughness in the fluvial-to-tidal transition zone can be predicted from dune geometry and agrees with calibrated model roughness.
- Variation in dune symmetry and leeside angle across a fluvial-to-tidal transition zone has little impact on reach-scale hydraulic roughness.
- Predicted spatial bedform patterns from modelled shear stress match measured bedform patterns, but absolute dune heights do not.

Corresponding author: Sjoukje de Lange, `sjoukje.delange@wur.nl`

Abstract

In deltas and estuaries throughout the world, a fluvial-to-tidal transition zone (FTTZ) exists where both the river discharge and the tidal motion drive the flow. It is unclear how bedform characteristics are impacted by changes in tidal flow strength, and how this is reflected in the hydraulic roughness. To understand bedform geometry and variability in the FTTZ and possible impacts on hydraulic roughness, we assess dune variability from multibeam bathymetric surveys, and we use a calibrated 2D hydrodynamic model (Delft3D-FM) of a sand-bedded lowland river (Fraser River, Canada). We focus on a period of low river discharge during which tidal impact is strong. We find that the fluvial-tidal to tidal regime change is not directly reflected in dune height, but local patterns of increasing and decreasing dune height are present. The calibrated model is able to predict local patterns of dune heights using tidally-averaged values of bed shear stress. However, the spatially variable dune morphology hampers local dune height predictions. The fluvial-to-tidal regime change is reflected in dune shape, where dunes have lower leeside angles and are more symmetrical in the tidal regime. Those tidal effects do not significantly impact the reach-scale roughness, and predicted dune roughness using dune height and length is similar to the dune roughness inferred from model calibration. Hydraulic model performance with a calibrated, constant roughness is not improved by implementing dune-derived bed roughness. Instead, large-scale river morphology may explain differences in model roughness and corresponding estimates from dune predictors.

Plain Language Summary

Where rivers meet the sea, the flow will be driven by tides from the sea and by river flow, resulting in a fluvial-to-tidal transition zone. The transition can be abrupt or gradual, which might influence the bed of the river, which is covered by bedforms (dunes and ripples). Bedform geometry is important in understanding the degree of friction in the river, which in turn determines water levels. It is unclear how bedform characteristics and the related friction are impacted by change in tidal flow strength. This study of the Fraser River in Canada used survey data of the river bed and a computer model of the river flow to study the geometry of dunes and the corresponding friction in this transitional region. We find that dune height and length vary considerably, but that it was unrelated to this regime change. Instead, only the dune leeside, i.e. the downstream facing side, was impacted. The difference in leeside angle before and after the regime change, did not result in a different friction produced by the dunes. Using the friction produced by dunes in the model, instead of a constant friction, does not improve model performance. Instead, large-scale river morphology determines roughness variations.

1 Introduction

Rivers debouching into a water body subject to tides have a fluvial-to-tidal transition zone (FTTZ). The FTTZ can be defined as the part of the river that is fully dominated by fluvial processes at its upstream end, and dominated by tidal and coastal processes at the downstream boundary (Phillips, 2022). The transition from fluvial to tidal can be gradual, but is often impacted by processes that modify the character of this transition by altering the channel bathymetry and adding friction (Godin, 1999; Horrevoets et al., 2004), such as an irregular underlying channel geology, bifurcations or confluences (Kästner et al., 2017), or dredging works (Gisen and Savenije, 2015). These changes can cause the gradual transition to become more abrupt, and a sudden change in tidal flow strength can lead to a change in hydraulic regime from a more fluvial to a more tidally dominated system. It is unclear how bedforms and their corresponding roughness respond to a change in hydraulic regime, while dune geometry and roughness prediction is essential for river management (ASCE Task Force, 2002; Best, 2005; Warmink et al., 2013), interpreting sedimentary rock records (Das et al., 2022), and understanding sediment fluxes (Venditti and Bradley, 2022).

Bedforms adjust to changes in the hydraulic regime, but not in a consistent manner. Until recently, it was often assumed that any spatial variability in dune geometry was caused by dunes that are not in equilibrium (Carling et al., 2000; Bridge, 2003; Holmes and Garcia, 2008), and the primary geometry (dune height and length) of equilibrium dunes was assumed to scale with water depth (Yalin, 1964). However, recent research has shown significant local spatial variation in dune height (Bradley and Venditti, 2017; Murphy, 2023; Venditti and Bradley, 2022) in riverine systems, independent of the water depth. In the FTTZ, this variability is expected to be even more pronounced, since tidally-influenced currents impose spatially-varying water level fluctuations (and therefore bed shear stress changes) on diurnal and semi-diurnal time scales (Sassi et al., 2011; Hoitink et al., 2003). The resulting spatial longitudinal variability of dune geometry in the FTTZ is understudied, but two key studies exist.

Prokocki et al. (2022) studied dunes in the lower 90 km of the Lower Columbia River (USA), and recognized differences in shape and 3D planform of dune geometry across the study reach. They related the changing dune morphology to downstream variations in grain size and spatiotemporal changes in tidal and fluvial flow. In the thalweg, they observed small-scale upstream-oriented dunes downstream, and larger scale downstream-oriented dunes upstream. Unfortunately, they did not report on flow conditions in those distinct regions, or on the resulting hydraulic roughness differences. Lefebvre et al. (2021) studied 4-year long bathymetric data of the downstream 160 km of the Weser Estuary in Germany. They did not observe a clear trend in dune geometry in the longitudinal direction, but found dunes that are generally smaller than predicted based on the water depth. They did not provide information on the flow conditions or resulting roughness. Beyond these recent studies, the response of dune geometry in the FTTZ to shear-stress variation at the change from a fluvial to tidal regime is unknown, and it is uncertain if dune geometry predictors apply here.

To date, it remains unclear to what extent variability in dune geometry is relevant for the large-scale roughness needed to model the FTTZ. Bedforms, especially dunes, are known to be a major source of roughness in lowland rivers (Gates and Al-Zahrani, 1996; Julien et al., 2002), and dune variability can impact roughness parametrizations. When modelling the FTTZ hydraulically, a roughness value must be chosen. Roughness is often represented by a single constant coefficient (Paarlberg et al., 2010), found by calibration, and is therefore a conceptualized and simplified representation of the physical process. To better include spatial variation in roughness in the FTTZ, De Brye et al. (2011) used a linearly decreasing roughness coefficient from a delta apex to the coast, to include the gradual transition from the riverine to the marine environment. However, proof for the validity of this approach is lacking. There is a need to improve hydraulic roughness parametrization in the FTTZ, since the output of hydrodynamic models strongly depends on an accurate specification of roughness (Lesser et al., 2004; Morvan et al., 2008; Wright and Crosato, 2011).

In this research, we aim to increase understanding of bedform variability and related roughness that occurs at the transition from a shallow mixed tidal-fluvial regime to a tidal regime. To do so, we assess the bedform characteristics and the resulting hydraulic roughness of the FTTZ of the Lower Fraser River. The lower Fraser River is a sand-bedded lowland river in British Columbia, Canada, with a significant decrease in tidal energy 40 kilometer landward of the river mouth (Wu et al., 2022). We aim to answer three research questions. 1) How are bedform characteristics impacted by the sudden change in tidal flow strength? 2) How can dune variability in the fluvial-to-tidal transition zone be explained and predicted? 3) To what extent does dune geometry and variability exert an impact on reach-scale hydraulic roughness, and which other factors can play a role in determining this bed roughness? Bathymetric field data from base flow conditions were used, allowing us to focus on the impact of the tides, which penetrate further upstream during base flow. A 2D hydrodynamic model is created to assess hydraulic roughness, and to explore the impacts of spatial variation in river and tidal flow.

2 Field site

The Fraser River (Figure 1) is located in British Columbia, Canada, and drains 228,000 km^2 of mountainous terrain. The Fraser exits a series of bedrock canyons approximately 185 km upstream of the river mouth at Sandheads, where it enters the gently-sloping Fraser Valley, past the towns of Hope (river kilometer (RK) 165) and Mission (RK 85). The Fraser River has an annual river discharge of 3,410 m^3 s^{-1} at Mission (Water Survey of Canada (WSC) Station 08MH024), but flow rates vary between a mean low discharge of 1,000 m^3 s^{-1} in winter time (November - April) and a mean high discharge of 9,790 m^3 s^{-1} during the snow melt-dominated freshet in May, June and early July (Attard et al., 2014; McLean et al., 1999). At New Westminster, 34 km upstream from the river mouth, the river bifurcates, forming the Fraser Delta where the Main Channel splits into two tributaries: the North Arm and the Main Channel. The Main Channel carries 88% of the flow, until it bifurcates into Canoe Pass (RK 13), which conveys approximately 18% of the total flow (Dashtgard et al., 2012; WCHL, 1977; NHC, 2008). The fluvial-to-tidal transition zone of the river is influenced by a predominantly semi-diurnal tide (Wu et al., 2022), with a mean tidal range at the mouth of approximately 3 m (Kostaschuk and Atwood, 1990). The tidal motion influences water levels up to Mission during high flow, but can penetrate up to Chilliwack (RK 120) during low flow creating a strong backwater effect (Kostaschuk and Atwood, 1990). It is an undammed, unregulated flow, which reflects climatic conditions. Human-made influences include dikes (90% of the reach), pipelines and bridge constructions, and dredging of the Main Channel occurs.

The Port of Vancouver dredges from the river mouth (RK 0) to the Port Mann Pumping Station (RK 42), with the most significant dredging in the deltaic reach from RK 35 to the river mouth (Nelson, 2017) to maintain a constant fairway depth (McLean and Tassone, 1989; Stewart and Tassone, 1989). The depth is larger in the tidal region, and has been made deeper by dredging. This results in a large decrease in momentum flux (Wu et al., 2022) at the upstream limit of the dredging works. Additionally, Wu et al. (2022) related this decrease in momentum flux to the influence of the Pitt River. They identified the junction of the Pitt River as the transition from a tidally-dominated to a river-dominated regime, and they noted the importance of this system for tidal attenuation. Therefore, two different regimes can be identified in the study area. The first regime, hereafter called the tidally-dominated regime, is characterized by a strong influence of tides and a large tidally-averaged water depth, and occurs seaward of RK 40. The second regime is the mixed tidal-fluvial regime, in which tides are less strong and the water depth is shallower, which occurs landward of RK 40. This roughly coincides with the upstream end of the modern Fraser Delta (RK 35) (Venditti et al., 2015; Venditti and Church, 2014), where the Fraser River bifurcates into the North Arm and the Main Channel.

The difference in tidal strength in the two regimes does not impact grain sizes of bed sediments in the thalweg. The main transition of grain size characteristics occurs around RK 100. Upstream of RK 100, the bed of the Fraser River consists of gravel, and downstream of a gravel-sand-transition near Mission, the main bed material is sand (Venditti and Church, 2014) (median grain size (D_{50}) 351 μm, mean 415 μm; Figure 2). There is a minor trend of downstream fining in the thalweg of the lower 50 km of the river, (1.14 μm per kilometer, Figure 5c), resulting on average in a decrease in D_{50} of approximately 100 μm over this reach, although there is a lot of scatter which can be related to gravel and mud deposits along the banks. The data underlying this figure is a compilation of multiple sources. The samples up until RK 48.5 were collected by McLaren and Ren (1995), who sampled bed material in the Main Channel and delta front at 0.5 km increments with a Shipek sampler. Although this grain size data is decades old, broad patterns are likely to be consistent with present conditions (Venditti and Church, 2014), and grain size shows little seasonal or year-to-year variation (Kostaschuk et al., 1989; McLean et al., 1999; Pretious, 1956). Venditti and Church (2014) measured 33 samples of RK 48.5 - 80, with a dredge sample in 2009, and Murphy (2023) collected 115 additional samples in this same reach using a pipe dredge.

They did not perform analysis on the fraction smaller than 63 μm. The Pitt system does not impact the sediment composition of the Fraser, since the net bedload transport is directed upstream toward Pitt lake (Ashley, 1980). In the delta, the river deposits its sand load in the channel and its banks, and its silt load on the distal margins and tidal flats (Venditti and Church, 2014) (Figure 2a, c, d). Seaward of the river mouth, the grain size decreases dramatically to a D_{50} of 22 μm. Locally, the river interacts with its bank and bed substrate. Gravel and clay patches are present at the outer banks on the north and south sides of the river. These patches are either modern deposits, such as gravel bars, or older Pleistocene glacial deposits (fine outwash deposits and coarse glacial till) (Nelson, 2017) (Supplementary Figures S1), constraining the river's course.

This study focuses on the Main Channel of the Fraser River, from the confined part of delta mouth at Steveston Harbor at RK 10, to Mission at RK 85 (Figure 1). The area is located in the FTTZ, and low-angled dunes (Bradley et al., 2013; Kostaschuk and Best, 2005; Kostaschuk and Villard, 1996), with no or intermittent flow separation, cover the river bed. When assessing local scale processes, we focus on three zones in the FTTZ (Figure 2, and Supplementary Figure S7).The zones are located at RK 21.5-23 (zone 1; tidal regime), 50-52.5 (zone 2; fluvial-tidal regime) and 57-59.5 (zone 3; fluvial-tidal regime). The selection of zones is based on three criteria. Firstly, a decreasing amount of tidal energy from zone 1 to 3. Secondly, a simple geometry, without bifurcations or confluences, to limit the influence of complex currents on dune geometry. Thirdly, a limited amount of human influence on the river bed. Zone 1 is 1 km shorter than the other zones due to dredging along the downstream side and an engineering structure on the upstream side.

3 Methods

3.1 Hydraulic model setup

A 2DH (two dimensional horizontal) hydraulic model was set up in the Delft3D Flexible Mesh (FM) model suite (Kernkamp et al., 2011). The model simulates depth-averaged flow quantities based on the two-dimensional shallow water equations. The numerical domain covers the Fraser River from river kilometer 85, to the offshore region of the Strait of Georgia reaches where depth exceeds >200 m. Bathymetry for the Main Channel is interpolated on an unstructured curvilinear grid with a median cell size of 30 m, and varies between 5 m in the river and 1000 m offshore. The bathymetry of the model of Wu et al. (2022) was taken as a basis, and the higher resolution MBES data described above were used for the bathymetry of the channels in the estuary. Bars that do not get submerged during an average yearly freshet (flood) were not well-represented in the bathymetry data, and its elevation in the model was manually increased till 10 m above mean sea level to prevent flooding.

The main imposed upstream boundary condition is the discharge at Mission (RK 85) for the time period of November 2017 till October 2018. The discharge at Mission is estimated using a rating curve if the discharge exceeds 5,000 m^3 s^{-1}. At lower discharge conditions, tidal influences make the rating curve at Mission inaccurate, and therefore the discharge was calculated using the discharge at Hope (RK 165) and two smaller tributaries (Chilliwack River and Harrison River). Using this calculation method, discharges measured at Mission (larger than 5,000 m^3 s^{-1}), were on average underestimated by 3%, and no significant temporal delay was observed. Additionally, at two downstream confluences, a constant discharge of 315 m^3 s^{-1} at Stave River (RK 74) and 130 m^3 s^{-1} at Pitt River (RK 45) were added to the Fraser flow. Stave River is dammed at 3 km upstream, therefore having a controlled flow. The Pitt River drains a lake and has therefore a nearly constant outflow. At the downstream boundary, water levels influenced by tides are imposed. Eight primary tidal constituents, the most important overtide (M4) and compound tides are determined via the Delft Dashboard toolbox (Van Ormondt et al., 2020), using the TPXO8.0 database (Egbert and Erofeeva, 2002).

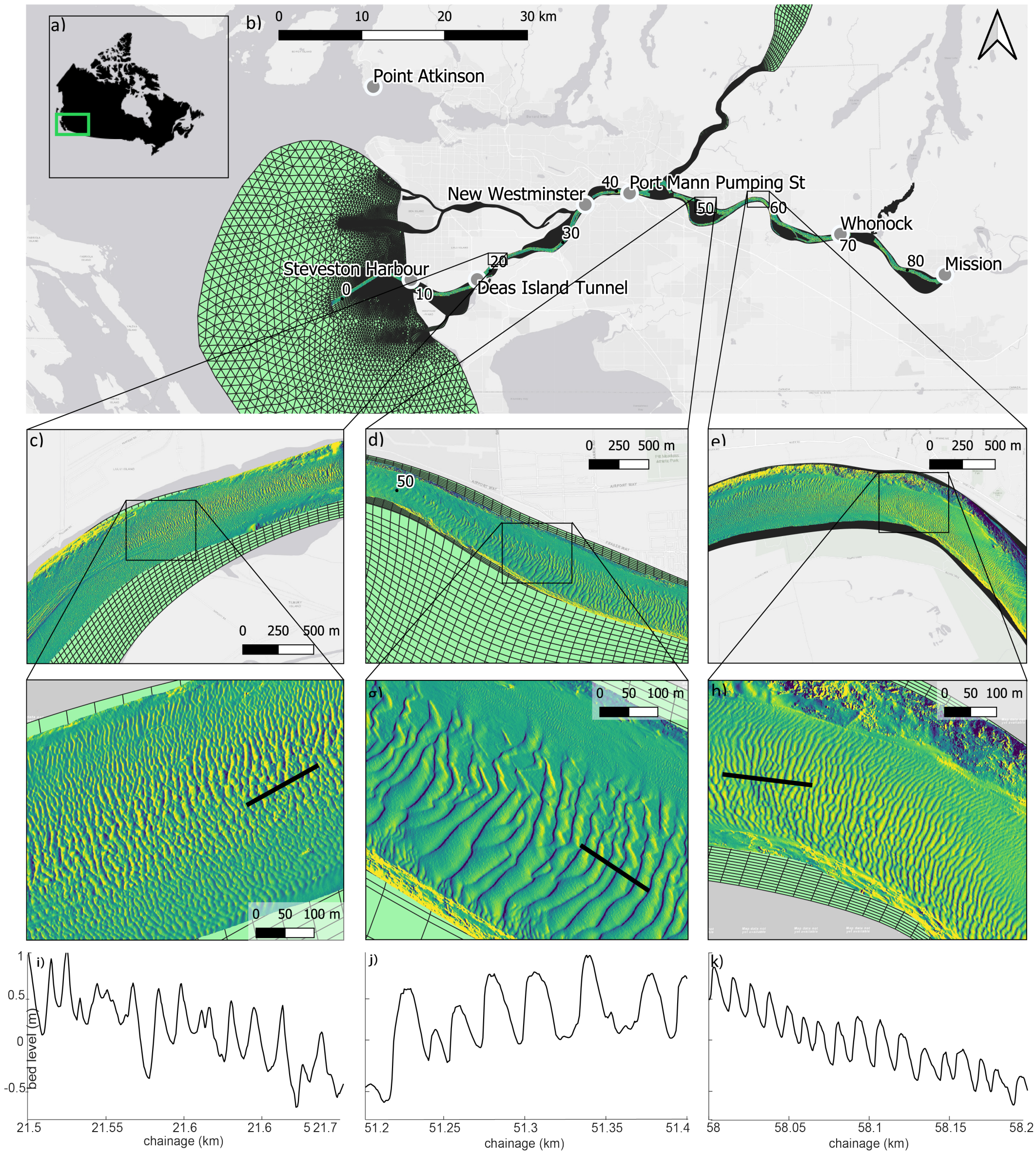

Figure 1. Study area of the Fraser River in British Columbia, Canada (a). b) The Fraser River from river kilometer 10 (Steveston Harbor) to 85 (Mission). Green shaded area indicates the model domain. Grey markers indicate gauging stations. c-e) three focus zones examined in this study, f-h) example zoom ins of the dune fields. i-k) example profiles of the dune fields.

The amplitudes and phases at the downstream boundary were corrected to minimize the error in the model-data comparison at the Point Atkinson tidal gauging station. This correction was on average 0.8% of the tidal amplitude and 20° for the tidal phases, for the 13 tidal components. The model was calibrated for low discharge (<1600 $m^3\ s^{-1}$; Figure 3b), to simulate flow conditions that correspond to the low-discharge bathymetry. The calibration was performed by varying the Manning's roughness coefficients and evaluating the resulting water levels and tidal amplitudes of the three most important tidal constituents at 7 gauging stations (RK 0, 9, 18.5, 35, 42, 70, 85) (Figure 2). The principal tidal constituent M_2 is used for calibration, together with M_4 and K_1. Relative phase differences between M_2 and M_4 (the first overtide of M_2) influence tidal duration asymmetry, the main mechanism for

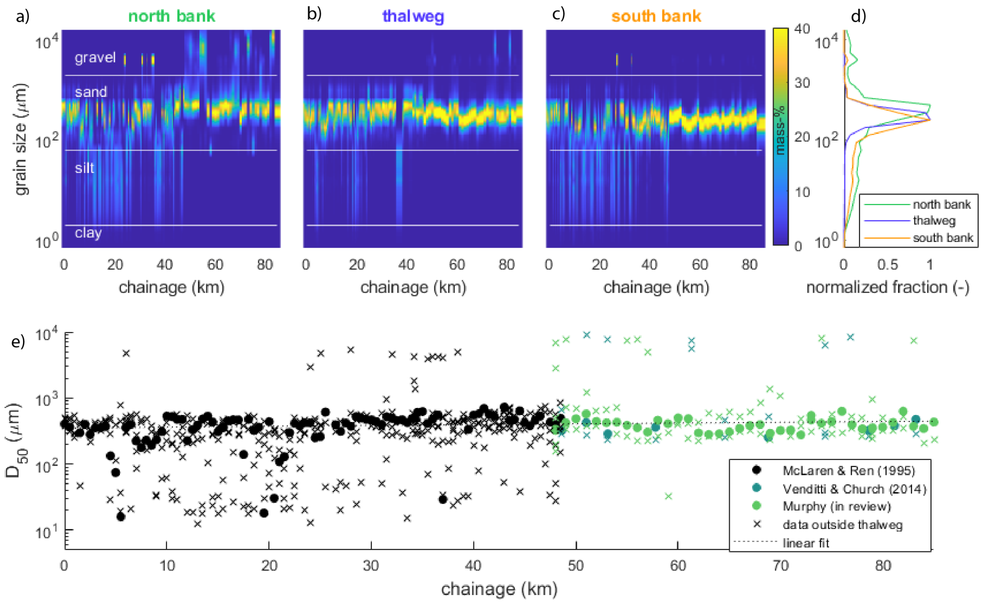

Figure 2. Grain size distributions of bed sediment in the Fraser River. a, b, c) grain size distribution along the north bank, thalweg and south bank. d) cumulative distribution at the north bank, thalweg and south bank. e) median grain size (D_{50}) in and outside of the thalweg. Markers differentiate between samples taken in the thalweg (solid marker) or outside along the river banks (indicated with 'x'). The data is from a data compilation by Venditti and Church (2014), which includes reanalyzed observations from McLaren and Ren (1995), and recent observations by Murphy (2023).

driving residual bed-load transport in estuaries (Van De Kreeke and Robaczewska, 1993). The diurnal tide K_1 is relatively large at the west coast of North America, and interaction between diurnal and semi-diurnal frequencies can produce asymmetric tides as well (Hoitink et al., 2003).

The tidal amplitudes were derived from harmonic analysis using t_tide (Pawlowicz et al., 2002). The best performing model had a uniform Manning's coefficient (roughness) of 0.026 s m$^{-1/3}$ (Figure 3). Disconnecting the hydraulic roughness at the regime transition at RK 40, thereby allowing for two different roughness values, did not improve the calibration (Supplementary materials Figure S3a). The uniform Manning's coefficient (roughness) of 0.026 s m$^{-1/3}$ is slightly higher than the calibrated Manning's coefficient of Wu et al. (2022), who used a uniform roughness of 0.015 s m$^{-1/3}$. The difference in roughness value is attributed to the difference in grid resolution. Our model grid in the river domain is overall coarser than the model of Wu et al. (2022) who used a 10 m resolution, so that the schematization of the bathymetric data on our grid results into slightly wider channels. Our value for roughness is considered to be more appropriate for natural sand-bedded rivers (Chow, 1959).

3.2 Field data and preprocessing

Raw multibeam echosounder (MBES) riverbed data were provided by the Public Works and Government Services, Canada. The measured bathymetry comprises data of the Main Channel between river kilometer -1 to 85 and covers the navigation, but does not provide full bank-to-bank spatial coverage. Data were collected during base flow conditions in January,

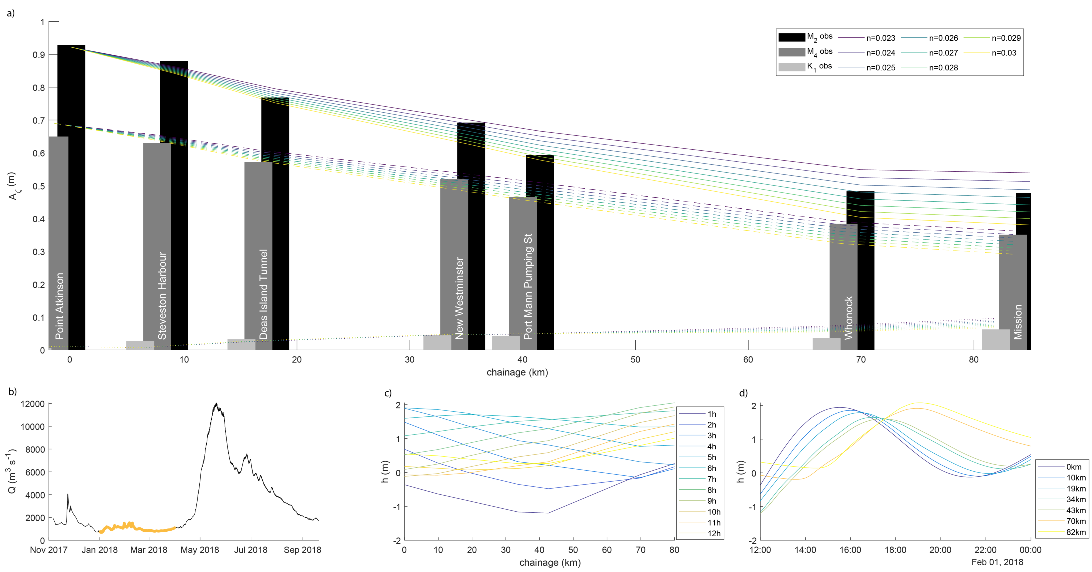

Figure 3. a) Calibration of the model with uniform roughness. The observed tidal amplitude of the tidal constituents M2 (black bars), K1 (dark grey bars), and M4 (light grey bars), and the corresponding modelled tidal amplitudes are indicated. b) Discharge at Mission. Highlighted part of the discharge curve indicates the timeframe of MBES data collection. c) Modelled water surface slope over time, simulated with the model with n_{man} = 0.026 s $m^{-1/3}$. d) Modelled propagation of the tidal wave per station, simulated with the model with n_{man} = 0.026 s $m^{-1/3}$.

February and March of 2021. This period is characterized by relatively constant discharge and little change to the bed surface (Bradley and Venditti, 2021). During the survey period, the measured discharge (at an hourly interval) was relatively constant, with monthly mean values of 1416 m^3 s^{-1} (SD 184 m^3 s^{-1}), 1051 m^3 s^{-1} (SD 140 m^3 s^{-1}) and 1074 m^3 s^{-1} (SD 35 m^3 s^{-1}) at Hope (RK 165) for the three months, respectively (Water Survey of Canada, Station 08MF005).

The MBES data is gridded onto a 1x1 m^2 grid, and the resulting MBES datasets contain x, y and z coordinates. Next, all bed level data is converted from Cartesian (x, y) coordinates to curvilinear coordinates (s, n) with the same spatial resolution (Vermeulen et al., 2014a). Herein, s is the longitudinal direction, parallel to the river, and corresponds with river kilometers (RK) and n is the cross-sectional direction, wherein n = 0 m is defined as the central river axis, which roughly coincides with the thalweg.

3.3 Data analysis

3.3.1 Analysis of river bathymetry: dune detection

Bathymetry was analyzed to derive dune characteristics. Three longitudinal profiles were taken, along the centerline and at approximately 80 m from the north and south bank. In three focus areas (Figure 1), a longitudinal profile was taken every 10 meters, resulting in 27, 41, 23 profiles for zones 1, 2 and 3 respectively, depending on the river width. To ensure that bedforms in all profiles were primarily caused by natural mobile bed conditions, we excluded bathymetry that showed extensive scour, human-made structures and dredging marks (Figure Supplementary Figures S2).

From the filtered profiles, bedform characteristics were determined by using a standard Bedform Tracking Tool (Mark et al., 2008). In the tool, the default filter span (c = 1/6) was suitable to filter out small features such as measurement errors or outliers. Three span values (P0), corresponding with bedforms with a length of 20 m ±10, 50 m ±20 and 100 m ±30, were used as input to detrend and smooth the profile. The span values in the tool are based on a spectral analysis yielding the dominant bedform wave lengths in each section.

Based on the detrended and smoothed profile, a zero-crossings profile was defined, based on which individual dunes were identified, and dune characteristics were calculated. Dune characteristics include dune height Δ (m), the vertical distance between the crest and downstream trough, dune length λ (m), the horizontal distance between two subsequent crests, leeside angle LSA (°), the slope from a linear fit of the dune's leeside, excluding the upper and lower 1/6 of the dune height, and the stoss side angle SSA (°) calculated in the same maner as the leeside angle. The bedform slipface angle SFA (°), the steepest part of the leeside angle, and is defined as the 95-percentile of the leeside angle. Finally, bedform asymmetry is calculated as the ratio between the length of the (seaward) leeside and the total bedform length (Lefebvre et al., 2021).

Bedforms with heights smaller than 0.1 m are not distinguishable from the error of the survey, and are excluded from the analysis. Bedform lengths smaller than 3 m are excluded as well, since the resolution of the bathymetric data (1 m) is too small to detect small bedform features. Features with a height greater than 2.5 m (2% of all detected bedforms) or a length greater than 200 m (0.08% of all detected bedforms) are considered another type of bed fluctuation unrelated to dunes such as scour holes or wake deposits downstream of human-made structures. These had a different geometry than mobile dunes, which was confirmed by visual inspection of the batymetric data. Large dunes (>2.5 m) as found in previous studies (Kostaschuk and Luternauer, 1989; Venditti et al., 2019; Pretious and Blench, 1951) were not observed in the low-discharge bathymetry used in this study.

3.3.2 Analysis of river geometry

River geometry was parametrized by river width, curvature, transverse bed slope and excess depth. River width W (m) was determined from a polygon following the longitudinal low water line, which is considered to be the discharge carrying section of the river under low discharge conditions. Cross-sectional area A (m^2) was subsequently approximated from the tidally-averaged water depth and river width, assuming a trapezoidal shape of the cross-sectional area, where the river bank has a 60° slope. Curvature r (km^{-1}) was defined as the inverse of bend radius following the approach of de Ruijsscher et al. (2020). Local transverse bed slope ξ (-) was defined as the slope between the two sides of the main river channel, longitudinally discretized at intervals of 100 m. Finally, an excess depth parameter D_e (-) was used as a measure to identify pools and scour holes (Vermeulen et al., 2014b), and was defined as:

$$D_e = \text{sign}(r)\left(\frac{D_{max}}{D_r} - 1\right) \tag{1}$$

where D_r is the regional mean depth of a discretized section of 500 m long, and D_{max} the local maximum depth in this section. Sign indicates the signum function, which returns the sign of a real number.

3.3.3 Analysis of river hydrodynamics

To assess local flow conditions and tidal attenuation, the hydrodynamic model was evaluated during low flow conditions in March 2018 (Figure 3b). The flow magnitude and direction, water depth and bed shear stress magnitude and direction per grid cell were saved every ten minutes in the simulation. The calculation of bed shear stresses in Delft3D is based on a logarithmic approximation of the near bed velocity and is explicitly solved. All output data were tidally-averaged using a Godin filter (Godin, 1972). The Godin filter removes the tidal and higher frequency variance to obtain a low-passed signal primarily caused by the river flow.

Besides transforming the data into along and across-channel coordinates (s,n) (Vermeulen et al., 2014a), the flow and shear stress vectors were rotated, to transform their orientation to along-channel direction (s-direction). This allowed differentiation between the in- and outgoing currents, which are in -s and s-direction, respectively. The percentage of time that the flow reverses and flows upstream (reversal time t_{rev} (%) was then calculated.

3.3.4 Dune geometry prediction

Flow data from the model was used to predict dune height Δ (m), using dune height predictors that include some measure of flow strength (Van Rijn, 1984; Yalin, 1964; Karim, 1995; Venditti and Bradley, 2022). Firstly, dune height was predicted using the widely applied dune geometry predictor of Van Rijn (1984). This predictor is based on 84 laboratory experiments, with grain sizes ranging from 190 - 2300 μm, and 22 field data sets (490 - 3600 μm) of relatively wide rivers (width / depth > 0.3) with unidirectional flow. This corresponds well with conditions found in the Fraser River, except that the Fraser experiences bidirectional currents. To account for this, values of water height and shear stress are tidally averaged, since bed-material sediment transport in the Lower Fraser River generally follows the pattern of mean velocity over the tidal cycle (Kostaschuk and Best, 2005). The tidal averaging is described in section 3.3.3. Dune height is thus:

$$\Delta_{vRijn} = 0.11h\left(\frac{D_{50}}{h}\right)^{0.3}(1 - e^{-0.5T})(25 - T) \tag{2}$$

in which D_{50} is median grain size (m), h is the water dept (m) and transport stage T is:

$$T = \frac{(u^*)^2 - (u_c^*)^2}{(u_c^*)^2} \tag{3}$$

where u^* is the shear velocity (m s^{-1}), and u_c^* is the critical shear velocity (m s^{-1}). Shear stress (τ, N m^{-2}) relates to shear velocity and can be expressed non-dimentionally as the Shields number (θ) as in:

$$\tau = u^{*2} * \rho_w \tag{4}$$

$$\theta = \frac{\tau}{(\rho_s - \rho_w) g D_{50}} \tag{5}$$

in which g is the gravitational acceleration (9.81 m s^{-2}), ρ_s is the sediment density (2,650 kg m^{-3} for quartz) and ρ_w is the water density (1,000 kg m^{-3} for fresh water). Therefore, equation 3 can be rewritten as:

$$T = \frac{\tau - \tau_c}{\tau_c} = \frac{\theta - \theta_c}{\theta_c} \tag{6}$$

When 50 μm $< D_{50} <$ 5,000 μm, the critical shields number θ_c (-) can be approximated as (Zanke, 2003). The resulting values of θ_c are approximately 0.03 (medium sand).

$$\theta_c = 0.145 Re_p^{-0.333} + 0.045 * 10^{-1100 Re_p^{-1.5}} \tag{7}$$

in which the particle Reynolds number Re$_p$ is:

$$Re_p = D_{50}^{3/2} \frac{\sqrt{Rg}}{\nu} \tag{8}$$

where the relative submerged density R = $(\rho_s - \rho_w)/\rho_w$ (-) and ν is the kinematic viscosity (m^2 s^{-1}), which is slightly dependent on water temperature as $\nu = 4 * 10^{-5}/(20 + t)$ in which t = temperature (°C). Here, ν = 1.3 * 10^{-6} is used for 10 °C.

We also predict dune height using the predictor of Yalin (1964):

$$\Delta_{Yalin} = \frac{h}{6} \left(1 - \frac{\tau_c}{\tau}\right) \tag{9}$$

The predictor of Karim (1995) builds on that of Van Rijn (1984) and Allen (1978), and is based on the suspension criterion which utilizes the shear velocity and the particle fall velocity (w$_s$). The predictor of Allen (1978) is not included in this research, since it is mostly based on laboratory experiments.

$$\Delta_{Karim} = h \left(0.04 + 0.294(\frac{u^*}{w_s}) + 0.00316(\frac{u^*}{w_s})^2 - 0.0319(\frac{u^*}{w_s})^3 + 0.00272(\frac{u^*}{w_s})^4\right) \tag{10}$$

where w$_s$ can be defined as (Ferguson and Church, 2004):

$$w_s = \frac{RgD_{50}^2}{C_1 \nu + (0.75 C_2 R g D_{50}^3)^{0.5}} \tag{11}$$

in which C_1 and C_2 are constants with values of 18 and 1.0, respectively, for slightly irregular particles.

Finally, we test the equation of Venditti and Bradley (2022).

$$\Delta_{VB} = h\left(10^{\left(-0.397(log\frac{\theta}{\theta_c}-1.14)^2-0.503\right)}\right) \quad (12)$$

3.3.5 Hydraulic roughness estimation

To estimate the impact of dunes on the water levels in the study reach, the hydraulic roughness was determined. The total predicted hydraulic roughness, expressed as a friction factor $\hat{f}$, results from form friction and grain friction (Einstein, 1950). Assuming dunes are the dominant structures causing form resistance, the total hydraulic roughness was predicted as in Van Rijn (1984):

$$\hat{f} = \frac{8g}{(18\log(\frac{12d}{k_s}))^2} \quad (13)$$

Herein, k_s consists of form roughness height k_{sf} and grain roughness height k_{sg}:

$$k_s = k_{sg} + k_{sf} \quad (14)$$

$$k_{sg} = 3D_{90} \quad (15)$$

where D_{90} is the 90$^{\text{th}}$ percentile of the grain size distribution, and

$$k_{sf} = 1.1\gamma_d\Delta(1-e^{\frac{-25\Delta}{\lambda}}) \quad (16)$$

where the calibration constant γ_d is taken as 0.7 in field conditions (Van Rijn, 1984).

In the modelling suite of Delft3D, roughness values of Manning's n, n_{man} (s $m^{-1/3}$), are converted to a Chézy coefficient C ($m^{1/2}s^{-1}$) via (Manning, 1891):

$$C = \frac{R_h^{1/6}}{n_{man}} \quad (17)$$

in which R_h is the hydraulic radius, which can be simplified to the water depth h (m) for rivers that satisfy W $\gg$ h.

The Chézy coefficient is converted to the dimensionless Darcy-Weisbach friction factor f_m according to Silberman et al. (1963):

$$f_m = \frac{8g}{C^2} \quad (18)$$

4 Results

4.1 Hydraulics and morphology of the fluvial-to-tidal transition zone

The tidally-averaged water depth in the study area fluctuates between 3 and 18 m (Figure 4a). In the mixed-fluvial tidal regime of the river (RK > 40), it increases gradually in seaward direction, and in the tidal regime (RK < 40) it remains constant. The local increase in water depth is reflected in the tidally averaged and instantaneous shear stress profiles (Figure 4b). The downstream-directed maximum shear stress increases from 0.4 N m^{-2} in the upstream area to 10 N m^{-2} at the river mouth. Similarly, the upstream-directed maximum shear stress in relation to flow reversal (indicated by a minus sign in Figure 4c) increases to 6 N m^{-2}. In contrast, the tidally-averaged shear stresses remain relatively constant over distance (fitting a linear model gives a slope of 10^{-5} N m^{-2} km^{-1}). The tidally averaged shear stress is on average 0.64 N m^{-2} and fluctuates between -1.0 N m^{-2} (indicating an upstream directed shear stress at the most downstream area, RK 0) and 2.2 N m^{-2} (at RK 67).

The tidal effect on the water levels and flow direction weakens in the upstream direction, and the amplitude of the tidal constituents M_2 and K_1 decreases as the tides attenuate (Figure 4d). The M_2 tidal constituent shows a particularly strong decrease from RK 10 to 40, while landwards the tidal attenuation is minimal. In the most upstream reach, bidirectional currents can still be observed (Figure 4c). During low flow conditions, upstream (flood) flow occurs for 45% of the time at the river mouth (about RK 10), and decreases to 25% at the most upstream location of the study reach.

The morphology of the Fraser River does not show consistent trends in the stream-wise direction. The river width fluctuates between 500 and 1100 m (Figure 5a). The cross-sectional area of the river remains relatively constant in the more upstream part of the river (RK > 40), since river depth varies inversely with river width. The more downstream part experiences larger fluctuations in cross-sectional area, since water depth remains relatively constant (Figure 5a). The bed level (Figure 5b) shows large variations, but remains relatively constant in the downstream part. River curvature, transverse bed slope and depth excess are strongly related (R^2 = 0.15 - 0.61, $p < 0.005$, Figure 5c), which reflects the low-sinuosity meandering morphology.

4.2 Morphological response of dunes to tidal hydraulics

Dune geometry in the study reach varies considerably (Figure 6), with dune heights up to 2.4 m (mean: 0.46, median: 0.39 m, SD: 0.28 m) and dune lengths up to 194 m (mean: 24 m, median: 16, SD: 22 m). Multiple scales of superimposed bedforms co-exist, although most of the bed is covered by only primary dunes. Patterns in dune geometry are apparent, with some areas of relatively low and short dunes, and others with increasing or decreasing dune heights and lengths. For example, the thalweg has large dunes around RK 68, 77 and 85, with increasing and decreasing dune heights upstream and downstream of those local maxima. Such patterns are not consistent over whole river width however, and where relatively large dunes prevail on one part of the river (e.g. north side), dunes can be small on the other parts (see for example around RK 68). This variation in dune height and length, along the cross-section and longitudinally, is expressed as the standard deviation of all dunes present in one unit of channel width. This allows for comparison between longitudinal and cross-sectional variability. The mean standard deviation in dune height and dune length in cross-sectional direction (0.20 m and 13.0 m, respectively) is twice as high as the variation along the longitudinal direction (on average 0.11 m and 6.8 m, respectively) (Figure 6).

Local patterns in dune height and length are difficult to explain, and do not reflect the regime change around RK 40 or trends in grain size in the thalweg. However, visual inspection reveals dune occurrence is primarily determined by grain size along the outer banks – when the grain size is too large (gravel) or too small (clay), dunes will be absent (Supplementary Figure S2e and f). When the river cuts into a clay or gravel layer on the north or south sides of the channel, abrupt changes in dune geometry can result.

The gradual increase in strength and duration of tidal currents in the seaward direction influences dune shape. Firstly, the dune crests become sharper (Figure 1 i-k). Secondly, the leeside and slipface angle of the dunes decrease in downstream direction (Figure 7a, b). In particular the slipface angle decreases faster in the tidal regime than in the fluvial-tidal regime. Since the stoss side angle remains relatively constant (with a slight increase in the tidal regime), dunes become more symmetrical in seaward direction (Figure 7c). When the asymmetry is equal to 0.5, dunes are perfectly symmetric. This is possible at nearly every

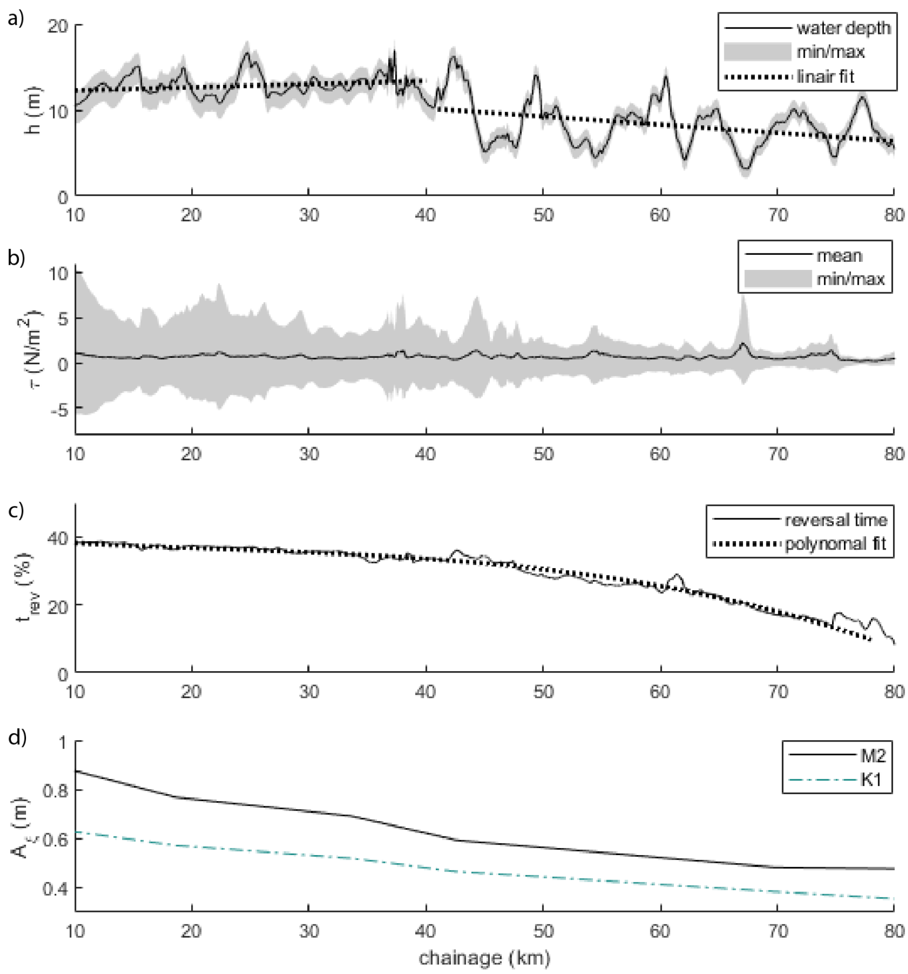

Figure 4. Hydraulic characteristics of the Lower Fraser River. a) water depth (h), b) tidally-averaged, maximum and minimum shear stress (τ), c) reversal time (t_{rev}), d) tidal amplitude (A_{ξ}) of the M_2 and K_1 tide.

location up to a distance of 75 km from the river mouth, and becomes consistent at around 40 km from the river mouth, indicating the impact of the regime change. Results from a two-paired student t-test shows that the leeside angle, slip face angle and asymmetry is significantly different (at a 95% confidence level) in the tidal and the fluvial-tidal regime, while stoss side angle is not. The leeside angle directly correlates with flow-reversal time (Figure 7d) and maximum shear stress (Figure 7e), showing lower leeside angles and more symmetric dunes in seaward direction, however large variation is observed.

4.3 Dune geometry prediction from model output

Dune height predictors whre applied to the FTTZ of the Fraer River at both small and large scales. The models were not specifically developed for tidal rivers with bidirectional currents, so input values were tidally-averaged.

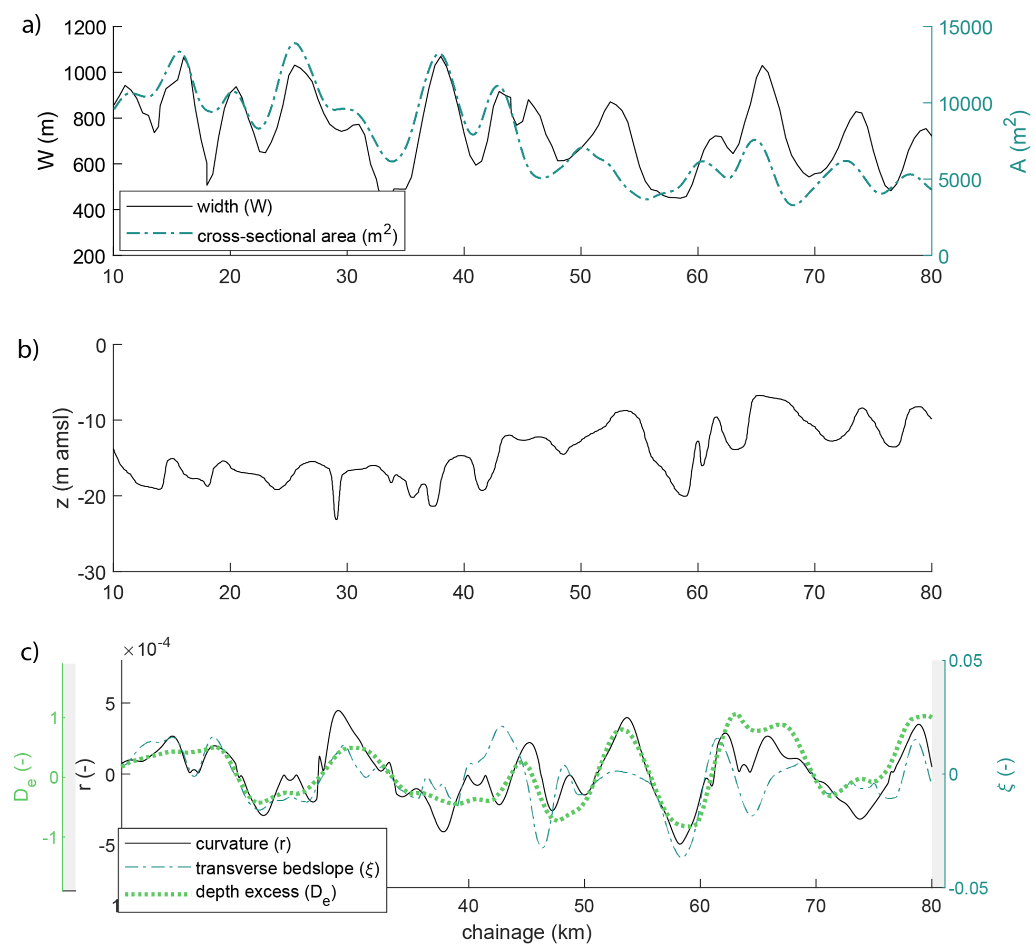

Figure 5. Morphological characteristics of the Lower Fraser River. a) smoothed channel width (W) and smoothed cross-sectional area (A), b) bed level z in meters above sea level, c) channel shape, expressed in depth excess (D$_e$), transverse bed slope (ξ) and curvature (r)

The predictor of Van Rijn (1984) works well when all data is reach-averaged (predicted Δ_{vRijn} = 0.52 m, compared to measured Δ = 0.50 m; Figure 8 a). However, it underestimates dune height in the mixed fluvial-tidal regime (by about 20 cm at RK 80), and overestimates it in the tidally-dominated regime (by about 24 cm at RK 10). All other predictors are inaccurate and overestimate the dune height significantly, with an increasing error in the downstream direction (Figure 8 b-d). For example, the reach-averaged predicted dune heights are 0.87 m, 1.27 m and 1.83 m for the predictors of Yalin (1964), Karim (1995) and Venditti and Bradley (2022), respectively.

Local variability in dune height in the study area is not captured in dune geometry predictors because of the considerable spatial variability in the measured dune geometry. To establish the degree to which local variability in dune properties relates to flow properties obtained with the 2DH hydraulic model assuming a constant roughness, we focus on three zones in the FTTZ (Figure 2). In those zones, flow characteristics are modelled (see Supplementary Figures S7-S11) and the dune height predictor of (Van Rijn, 1984) (equation

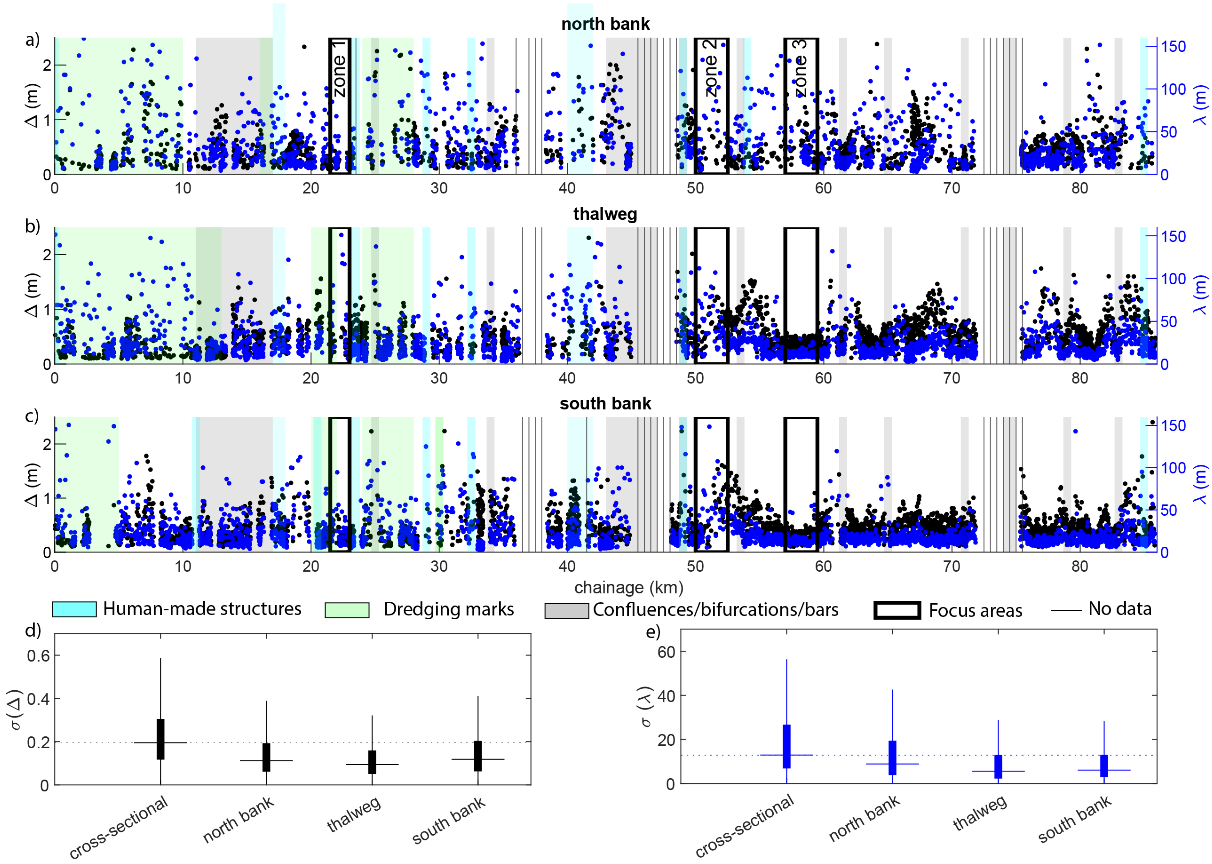

Figure 6. Dune geometry. a, b, c) Dune height (Δ; black) and dune length (λ; blue) throughout the research area. Human-made structures, dredging marks, confluences, bifurcations and bars, focus areas, and zones with no data are indicated (see legend). d, e) Standard deviation (σ) within the mean multibeam echosounder coverage width (230 m) of dune height and dune length over the cross-section, north bank, thalweg and south bank. In each bar, the central mark indicates the median, and the bottom and top edges of the box indicate the 25^{th} and 75^{th} percentiles, respectively. The whiskers extend to the most extreme data points, and outliers are not shown.

2) is applied to each zone using model output per grid cell. The dune height predictor of Van Rijn (1984) performs reasonably well in predicting the local spatial pattern of dune height in the three zones (Figure 9 a-c), but the mean dune height is overestimated for zone 1 and 3, and underestimated for zone 2. To assess the performance of the van Rijn model in predicting dune patterns, a bias correction is performed. Numerical values were added to or subtracted from the predicted dune height in order to minimize the RMSE, and assess the overall patterns in the dune field rather than the actual value (Supplementary Figure S5). The bias-corrected RMSE values of dune height average 0.13 m, which indicates that the spatial pattern of dune heights is relatively well captured by the predictor. The van Rijn dune height predictor captures the main processes that determine dune height in tidal environments, but does not reliably predict absolute values. The dune height predictors of Yalin (1964), Karim (1995) and Venditti and Bradley (2022) perform worse on the local scale pattern (Figure 9 d-l). Notably, the bias correction improves their performance, (Supplementary Figure S6), but they capture the pattern less than well than the predictor of Van Rijn (1984).

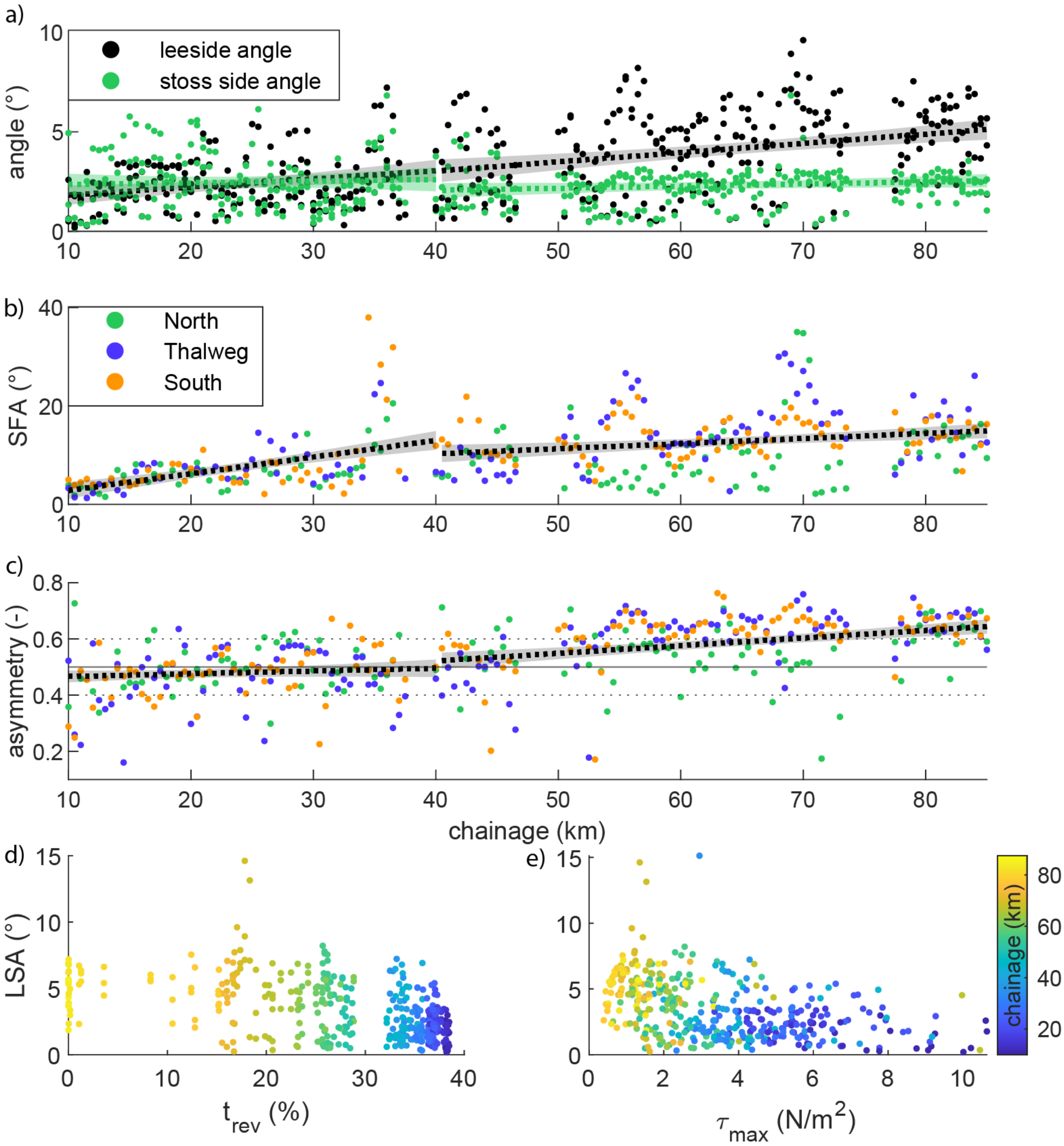

Figure 7. Dune shape in the study area. a) leeside angle (LSA) and stoss side angle (SSA), b) dune slipface angle (SFA), c) dune asymmetry, expressed as the ratio between the length of the (seaward) leeside and the total bedform length. A value of 0.5 indicates symmetric dunes, values of asymmetry smaller than 0.4 are defined as flood-asymmetric, while values larger than 0.6 are ebb-asymmetric. Confidence intervals of linear regressions are shown. Subfigure d) and e) show dune leeside angle against against reversal time (t_{rev}) and against maximum shear stress (τ_{max}), respectively.

4.4 Comparison of observed dune roughness and model roughness

The variability in dune geometry is reflected in the hydraulic roughness generated by the dunes, which ultimately can be used in the hydraulic model to assess the importance of dunes for the large-scale hydraulic roughness.

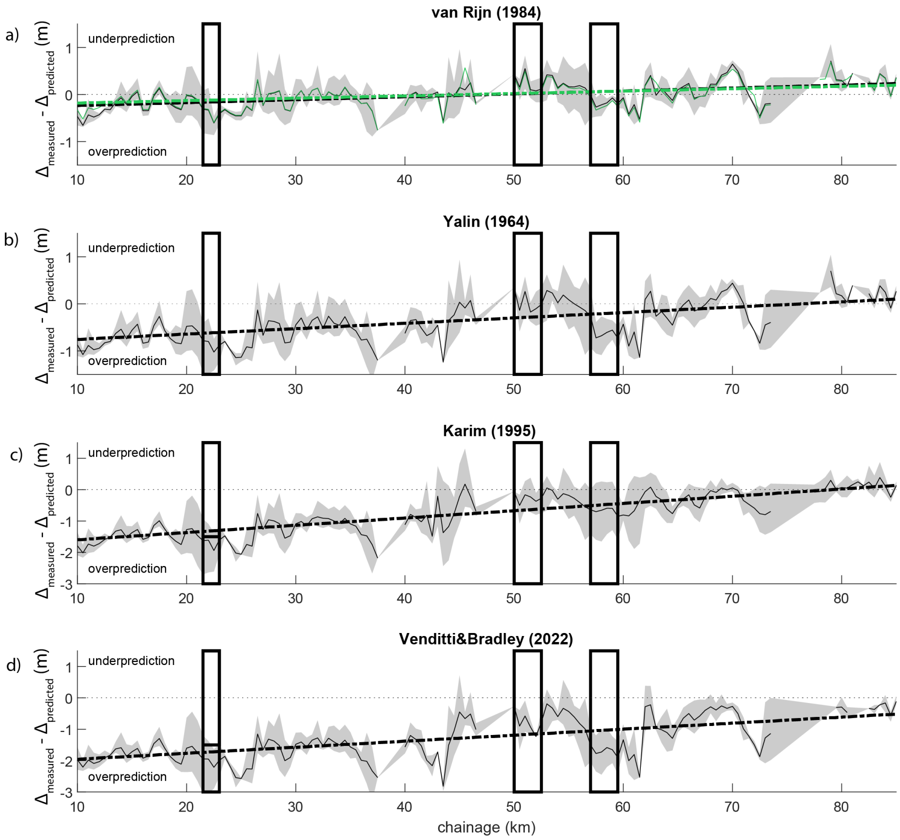

Figure 8. Residual dune height (measured minus predicted) to assess dune height predictor performance of the predictor of a) Van Rijn (1984), b) Yalin (1964), c) Karim (1995) and d) Venditti and Bradley (2022). The measured data is based on the average of three longitudinal transects, and includes the minimum and maximum values in a grey shading. The modelled data is based on the model with a constant roughness of $n_{man} = 0.026$ s m$^{-1/3}$. In subfigure a) predicted dune height with dune-adjusted roughness (varying between 0.024 and 0.028 s m$^{-1/3}$) is displayed in green.

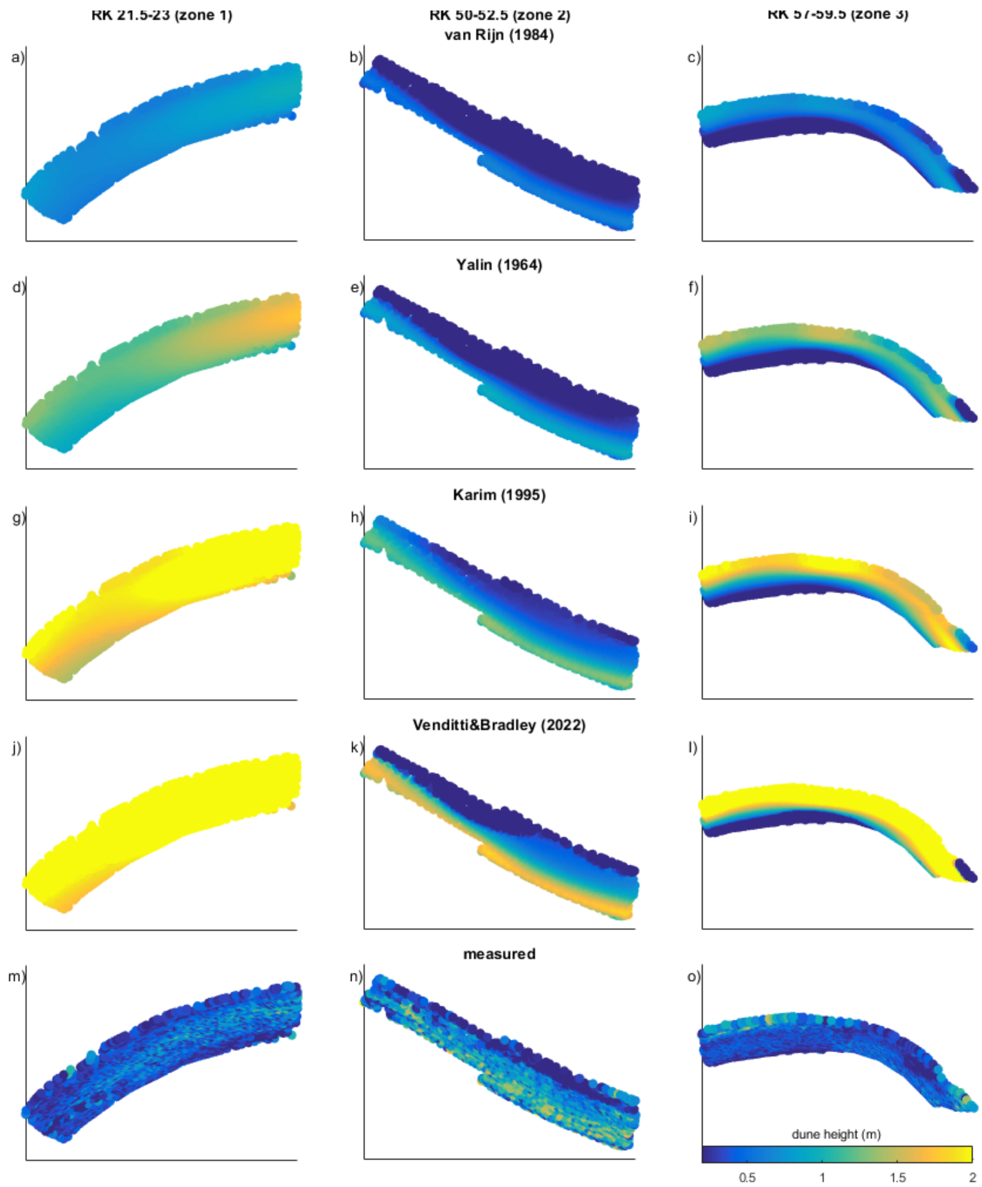

Figure 9. Dune height predictor performance of the predictor of Van Rijn (1984) (a,b,c), Yalin (1964) (d,e,f), Karim (1995) (g,h,i) and Venditti and Bradley (2022) (j,k,l), compared to the measured dune height (m,n,o).

Hydraulic roughness generated by dunes was calculated using equation 13, which includes dune height and length, but does not include the leeside or stoss side angles. The predicted roughness decreases in the downstream direction (Figure 10), which is mainly caused by an increase in water depth. The main variability in roughness is due to variability in water depth, which is most pronounced in the upstream part (RK > 40) of the river (Figure 4). Additionally, local fluctuations in roughness correspond to the local patches of higher dunes, for example at RK ∼54, 63 and 68. The decrease in grain roughness due to a subtle degree of downstream fining has a small impact on overall roughness, because grain roughness values are only around 3% of typical form roughness values. In the downstream reach (RK < 40), smoothed roughness shows a persistent out-of-phase relation with the gradient in smoothed bed elevation (moving average filter of 8 km) (Figure 10a) that is absent in the upstream part of the river.

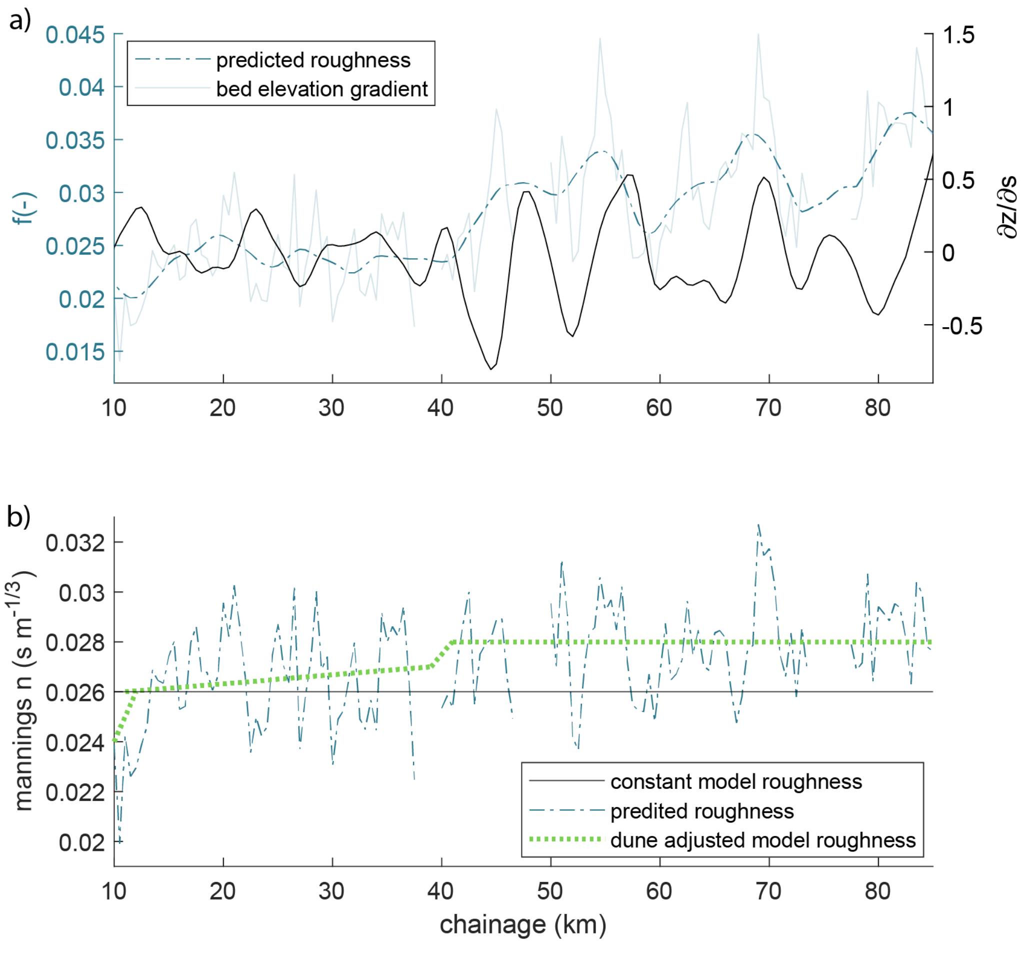

Figure 10. Hydraulic roughness in the study area. a) smoothed roughness (f) (and original roughness in grey) calculated from dune geometry (equation 13)(blue) and the gradient of the smoothed bed level (∂z/∂s; black). b) roughness expressed in Mannings' roughness coefficient n_{man}. Model roughness with a constant n_{man} of 0.026 s $m^{-1/3}$ (black), roughness calculated from dune geometry (equation 13 and 17)(blue), and dune-adjusted model roughness (green).

.

The calculated dune roughness differs slightly from the uniform roughness used in the from model (Manning's roughness of $n_{man} = 0.026$ s $m^{-1/3}$). The derived friction coefficient f_m from the model's roughness (equation 17 and 18) displays the expected decrease in seaward direction, reflecting the increase in water depth. Dune roughness agrees reasonably well to the uniform model roughness (Figure 10b), but local fluctuations are not well-represented. In the upstream region (RK > 40), the model roughness is slightly lower than the dune roughness, while they are similar in the downstream region.

To represent the effect of dune height variation on roughness in the hydrodynamic model, and to investigate if this can improve the calibration, the dune roughness as calculated by equation 13 is divided into three linear components: a uniform roughness of $n_{man} = 0.024$ s $m^{-1/3}$ from RK 0 - 10, a linearly increasing roughness of $n_{man} = 0.026$ to 0.027 s $m^{-1/3}$ in the tidally dominated regime (RK 10 - 40), and a constant roughness of $n_{man} = 0.028$ s $m^{-1/3}$ in the mixed fluvial-tidal regime (RK > 40). A small transition area between the breaks is implemented to ensure a smooth transition to the new roughness regime. These roughness transitions correspond with the transition from the fluvial regime to the deltaic regime around RK 40, and the downstream change from a confined to a less confined channel at around RK 10 (Figure 1).

The dune-derived roughness has little impact on the calibration of water levels and tidal amplitude of the M_2, K_1 and M_4 tidal components (Supplementary Figure S3b). On average, the RMSE value of the modelled water height decreases from 0.36 m to 0.35 m, and the difference between the modelled and observed M_2 amplitude increases from 3% to 4% and K1 from 4% to 6%. Additionally, using the dune-derived roughness for dune height prediction with the Van Rijn predictor only slightly improves the predicted values (17 cm at RK 80 and RK 10) (Figure 8).

5 Discussion

5.1 How are bedform characteristics impacted by the sudden change in tidal flow strength during periods of low river discharge?

During low river discharge conditions like studied in this research, the increase in water depth around RK 40 results into two different hydrodynamic regimes (Figure 11). The tidally-dominated regime is characterized by a large maximum absolute shear stresses, a large tidally-averaged water depth, relatively symmetrical dunes, low leeside and slipface angles and low hydraulic roughness. The mixed tidal-fluvial regime is characterized by a weaker tidal influence, a shallower and more variable water depth, lower maximum absolute shear stresses, asymmetric dunes, higher leeside and slipface angles, and a rougher hydraulically regime. The increase in depth is the main reason that hydraulic roughness is lower in the tidal regime (Equation 13), since the sources of roughness in the Main Channel, sediment composition and dune height, are relatively constant.

Contrasting flow conditions in the two regimes are not reflected in dune height or length. In other systems, dune height is sometimes found to decrease in tidally-influenced regions (Prokocki et al., 2022). Rapid local deposition of the sediment in the deltaic part of the Fraser might result in tidal dunes that are larger than expected (Villard and Church, 2005), leading to a relatively constant dune height. The change in flow regime is reflected in the leeside angle, slip face angle, dune symmetry and dune crest shape. In particular slipface angles are significantly larger in the fluvial-tidal regime, on average 13° compared to 7° in the tidal regime. Dunes are on average asymmetric upstream of the bifurcation at RK 40 (Figure 7), and symmetric downstream of RK 40. This agrees with the findings of Kostaschuk and Villard (1996), who relate the symmetric dunes to high sediment transport rates due to the tides. Indeed, high maximum shear stresses (Figure 11b) are observed in the tidal regime, although tidally-averaged shear stresses remain relatively constant (Figure 4b).

The reversal of the current switches the leeside and stoss side every tidal cycle, steepening both sides in a similar manner (Lefebvre and Winter, 2016). This could be one of the reasons for the large observed variability in angles, since the MBES data is simply a snapshot of the riverbed. Bidirectional currents cause crest orientation to be time-dependent (Hendershot et al., 2016). Both the duration (t_{rev}) and the strength of the flow reversal (τ or Q) determine the dune shape. During low river discharge conditions, the maximum upstream-oriented discharge at RK 22 varies between 4000 and 6000 m^3 s^{-1}, depending on the spring-neap tide cycle. Only 30 km further upstream this has decreased by 66-75%, although the reversal time has only dropped by 9%.

These observations partially agree with the findings of Lefebvre et al. (2021) and Prokocki et al. (2022). Prokocki et al. (2022) observed two different regimes in the Lower Columbia River, USA, based on dune geometry: (fluvial-)tidal dunes, and fluvial dunes. The former were restricted to the most downstream reach (RK $<$ 30 km), and were upstream oriented, predominately low-angled (based on maximum LSA), 2D dunes. Fluvial dunes were downstream oriented, and were higher and longer than the tidal dunes. The division of the regimes in the Columbia is clearer than in the Fraser, most likely because the division in the Columbia coincides with a change in grain size. In addition, the division between the two regimes in the Columbia shifts downstream with an increased discharge. During low discharge, the division is located slightly more downstream (RK 30) than in the Fraser (RK $\sim$40), which could be attributed to the Columbia's lower tidal range.

Lefebvre et al. (2021) also found an increase in dune symmetry in the downstream direction in the Weser Estuary, Germany, but they did not distinguish between two different regimes. However, their data shows that around 60 km from the river mouth, upstream of the estuarine turbidity maximum, the leeside angle of dunes decreases, and dunes become more symmetric. This transition seems to be slightly more gradual than in this study or in the study of Prokocki et al. (2022). The gradual transition is almost twice as far upstream as in the Fraser River, which is likely because the tidal effect in the Weser extends much further upstream than in the Fraser. In this study, and in those of Prokocki et al. (2022) and Lefebvre et al. (2021), the transition in dune morphology coincides with an increase in channel cross-sectional area, either by widening, deepening or both. The deeper regimes are more tidally-dominated, and the constriction upstream of the cross-sectional area leads to a rapid dissipation of tidal energy, that is reflected in the dune leeside angle and symmetry.

5.2 How can dune variability in the fluvial-to-tidal transition zone during low river discharge be predicted and explained?

Tidally-averaged bed shear stresses from the hydrodynamic model can be used to reliably predict reach-averaged dune height using the predictor of Van Rijn (1984). Furthermore, the shear stress distribution predicted by the hydrodynamic model with constant roughness can predict local dune patterns (Figure 8b-g), thereby capturing the cross-sectional variability in dune heights as observed in Figure 6. Cross-sectional shear-stress variation, which is one of the input parameters of the dune predictor of Van Rijn (1984), largely explains the observed patterns. For example, in zone 1, dune height decreases downstream, becasue river width increases and vflow velocity decreases, resulting in lower shear stresses (Supplementary Figure S10). In zone 2, dunes are the highest on the south side of the channel where the river is deepest and the flow velocity and shear stresses are highest. Finally, in zone 3, centrifugal acceleration generates higher flow velocity and larger dunes on the outside of the bend, whereas upstream the dunes are the largest on the inner bend because flow is accelerated by the momentum inherited from the bend upstream (Jackson, 1975).

Van Rijn (1984) and other dune height predictors tested did not accurately predict absolute magnitude of local dune height using tidally-averaged bed shear stresses from the hydrodynamic model. However, they do a good job of predicting the overall patterns of

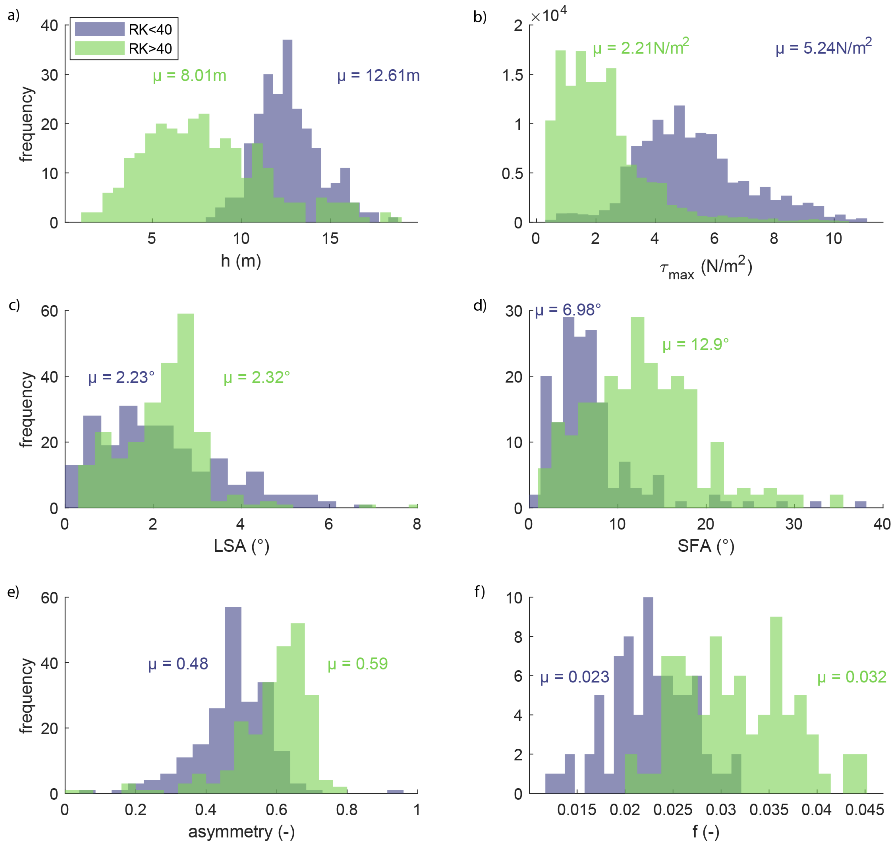

Figure 11. Characteristics of the tidally-dominated regime, seaward of river kilometer (RK) 40, and the mixed tidal-fluvial regime, landward of RK 40. a) water depth (h), b) maximum absolute shear stress (τ_{max}), c) leeside angle (LSA), d) slipface angle (SFA), e) asymmetry, f) friction coefficient (f) derived from dune geometry with equation 13. Mean values are indicated in the figure.

dune height, suggesting that the right processes are captured by the predictors. The poor prediction of absolute values is likely related to number of factors that are not included in the predictors, including self-organization dunes in a shear stress field (Bradley and Venditti, 2019) (such as merging and splitting (Hendershot et al., 2018; Gabel, 1993), crest line deformation (Venditti et al., 2005)), local sediment dynamics not captured by low resolution bed sediment sampling such as local scour (Leclair, 2002), discharge fluctuations and associated hysteresis (Bradley and Venditti, 2021; Julien et al., 2002) and the potential presence of remnant dunes from earlier high-flow conditions. The influence of local factors can be seen in our three focus zones. The larger dunes observed in zone 2 may be related to the local sediment supply being higher here, so dunes develop to a maximum equilibrium size compared to zones 1 and 3. The dunes in zone 2 become longer in the downstream direction until they disappear, even though flow velocity and grain size do not change significantly. The disappearance of dunes in this area could be because the surface of the bed consists of a thin layer of medium sand overlying a deposit of Pleistocene or early Holocene sediment, such as cohesive clay (Clague et al., 1983) (see Supplementary Figure S1), that is not conducive to dune formation. Similarly, in zones 1 and 3, dunes do not develop where the outer bank cuts into a clay layer (Supplementary Figure S9). Additionally, the dunes could be reworked remnants from the previous freshet (Bradley and Venditti, 2021) and their geometry could be related to the much stronger and predominantly downstream currents associated with high river discharge. However, Kostaschuk et al. (1989) found that dunes near Steveston (RK 10) adjusted to the post-freshet decline in discharge over a period of weeks, supporting our contention that the dunes observed herein (more than 6 months after the last freshet) are at least in quasi-equilibrium with low-flow conditions. Additionally, Bradley and Venditti (2021) interpreted low-amplitude bed undulations at RK $\sim$35 as relics from higher flow conditions with smaller dunes superimposed, the latter formed by the low-flow conditions. Kostaschuk et al. (1989) interpreted similar features as 'washed-out' dunes that represented a transition from large, freshet bedforms to small dunes adjusted to low river discharge. In this study we detrended the bed level prior to measuring dune geometry, thereby ensuring that the dunes that we analyzed were representative of low flows.

The poor prediction of local dune geometry in the FTTZ and the observed variability in dune morphology has practical implications for scientists and engineers. Firstly, fairway depth cannot be maintained solely on the basis of on an average dune height, because height varies unpredictably over the river bed. Secondly, measurements of dune height from rock records cannot be reliably used to estimate paleo-hydraulic conditions (Das et al., 2022). Thirdly, models based on reach-averaged dune geometry may result in inaccurate estimates of form roughness and water levels and local values should be used instead. Finally, because the variability in dune height across the channel is twice that of dune height variation along the channel, the grid cell size in hydraulic models should be twice as large in the longitudinal direction than in the cross-river direction.

5.3 To what extent does dune geometry and variability exert an impact on reach-scale hydraulic roughness?

Hydraulic roughness is traditionally predicted using dune height and length (Bartholdy et al., 2010; Lefebvre and Winter, 2016; Soulsby, 1997; Van Rijn, 1984). However, recent research shows that the leeside angle of dunes might be important for roughness prediction (Lefebvre and Winter, 2016) and is poorly represented by dune height and length. Characteristics of the leeside angle determine the strength of flow separation zone (Lefebvre et al., 2014) which impacts form roughness (Lefebvre et al., 2013) induced by dunes. Large rivers are covered by low-angled dunes (LAD) with slip face angles (SFA) $< 30°$ (Cisneros et al., 2020; Kostaschuk and Venditti, 2019) that generate less flow separation than high-angled dunes that have steeper slip face angles (Kwoll et al., 2016). However, weak or intermittent flow separation, with mean leeside angles (LSA) of only 10° still generate flow resistance (Kwoll et al., 2016). Lefebvre and Cisneros (2023) show that not only the leeside angle itself, but also the shape of the leeside impacts flow properties and turbulence. Based on numerical experiments, they found that LADs with a mean LSA of $<10°$ and a SFA of $<20°$ are not capable of permanent flow separation. LADs are still able to generate turbulence (Kostaschuk and Villard, 1996; McLean and Smith, 1979) however, because the decelerated downstream flow generates a shear layer that causes eddy generation (Kostaschuk and Villard, 1999; Best and Kostaschuk, 2002), sand resuspension and roughness.

In this study, the transition from a fluvial-tidal to a tidal regime and the corresponding change in dune leeside and slipface angle are not reflected in the reach-scale hydraulic roughness needed to attenuate the tidal motion in the model. Implementing a roughness change at the depth break at RK 40 could be used to parameterize the change in dune leeside angle at the regime transition. However, models with a higher roughness downstream than upstream performed slightly better than models with the highest roughness upstream (Supplementary Materials Text S3). This is contrary to the expectations based on the leeside angle observations and suggests a different source of roughness in the tidal regime (see below). Additionally, the dune roughness predictor (equation 2), based on dune height and dune length, yields very similar values to the calibrated model roughness (RMSE $f = 0.0053$).

This supports the application of the dune roughness predictor in a tidal environment and also indicates that dune leeside angle might not be important in determining reach-scale model roughness. Finally, local values of dune height and length are not required to accurately predict reach-scale model roughness, because hydraulic model performance is not improved by using local dune geometry. This in turn suggests that variable dune roughness might not be needed to simulate large-scale (tidal) flow. Similar conclusions were drawn from a fluvial system where dune roughness calculated from dune geometry explained only 31% of the variance of the roughness inferred from the water surface slope (deLange et al., 2021) and the remaining variance could not be explained by leeside angle statistics.

The limited impact of local dune height, length and leeside angle on the hydraulic model could be due to several factors. Firstly, 3-dimensional dune fields such as those in our study area, generate less roughness than 2-dimensional dune fields (Venditti, 2007), which could explain the lack of model improvement when implementing dune-related roughness. Secondly, a complex leeside shape might have an effect on flow separation (Lefebvre and Cisneros, 2023) and form roughness. So even though the SFAs found in this study are large enough to generate flow separation, the shape of the leeside might prevent it. Thirdly, we evaluated the hydraulic model by assessing tidal attenuation and water level fluctuations and found minimal impact of local dune geometry. However, incorporating dune roughness could be important for prediction of residual sediment transport (Herrling et al., 2021), which is not implemented in our hydraulic model. Local values of shear stresses (for which detailed MBES data is needed) might be required for morphodynamic modelling, even if they are not needed for modelling tidal propagation in a hydrodynamic model. Finally, we evaluated the model on the reach-scale where other components of roughness dominate (see below). However these components are less relevant on the local scales, where dunes might be the main source of roughness. In addition, the prediction of hydraulic roughness generated by dunes deviates locally from the constant model roughness. As a result, in the mixed tidal-fluvial regime the dune-induced roughness is larger than needed for attenuation based on the calibrated roughness. For example, Davies and Robins (2017) found that the overall effective roughness of the bed is about half of the maximum local dune-induced roughness (expressed in k_s). Halving the k_s value in equation 13 results in a comparable dune roughness and calibrated roughness in the mixed fluvial-tidal regime (RMSE 0.0034 for RK > 40) (Supplementary Figure S4) but not in the tidally-dominated regime where dune roughness remains lower than calibrated roughness. This could be a result of the lower LSA in the tidal regime. However, including the LSA in roughness prediction using the equation developed by Lefebvre and Winter (2016) results in unrealistically low values of roughness. In general, evidence that the LSA impacts reach-scale model roughness is lacking.

In our research area there are several reach-scale sources of roughness. Firstly, large-scale river geometry, which is included in the hydraulic model by the bathymetry. We observed an out-of-phase relation between hydraulic roughness and the smoothed gradient of the bed level in the tidally-dominated regime of our study area (Figure 10). A similar relation was observed in the Rhine and Waal rivers in the Netherlands by deLange et al. (2021), and they hypothesised that multi-kilometer depth oscillations induce flow divergence associated with depth increase, which in turn causes energy loss. This in turn is reflected in an elevated hydraulic roughness. However, this out-of-phase relation is not observed in the mixed tidal-fluvial regime in the Fraser, where increases in depth coincide with decreases in width, keeping the cross-sectional area relatively constant. As a result, changes in depth do not result in flow divergence or convergence and the out-of-phase relation does not develop. Secondly, intertidal areas affect reach-scale roughness. The calibrated friction in our model is an indication of the friction required to attenuate the tide. The model calibrated with a uniform Manning's roughness ($n_{man} = 0.026$ s m$^{-1/3}$) performs reasonably well in modelling of water level and tidal amplitude, but regions with a significant decrease in tidal energy (between RK 9-18.5 and 35-42) are not well captured by the model (Figure 3). These regions possess intertidal areas (Supplementary Figure S11) which flood during high tide and are not properly represented in the model due to the lack of topographical data, resulting in a local tidal attenuation that is too low. Finally, engineering works, such as the tunnel at RK 18 and the bridge at RK 36, could be an extra source of roughness.

6 Conclusions

During low flow discharge, the Fraser River deepens downstream of 40 km from the river mouth, separating a fluvial-tidal regime landward and a tidal regime seaward. Bathymetric data and a hydraulic model of the lowermost 85 km of the river were used to explore the spatial variability and controls of dune morphology in this fluvial-to-tidal transition zone (FTTZ). Dune height was predicted using several semi-empirical equations to explore the potential for local and regional dune height prediction. Finally, the hydraulic model was used to assess the importance of dune generated roughness on model performance. From these investigations we conclude that:

- There are no significant spatial trends in dune height or length, even though the river deepens at 40 km. Local variability in dune height and length dominates, and variability in dune height and length is two times as large in the cross-sectional direction than in the longitudinal direction.
- Dune height predictors provide a good first approximation of regional dune height and local spatial patterns, but local shear stress predictions need to be improved to enable prediction of local dune heights. Using shear stresses from the hydraulic model calibrated with a constant roughness of $n_{man} = 0.026$ s $m^{-1/3}$, the dune height predictor of Van Rijn (1984) is able to predict local local patterns of dune heights using tidally-averaged values of bed shear stress. Other tested predictors of dune height do a worse job.
- Mean leeside angle and stoss side of dunes are lower in the tidal regime compared to the fluvial-tidal regime, and dunes become symmetric due to the stronger tidal influence. These changes in dune morphology however do not affect reach-scale hydraulic roughness, because the calibrated model roughness is similar to the dune-derived roughness based on dune height and dune length. As a result, hydraulic model performance using a calibrated, constant, roughness is not improved by implementing dune-derived bed roughness.
- Large-scale variations river morphology are more important than dune morphology in controlling variations in reach scale roughness. Reach-scale variations in depth can elevate hydraulic roughness in the tidal region, but this does not occur in the fluvial-tidal regime because changes in depth are compensated by changes in width, keeping the cross-sectional area of the channel relatively constant. Intertidal areas in the Fraser are likely a significant source of roughness, but are difficult to incorporate into hydraulic models because of limited topographic information.

Acknowledgments

SdL and RS were funded by the Netherlands Organisation for Scientific Research (NWO), within Vici project "Deltas out of shape: regime changes of sediment dynamics in tide-influenced deltas" (Grant NWO-TTW 17062). RB, DM, and JV were funded through a Natural Sciences and Engineering Research Council of Canada (NSERC) Discovery Grant and Accelerator Supplement. T. Cain and I. Darke at Public Service and Procurement Canada graciously provided the bathymetric data. Reviewers and editors will be thanked. Data is publicly available via DOIxxx

References

Allen, J. R.L. (1978). "Computational models for dune time-lag: calculations using Stein's rule for dune height". In: *Sedimentary Geology* 20.C, pp. 165–216. ISSN: 00370738. DOI: 10.1016/0037-0738(78)90054-4.

ASCE Task Force (2002). "Flow and transport over dunes". In: *Journal of Hydraulic Engineering* 127, pp. 726–728.

Ashley, G. M. (1980). "Channel morphology and sediment movement in a tidal river, Pitt River, British Columbia." In: *Earth Surface Processes* 5.4, pp. 347–368. ISSN: 03601269. DOI: 10.1002/esp.3760050406.

Attard, Maureen E., Jeremy G. Venditti, and Michael Church (2014). "Suspended sediment transport in Fraser River at Mission, British Columbia: New observations and comparison to historical records". In: *Canadian Water Resources Journal* 39.3, pp. 356–371. ISSN: 07011784. DOI: 10.1080/07011784.2014.942105. URL: http://dx.doi.org/10.1080/07011784.2014.942105.

Bartholdy, J. et al. (2010). "Hydraulic roughness over simple subaqueous dunes". In: *Geo-Marine Letters* 30.1, pp. 63–76. ISSN: 14321157. DOI: 10.1007/s00367-009-0153-7.

Best, Jim (2005). "The fluid dynamics of river dunes: A review and some future research directions". In: *Journal of Geophysical Research: Earth Surface* 110.4, pp. 1–21. ISSN: 21699011. DOI: 10.1029/2004JF000218.

Best, Jim and Ray Kostaschuk (2002). "An experimental study of turbulent flow over a low-angle dune". In: *Journal of Geophysical Research C: Oceans* 107.9, pp. 18–1. ISSN: 01480227. DOI: 10.1029/2000jc000294.

Bradley, R. W. et al. (2013). "Flow and sediment suspension events over low-angle dunes: Fraser Estuary, Canada". In: *Journal of Geophysical Research: Earth Surface* 118.3, pp. 1693–1709. ISSN: 21699011. DOI: 10.1002/jgrf.20118.

Bradley, Ryan W. and Jeremy G. Venditti (Feb. 2017). *Reevaluating dune scaling relations.* DOI: 10.1016/j.earscirev.2016.11.004.

— (2019). "Transport Scaling of Dune Dimensions in Shallow Flows". In: *Journal of Geophysical Research: Earth Surface* 124.2, pp. 526–547. ISSN: 21699011. DOI: 10.1029/2018JF004832.

— (2021). "Mechanisms of Dune Growth and Decay in Rivers". In: *Geophysical Research Letters* 48.20, pp. 1–10. ISSN: 19448007. DOI: 10.1029/2021GL094572.

Bridge, J.S. (2003). *Rivers and Floodplains: Forms, Processes, and Sedimentary Record.* Malden, Massachusetts: John Wiley & Sons, p. 491.

Carling, P. A. et al. (2000). "The morphodynamics of fluvial sand dunes in the River Rhine, near Mainz, Germany. I. Sedimentology and morphology". In: *Sedimentology* 47.1, pp. 227–252. ISSN: 00370746. DOI: 10.1046/j.1365-3091.2000.00290.x.

Chow, V.T. (1959). *Open-channel hydraulics.* McGraw-Hill Book Company, USA. ISBN: ISBN 0-07- 085906-X.

Cisneros, Julia et al. (2020). "Dunes in the world's big rivers are characterized by low-angle lee-side slopes and a complex shape". In: *Nature Geoscience* 13.2, pp. 156–162. ISSN: 17520908. DOI: 10.1038/s41561-019-0511-7.

Clague, John J., John L. Luternauer, and Richard J. Hebda (1983). "Sedimentary environments and postglacial history of the Fraser Delta and Lower Fraser Valley, British Columbia". In: *Canadian journal of earth sciences* 20.8, pp. 1314–1326. ISSN: 00084077. DOI: 10.1139/e83-116.

Das, Debsmita et al. (Sept. 2022). "The Influence of Transport Stage on Preserved Fluvial Cross Strata". In: *Geophysical Research Letters* 49.18. ISSN: 19448007. DOI: 10.1029/2022GL099808.

Dashtgard, Shahin E et al. (2012). "Sedimentation Across the Tidal-Fluvial Transition in the Lower Fraser River, Canada". In: *The Sedimentary Record* 10.4, pp. 4–9. ISSN: 15438740. DOI: 10.2110/sedred.2012.4.4. URL: http://www.wateroffice.ec.gc.ca/,.

Davies, A. G. and P. E. Robins (2017). "Residual flow, bedforms and sediment transport in a tidal channel modelled with variable bed roughness". In: *Geomorphology* 295, pp. 855–872. ISSN: 0169555X. DOI: 10.1016/j.geomorph.2017.08.029. URL: http://dx.doi.org/10.1016/j.geomorph.2017.08.029.

De Brye, Benjamin et al. (2011). “Preliminary results of a finite-element, multi-scale model of the Mahakam Delta (Indonesia)”. In: *Ocean Dynamics* 61.8, pp. 1107–1120. ISSN: 16167341. DOI: 10.1007/s10236-011-0410-y. URL: www.climate.be/slim.

de Ruijsscher, Naqshband, and Hoitink (2020). “Effect of non-migrating bars on dune dynamics in a lowland river”. In: *Earth Surface Processes and Landforms*.

deLange, S. I., S. Naqshband, and A. J.F. Hoitink (2021). “Quantifying Hydraulic Roughness From Field Data: Can Dune Morphology Tell the Whole Story?” In: *Water Resources Research* 57.12, pp. 1–22. ISSN: 19447973. DOI: 10.1029/2021WR030329.

Egbert, Gary D. and Svetlana Y. Erofeeva (2002). “Efficient inverse modeling of barotropic ocean tides”. In: *Journal of Atmospheric and Oceanic Technology* 19.2, pp. 183–204. ISSN: 07390572. DOI: 10.1175/1520-0426(2002)019<0183:EIMOBO>2.0.CO;2.

Einstein, H. A. (1950). “The bed-load function for sediment transportation in open channel flows”. In: *Technical Bulletins 156389, United States Department of Agriculture, Economic Research Service.*

Ferguson, R I and M Church (2004). *A simple universal equation for grain settling velocity.* Tech. rep. 6, pp. 933–937. URL: http://pubs.geoscienceworld.org/sepm/jsedres/article-pdf/74/6/933/2821499/933.pdf.

Gabel, Sharon L. (Apr. 1993). “Geometry and kinematics of dunes during steady and unsteady flows in the Calamus River, Nebraska, USA”. In: *Sedimentology* 40.2, pp. 237–269. ISSN: 0037-0746. DOI: 10.1111/j.1365-3091.1993.tb01763.x.

Gates, T. and M. Al-Zahrani (1996). “Spatiotemporal stochastic open-channel flow. II: simulation experiments.” In: *Journal of Hydraulic Engineering* 122.11, pp. 652–611. DOI: 10.1061/(ASCE)07339429(1996)122:11(652)..

Gisen, Jacqueline Isabella Anak and Hubert H.G. Savenije (Apr. 2015). “Estimating bankfull discharge and depth in ungauged estuaries”. In: *Water Resources Research* 51.4, pp. 2298–2316. ISSN: 0043-1397. DOI: 10.1002/2014WR016227.

Godin, G. (1972). *The analysis of tides.* University of Toronto Press, p. 264.

— (Mar. 1999). “The Propagation of Tides up Rivers With Special Considerations on the Upper Saint Lawrence River”. In: *Estuarine, Coastal and Shelf Science* 48.3, pp. 307–324. ISSN: 02727714. DOI: 10.1006/ecss.1998.0422.

Hendershot, Megan L. et al. (2016). “Response of low-angle dunes to variable flow”. In: *Sedimentology* 63.3, pp. 743–760. ISSN: 00370746. DOI: 10.1111/sed.12236.

Hendershot, Megan L. et al. (Dec. 2018). “Crestline bifurcation and dynamics in fluvially-dominated, tidally-influenced flow”. In: *Sedimentology* 65.7, pp. 2621–2636. ISSN: 13653091. DOI: 10.1111/sed.12480.

Herrling, Gerald et al. (Sept. 2021). “The effect of asymmetric dune roughness on tidal asymmetry in the Weser estuary”. In: *Earth Surface Processes and Landforms* 46.11, pp. 2211–2228. ISSN: 10969837. DOI: 10.1002/esp.5170.

Hoitink, A. J.F., P. Hoekstra, and D. S. Van Maren (Oct. 2003). “Flow asymmetry associated with astronomical tides: Implications for the residual transport of sediment”. In: *Journal of Geophysical Research: Oceans* 108.10. ISSN: 21699291. DOI: 10.1029/2002jc001539.

Holmes, Marcelo H. and Marcelo H. Garcia (2008). “Flow over bedforms in a large sand-bed river: A field investigation”. In: *Journal of Hydraulic Research* 46.3, pp. 322–333. ISSN: 00221686. DOI: 10.3826/jhr.2008.3040.

Horrevoets, A.C. et al. (July 2004). “The influence of river discharge on tidal damping in alluvial estuaries”. In: *Journal of Hydrology* 294.4, pp. 213–228. ISSN: 00221694. DOI: 10.1016/j.jhydrol.2004.02.012.

Jackson, Roscoe G. (1975). “Velocity-bed-form-texture patterns of meander bends in the lower Wabash River of Illinois and Indiana”. In: *Bulletin of the Geological Society of America* 86.11, pp. 1511–1522. ISSN: 19432674. DOI: 10.1130/0016-7606(1975)86<1511:VPOMBI>2.0.CO;2.

Julien, P. Y. et al. (2002). "Case study: Bed resistance of Rhine River during 1998 flood". In: *Journal of Hydraulic Engineering* 128.12, pp. 1042–1050. ISSN: 07339429. DOI: 10.1061/(ASCE)0733-9429(2002)128:12(1042).

Karim, F. (1995). "Bed configuration and hydraulic resistance in alluvial-channel flows". In: *Journal of Hydraulic Engineering* 121.1, pp. 15–25.

Kästner, K. et al. (Mar. 2017). "Distributary channels in the fluvial to tidal transition zone". In: *Journal of Geophysical Research: Earth Surface* 122.3, pp. 696–710. ISSN: 21699011. DOI: 10.1002/2016JF004075. URL: https://onlinelibrary.wiley.com/doi/abs/10.1002/2016JF004075.

Kernkamp, Herman W.J. et al. (Aug. 2011). "Efficient scheme for the shallow water equations on unstructured grids with application to the Continental Shelf". In: *Ocean Dynamics* 61.8, pp. 1175–1188. ISSN: 16167341. DOI: 10.1007/s10236-011-0423-6.

Kostaschuk, R.A. and L.A. Atwood (1990). "River discharge and tidal controls on salt-wedge position and implications for channel shoaling: Fraser River, British Columbia". In: *Canadian Journal of Civil Engineering* 17.3, pp. 452–459. ISSN: 03151468. DOI: 10.1139/l90-049.

Kostaschuk, R.A., M.A. Church, and J.L. Luternauer (1989). "Bedforms, bed material, and bedload transport in a salt-wedge estuary: Fraser River, British Columbia". In: *Canadian Journal of Earth Sciences* 26.7, pp. 1440–1452. DOI: https://doi.org/10.1139/e89-122.

Kostaschuk, R.A. and J.L. Luternauer (1989). "The role of the salt wedge in sediment resuspension and deposition: Fraser River Estuary, Canada". In: *J. Coastal Res.* 5, pp. 93–101.

Kostaschuk, R.A. and P.V. Villard (1999). "Turbulent sand suspension over dunes". In: *Proceedings of the 6th International Conference on Fluvial Sedimentology.* Ed. by N.D. Smith and Rogers. J. Blackwell Sci., Malden, Mass.

Kostaschuk, Ray A and Jeremy G Venditti (2019). "Why do large, deep rivers have low-angle dune beds?" In: *Geology* 47.10, pp. 919–922. ISSN: 19432682. DOI: 10.1130/G46460.1. URL: https://doi.org/10.1130/G46460.1.

Kostaschuk, Ray and Jim Best (Dec. 2005). "Response of sand dunes to variations in tidal flow: Fraser Estuary, Canada". In: *Journal of Geophysical Research: Earth Surface* 110.4. ISSN: 21699011. DOI: 10.1029/2004JF000176.

Kostaschuk, Ray and Paul Villard (Jan. 1996). "Flow and sediment transport over large subaqueous dunes: Fraser River, Canada". In: *Sedimentology* 45.1, pp. 849–863. ISSN: 00370746. DOI: 10.1111/j.1365-3091.1996.tb01506.x.

Kwoll, E. et al. (Mar. 2016). "Flow structure and resistance over subaquaeous high- and low-angle dunes". In: *Journal of Geophysical Research: Earth Surface* 121.3, pp. 545–564. ISSN: 21699011. DOI: 10.1002/2013JF002871.Received.

Leclair, Suzanne F. (2002). "Preservation of cross-strata due to the migration of subaqueous dunes: An experimental investigation". In: *Sedimentology* 49.6, pp. 1157–1180. ISSN: 00370746. DOI: 10.1046/j.1365-3091.2002.00482.x.

Lefebvre, A. and J Cisneros (2023). "The influence of dune lee side shape". In: *EGUsphere [preprint].*

Lefebvre, A. et al. (2014). "Flow separation and roughness lengths over large bedforms in a tidal environment: A numerical investigation". In: *Continental Shelf Research* 91, pp. 57–69. ISSN: 02784343. DOI: 10.1016/j.csr.2014.09.001. URL: http://dx.doi.org/10.1016/j.csr.2014.09.001.

Lefebvre, Alice, Verner B. Ernstsen, and Christian Winter (2013). "Estimation of roughness lengths and flow separation over compound bedforms in a natural-tidal inlet". In: *Continental Shelf Research* 61-62, pp. 98–111. ISSN: 02784343. DOI: 10.1016/j.csr.2013.04.030.

Lefebvre, Alice and Christian Winter (2016). "Predicting bed form roughness: the influence of lee side angle". In: *Geo-Marine Letters* 36.2, pp. 121–133. ISSN: 14321157. DOI: 10.1007/s00367-016-0436-8.

Lefebvre, Alice et al. (2021). “Morphology of estuarine bedforms, Weser Estuary, Germany”. In: *Earth Surface Processes and Landforms* 47.1, pp. 242–256. ISSN: 10969837. DOI: 10.1002/esp.5243.

Lesser, Giles R et al. (2004). “Development and validation of a three-dimensional morphological model”. In: *Coastal Engineering* 51.8-9, pp. 883–915. ISSN: 03783839. DOI: 10.1016/j.coastaleng.2004.07.014. URL: www.elsevier.com/locate/coastaleng.

Manning, R. (1891). “On the flow of water in open channels and pipes”. In: *Transactions of the Institution of Civil engineers of Ireland*.

Mark, C. F. van der, Astrid Blom, and S. M.J.H. Hulscher (2008). “Quantification of variability in bedform geometry”. In: *Journal of Geophysical Research: Earth Surface* 113.3, pp. 1–11. ISSN: 21699011. DOI: 10.1029/2007JF000940.

McLaren, Patrick and Ping Ren (1995). *Sediment transport patterns in the lower fraser river and fraser delta*. Tech. rep.

McLean, D.G and B.L. Tassone (1989). *Effects of Dredging on Fraser River Channel Regime*. Tech. rep. Public Works Canada and Environment Canada, Vancouver. Unpublished report 883-578, p. 25.

McLean, David G., Michael Church, and Bruno Tassone (1999). “Sediment transport along lower Fraser River 1. Measurements and hydraulic computations”. In: *Water Resources Research* 35.8, pp. 2533–2548. ISSN: 00431397. DOI: 10.1029/1999WR900101.

McLean, Stephen R. and J. Dungan Smith (1979). “Turbulence measurements in the boundary layer over a sand wave field”. In: *Journal of Geophysical Research* 84.C12, p. 7791. ISSN: 0148-0227. DOI: 10.1029/JC084iC12p07791.

Morvan, Hervé et al. (2008). “The concept of roughness in fluvial hydraulics and its formulation in 1D, 2D and 3D numerical simulation models”. In: *Journal of Hydraulic Research* 46.2, pp. 191–208. ISSN: 00221686. DOI: 10.1080/00221686.2008.9521855.

Murphy, Dan (2023). “Sediment Delivery and Bedform Variability of the Lower Fraser River and Delta”. PhD thesis. Simon Fraser University.

Nelson, Andrew (2017). *Effect of Longterm Navigation Channel Lowering on Scour and Degradation Processes on Lower Fraser River*. Tech. rep. URL: https://www.researchgate.net/publication/323413777.

NHC (2008). *Fraser River hydraulic model update final report*. Tech. rep.

Paarlberg, Andries J. et al. (2010). “Modelling the effect of time-dependent river dune evolution on bed roughness and stage”. In: *Earth Surface Processes and Landforms* 35.15, pp. 1854–1866. ISSN: 10969837. DOI: 10.1002/esp.2074.

Pawlowicz, Rich, Bob Beardsley, and Steve Lentz (2002). “Classical tidal harmonic analysis including error estimates in MATLAB using TDE”. In: *Computers and Geosciences* 28.8, pp. 929–937. ISSN: 00983004. DOI: 10.1016/S0098-3004(02)00013-4.

Phillips, Jonathan D. (2022). “Geomorphology of the fluvial–estuarine transition zone, lower Neuse River, North Carolina”. In: *Earth Surface Processes and Landforms* 47.8, pp. 2044–2061. ISSN: 10969837. DOI: 10.1002/esp.5362. URL: https://doi.org/10.1002/esp.5362.

Pretious, E.S. (1956). *Bed-load Measurement in the Main Arm Fraser River Estuary*. Tech. rep., Canada Department of Public Works. Fraser River Mo.

Pretious, E.S. and T. Blench (1951). *Final Report on Special Observations of Bed Movement in the Lower Fraser River at Ladner Reach during 1950 Freshet*. Tech. rep. Vancouver: Natl. Res. Counc. Can.

Prokocki, Eric W. et al. (2022). “The morphology of fluvial-tidal dunes: Lower Columbia River, Oregon/Washington, USA”. In: *Earth Surface Processes and Landforms* 47.8, pp. 2079–2106. ISSN: 10969837. DOI: 10.1002/esp.5364.

Sassi, Maximiliano G et al. (2011). “Tidal impact on the division of river discharge over distributary channels in the Mahakam Delta”. In: *Ocean Dynamics* 61.12, pp. 2211–2228. ISSN: 16167341. DOI: 10.1007/s10236-011-0473-9.

Silberman, E. et al. (1963). “Friction factors in open channels”. In: *J. Hydraul. Eng.* 89.HY2, pp. 97–143.

Soulsby, R. (1997). *Dynamics of marine sands*.

Stewart, I and B Tassone (1989). *The Fraser River delta: a Review of Historic Sounding Charts*. Tech. rep. Environment Canada, Conservation and Protection, Vancouver, B.C, p. 39.

Van De Kreeke, J and K Robaczewska (1993). *Tide-induced residual transport of coarse sediment: application to the Ems estuary*. Tech. rep. 3, pp. 209–220.

Van Ormondt, Maarten, Kees Nederhoff, and Ap Van Dongeren (2020). "Delft Dashboard: A quick set-up tool for hydrodynamic models". In: *Journal of Hydroinformatics* 22.3, pp. 510–527. ISSN: 14651734. DOI: 10.2166/hydro.2020.092.

Van Rijn, L.C. (1984). "Sediment transport, part III: Bedforms". In: *Journal of Hydraulic Engineering* 110.12, pp. 1733–1754.

Venditti, J.G. et al. (2019). "Supply-limited bedform patterns and scaling downstream of a gravel–sand transition". In: *Sedimentology* 66.6, pp. 2538–2556. ISSN: 13653091. DOI: 10.1111/sed.12604.

Venditti, Jeremy G. (Nov. 2007). "Turbulent flow and drag over fixed two- and three-dimensional dunes". In: *Journal of Geophysical Research* 112.F4, F04008. ISSN: 0148-0227. DOI: 10.1029/2006JF000650.

Venditti, Jeremy G. and Ryan W. Bradley (Jan. 2022). "Bedforms in Sand Bed Rivers". In: *Treatise on Geomorphology*. Elsevier, pp. 222–254. ISBN: 9780128182352. DOI: 10.1016/B978-0-12-409548-9.12519-9.

Venditti, Jeremy G. and Michael Church (2014). "Morphology and controls on the position of a gravel- sand transition: Fraser River, British Columbia". In: pp. 300–316. DOI: 10.1002/2013JF002871.Received.

Venditti, Jeremy G., Micheal Church, and Sean J. Bennett (Nov. 2005). "On the transition between 2D and 3D dunes". In: *Sedimentology* 52.6, pp. 1343–1359. ISSN: 00370746. DOI: 10.1111/j.1365-3091.2005.00748.x.

Venditti, Jeremy G. et al. (2015). "The gravel-sand transition: Sediment dynamics in a diffuse extension". In: *Journal of Geophysical Research: Earth Surface*, pp. 300–316. DOI: 10.1002/2013JF002871.Received.

Vermeulen, B., M. G. Sassi, and A. J. F. Hoitink (2014a). "Improved flow velocity estimates frommoving-boat ADCP measurements". In: *Journal of the American Water Resources Association* 50. ISSN: 1093-474X. DOI: 10.1111/j.1752-1688.1969.tb04897.x.

Vermeulen, B. et al. (2014b). "Sharp bends associated with deep scours in a tropical river: The river Mahakam (East Kalimantan, Indonesia)". In: *Journal of Geophysical Research: Earth Surface* 119.7, pp. 1441–1454. ISSN: 21699011. DOI: 10.1002/2013JF002923.

Villard, P. V. and M. Church (2005). "Bar and dune development during a freshet: Fraser River Estuary, British Columbia, Canada". In: *Sedimentology* 52.4, pp. 737–756. ISSN: 00370746. DOI: 10.1111/j.1365-3091.2005.00721.x.

Warmink, J. J. et al. (2013). "Quantification of uncertainty in design water levels due to uncertain bed form roughness in the Dutch river Waal". In: *Hydrological Processes* 27.11, pp. 1646–1663. ISSN: 08856087. DOI: 10.1002/hyp.9319.

WCHL (1977). *Feasibility Study, Development of a Forty-Foot Draft Navigation Channel, New Westminster to Sandheads: Vancouver, Western Canada*. Tech. rep., Hydraulic Laboratories, p. 107.

Wright, N and A Crosato (2011). "The Hydrodynamics and Morphodynamics of Rivers". In: *Treatise on Water Science*. Vol. 2, pp. 135–156. ISBN: 9780444531933. DOI: 10.1016/B978-0-444-53199-5.00033-6.

Wu, Yongsheng et al. (2022). "Tidal propagation in the Lower Fraser River, British Columbia, Canada". In: *Estuarine, Coastal and Shelf Science* 264.November 2021, p. 107695. ISSN: 02727714. DOI: 10.1016/j.ecss.2021.107695. URL: https://doi.org/10.1016/j.ecss.2021.107695.

Yalin, M.S. (1964). "Geometrical Properties of Sand Wave". In: *Journal of Hydraulic Engineering* 90, pp. 105–119.

Zanke, U.C.E. (2003). "On the influence of turbulence on the initiation of sediment motion". In: *International Journal of Sediment Research* 18.1, pp. 17–31. ISSN: 00298018. DOI: 10.1016/0029-8018(79)90021-0.

Supporting Information for "Dune geometry and the associated hydraulic roughness at the transition from a fluvial to tidal regime at low river discharge"

S.I. de Lange[1], R. Bradley[2,3], R.A. Schrijvershof [1], D. Murphy[3], K. Waldschläger[1], R. Kostaschuk[3], J.G. Venditti[3], A.J.F. Hoitink[1]

[1]Wageningen University, Department of Environmental Sciences, Hydrology and Quantitative Water Management, Wageningen, the Netherlands

[2]Northwest Hydraulic Consultants Ltd., North Vancouver, British Columbia, Canada

[3]School of Environmental Science, Simon Fraser University, Burnaby, British Columbia, Canada

Contents of this file

Introduction In these supplementary materials, six topics will be discussed and/or visualised. These include surface geology of the lower Fraser river, examples of bathymetric data where (human-made) irregularities are visible, the model calibration and evaluation, figures visualising the predictive capacity for dune patterns of several dune height predictors, some additional figures on the local focus areas, and a figure indicating the intertidal areas.

Text S1: Surface geology The surface geology (Figure S1) determines the underlying material of the Fraser river, and is often exposed on the channel margin. At the outer banks of the river, gravel and clay patches are present (Figure 2a and c). These patches of gravel and clay are either caused by modern deposits, such as gravel bars, or by earlier deposited sediments constraining the river's course. When the river cuts into a clay or gravel layer, abrupt changes in dune geometry can be visible.

Text S2: Examples of bathymetric data with (human-made) irregularities

see Figure S2

Text S3: Model calibration and evaluation

The model was calibrated by assessing the tidal amplitude of the M_2, M_4 and K_1 tidal constituents, during low water levels in winter 2018. A uniform roughness of 0.026 s $m^{-1/3}$ performs the best. The performance of best performing model, and the other tests using different values of uniform roughness, are summarized in Table S2, indicating the Root Mean Square Error of the observed and modelled water level (between 0.27 and 0.43 m), the correlation coefficient R^2 between the observed and modelled water level (between 0.67 and 0.87), and the difference in observed and modelled tidal amplitude of the M2, K1 and M4 tidal constituents (observed divided by modelled values), with a maximum over/under estimation of 5%, 6% and 390%, respectively).

When implementing a roughness break at the regime change and testing various roughness values before and after the regime change, the calibration can improve slightly for certain parameters at certain stations (Figure S3a). However, there is no model that performs better in all aspects than the uniform roughness model (Table S1).

When implementing dune-adjusted roughness, the calibration does not improve (Figure S3b and Table S2). When using 1/2 k_s in equation 2, following the suggestion of Davies and Robins (2017) that the total effective hydraulic roughness is half of the dune roughness, the dune roughness corresponds well with the calibrated model roughness in the mixed fluvial-tidal regime (RK > 40) (Figure S4).

Text S4: Dune height prediction see Figure S5 and S6

Text S5: Additional information on focus zones see Figure S7 , S8, S9 and S10

Text S6: Intertidal areas see Figure S11

References

Davies, A. G., & Robins, P. E. (2017). Residual flow, bedforms and sediment transport in a tidal channel modelled with variable bed roughness. *Geomorphology*, *295*, 855–872. Retrieved from http://dx.doi.org/10.1016/j.geomorph.2017.08.029 doi: 10.1016/j.geomorph.2017.08.029

Turner, R., Clague, J., Groulx, B., & Journeay, J. (1998). *GeoMap Vancouver, geological map of the Vancouver Metropolitan area.* Geological Survey of Canada, Open File 3511, 1998, 1 sheet. doi: https://doi.org/10.4095/209909

Van Rijn, L. (1984). Sediment transport, part III: Bedforms. *Journal of Hydraulic Engineering*, *110*(12), 1733–1754.

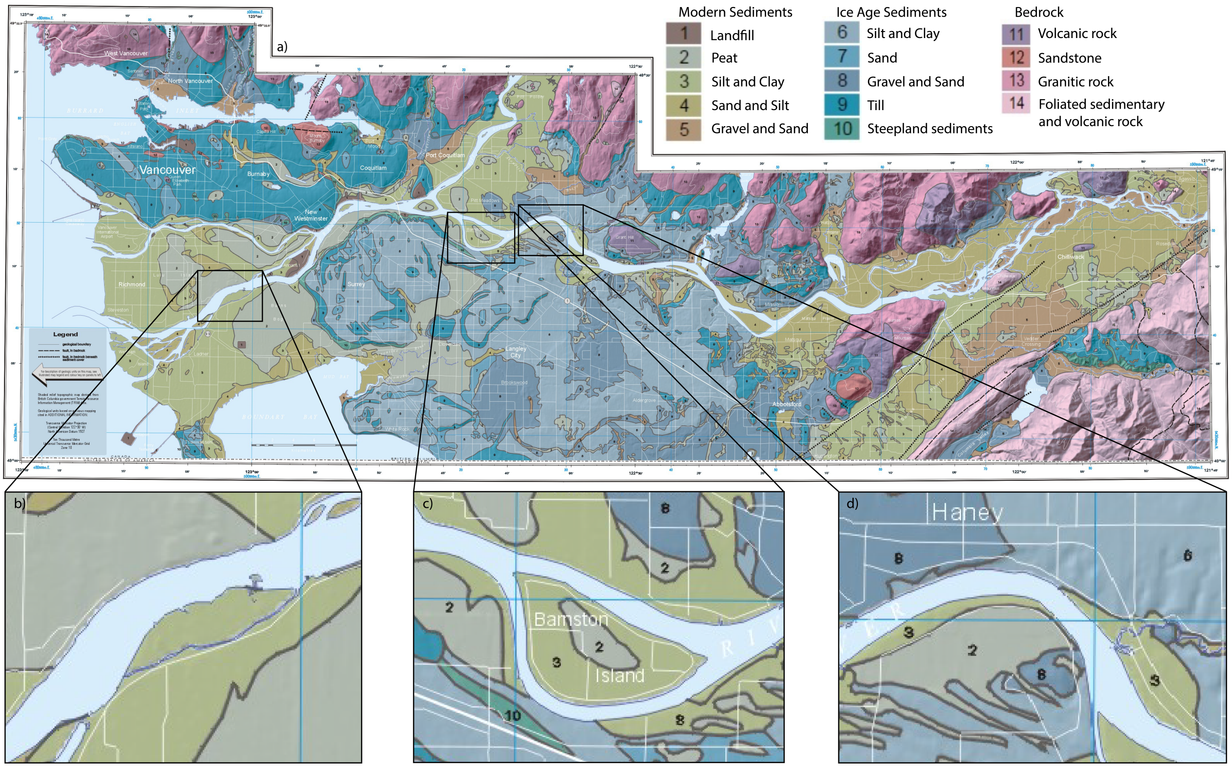

Figure S1. Surficial geology map (a), zoomed in on the focus areas (b, c, d). Adjusted from Turner et al. (1998).

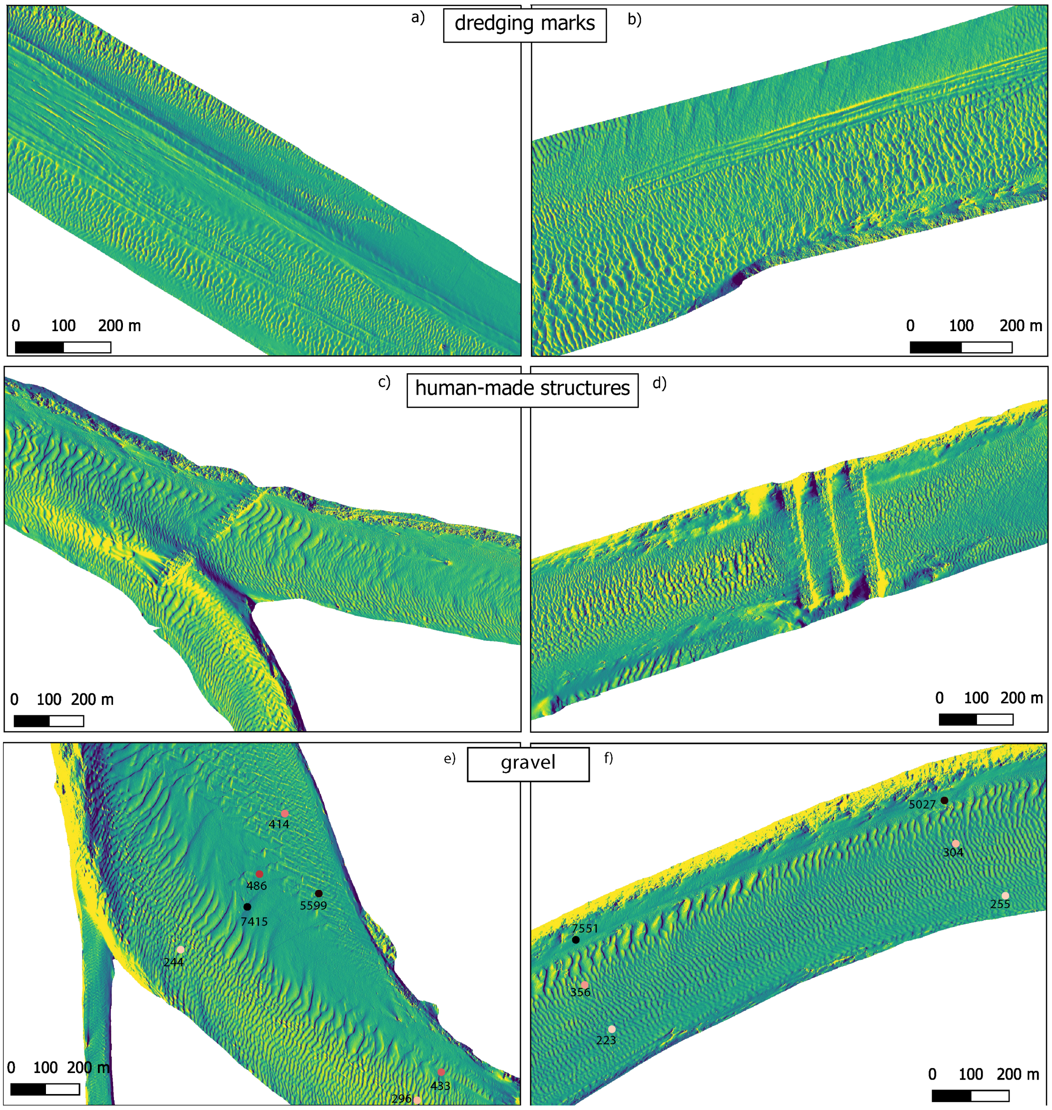

Figure S2. Example of bathymetric data with a, b) dredging marks, c, d) human-made structures e, f) gravel deposits, featuring no dunes. Median grain size (μm) is indicated.

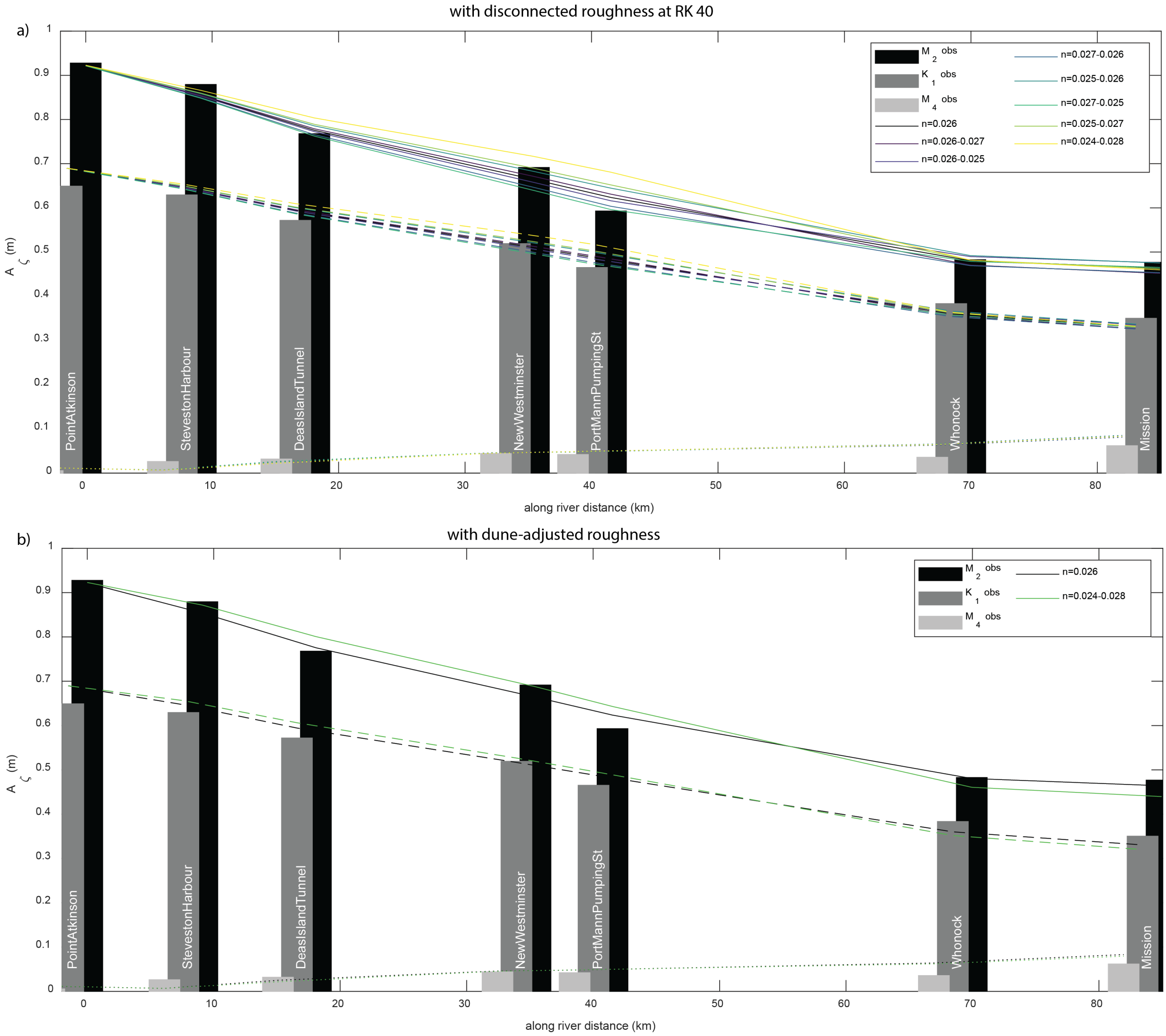

Figure S3. Performance of the model, with a disconnected roughness at the regime change at RK 40 (a) and dune-adjusted roughness (b). The observed tidal amplitude of the tidal constituents M2 (black bars), K1 (dark grey bars), and M4 (light grey bars) are indicated by bars, and the corresponding modelled tidal amplitudes for the various models are indicated with lines.

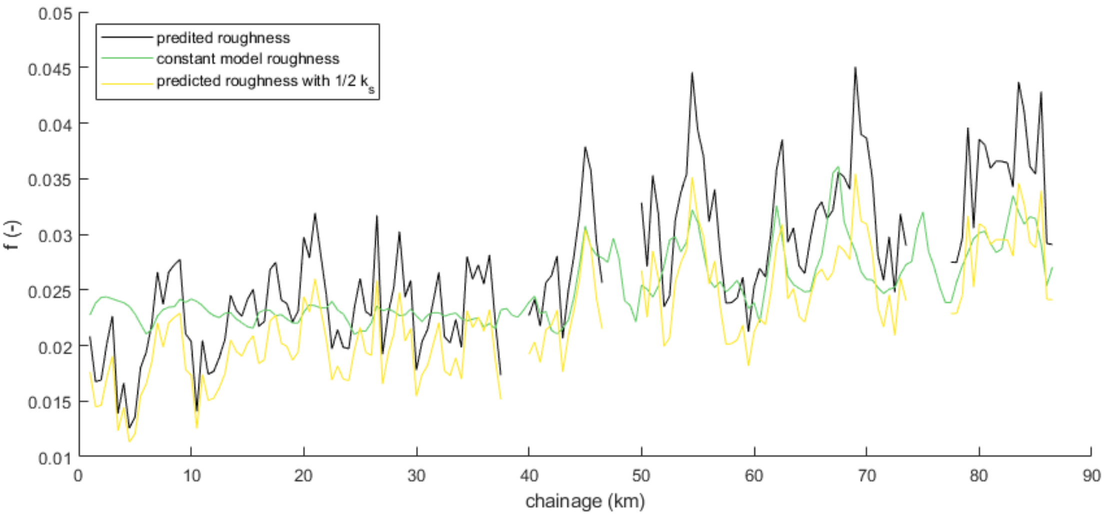

Figure S4. Hydraulic roughness in the study area expressed in f. Roughness calculated from dune geometry (equation13 in main manuscript)(black), model roughness with a constant Manning's n of 0.026 s $m^{-1/3}$ (green) and roughness calculated from dune geometry, using 1/2 k_s.

Table S1. Model evaluation of the model with uniform roughness (n_{man}=0.026) and a roughness break at RK 40, allowing two constant roughness value downstream and upstream of this break. The models are evaluated with the Root Mean Square Error (RMSE) of the observed and modelled water level (h), and the difference in observed and modelled tidal amplitude (Aζ) of the M2, K1 and M4 tidal constituents (observed divided by modelled values). The mean of the latter is calculated as the absolute values of Aζ - 1.

	Roughness model	Point Atkinson	Steveston Harbour	Deas Island Tunnel	New Westminster	Port Mann Pumping St	Whonock	Mission	Mean all stations
	0.026	0.341	0.363	0.346	0.430	0.380	0.305	0.266	0.347
	0.026-0.027	0.341	0.363	0.347	0.431	0.379	0.306	0.270	0.348
	0.026-0.025	0.341	0.362	0.345	0.429	0.381	0.305	0.264	0.347
	0.027-0.026	0.340	0.363	0.344	0.422	0.377	0.306	0.267	0.346
	0.025-0.026	0.341	0.363	0.348	0.439	0.385	0.305	0.265	0.349
	0.027-0.025	0.340	0.362	0.344	0.421	0.378	0.305	0.265	0.345
	0.025-0.027	0.341	0.364	0.348	0.439	0.384	0.305	0.269	0.350
RMSE h (m)	0.024-0.028	0.341	0.365	0.351	0.449	0.388	0.305	0.273	0.353
	0.026	1.01	1.03	0.99	1.04	0.95	1.00	1.03	0.024
	0.026-0.027	1.01	1.03	0.99	1.03	0.94	1.03	1.06	0.031
	0.026-0.025	1.01	1.03	0.99	1.05	0.96	0.99	1.00	0.021
	0.027-0.026	1.01	1.04	1.00	1.07	0.98	1.03	1.05	0.030
	0.025-0.026	1.01	1.02	0.98	1.01	0.92	0.98	1.00	0.024
	0.027-0.025	1.01	1.04	1.01	1.08	0.99	1.01	1.02	0.024
	0.025-0.027	1.01	1.02	0.97	1.00	0.91	1.00	1.03	0.026
A M2 (obs/mod)	0.024-0.028	1.01	1.02	0.96	0.97	0.87	1.00	1.04	0.038
	0.026	0.94	0.97	0.96	1.00	0.95	1.06	1.06	0.043
	0.026-0.027	0.94	0.97	0.96	1.00	0.95	1.08	1.08	0.047
	0.026-0.025	0.94	0.97	0.96	1.01	0.96	1.06	1.05	0.039
	0.027-0.026	0.94	0.98	0.97	1.03	0.98	1.08	1.08	0.046
	0.025-0.026	0.94	0.97	0.95	0.98	0.93	1.05	1.04	0.045
	0.027-0.025	0.94	0.98	0.97	1.03	0.98	1.07	1.06	0.042
	0.025-0.027	0.94	0.97	0.95	0.98	0.92	1.06	1.06	0.051
A K1 (obs/mod)	0.024-0.028	0.94	0.96	0.94	0.96	0.90	1.05	1.06	0.060
	0.026	0.48	3.90	1.27	0.96	0.88	0.56	0.75	0.65
	0.026-0.027	0.48	3.99	1.30	0.96	0.87	0.57	0.76	0.66
	0.026-0.025	0.48	3.80	1.25	0.96	0.88	0.55	0.73	0.64
	0.027-0.026	0.49	3.73	1.23	0.96	0.88	0.57	0.76	0.61
	0.025-0.026	0.47	4.03	1.32	0.97	0.87	0.55	0.73	0.68
	0.027-0.025	0.49	3.62	1.21	0.96	0.89	0.56	0.75	0.60
	0.025-0.027	0.47	4.09	1.35	0.97	0.87	0.56	0.75	0.69
A M4 (obs/mod)	0.024-0.028	0.46	4.12	1.45	0.98	0.87	0.56	0.75	0.71

Table S2. Model evaluation of the model with uniform roughness (n_{man}=0.026) and with dune adjusted roughness. The models are evaluated with the Root Mean Square Error (RMSE) of the observed and modelled water level (h), the correlation coefficient R^2 between the observed and modelled water level (h), and the difference in observed and modelled tidal amplitude (Aζ) of the M2, K1 and M4 tidal constituents (observed divided by modelled values). *the mean of the absolute values of Aζ - 1

	Roughness model	Point Atkinson	Steveston Harbour	Deas Island Tunnel	New Westminster	Port Mann Pumping St	Whonock	Mission	Mean all stations
RMSE h (m)	constant	0.34	0.36	0.42	0.43	0.38	0.31	0.27	0.36
	dune	0.34	0.36	0.34	0.44	0.37	0.31	0.27	0.35
R-squared h	constant	0.87	0.84	0.85	0.74	0.74	0.67	0.72	0.78
	dune	0.87	0.85	0.85	0.75	0.76	0.66	0.7	0.78
Aζ M2 (obs/mod)	constant	1.01	1.03	0.99	1.04	0.95	1.00	1.03	0.03*
	dune	1.00	1.00	0.96	1.00	0.92	1.04	1.08	0.04*
Aζ K1 (obs/mod)	constant	0.94	0.97	0.96	1.00	0.95	1.06	1.06	0.04*
	dune	0.94	0.96	0.95	0.99	0.93	1.09	1.09	0.06*
Aζ M4 (obs/mod)	constant	0.48	3.9	1.27	0.96	0.88	0.56	0.75	0.65*
	dune	0.46	3.89	1.47	0.97	0.88	0.57	0.78	0.67*

Table S3. Statistics (mean, *median in parenthesis), Root Mean Square Error (RMSE)) of the measured and predicted dune height (based on the uniform roughness model with n=0.026 s $m^{-1/3}$ and the predictor of Van Rijn (1984)) for the three focus zones and the total study area.

Δ (m)		**Zone 1**	**Zone 2**	**Zone 3**	**Whole area**
Measured		0.42 (0.39)	0.74 (0.73)	0.37 (0.36)	0.49 (0.44)
Predicted with tidally-averaged shear stress	Mean*	0.80 (0.78)	0.29 (0.27)	0.42 (0.46)	0.44 (0.47)
	RMSE	0.42	0.55	0.29	0.41
Predicted with maximum shear stress	Mean*	0.28 (0.30)	0.73 (0.76)	0.84 (0.85)	0.66 (0.65)
	RMSE	0.27	0.32	0.58	0.41

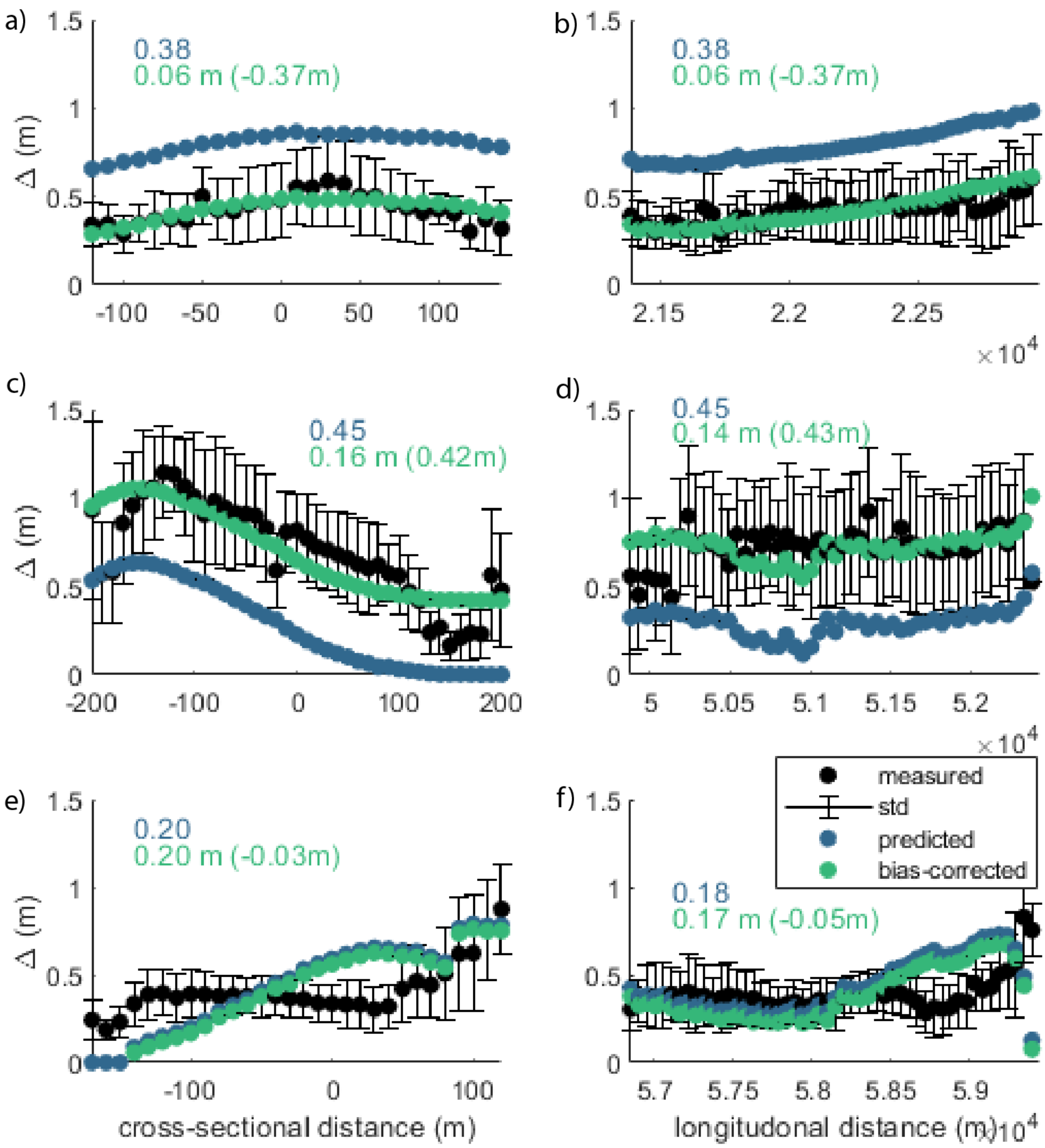

Figure S5. Predicted dune height compared to the measured dune height over the cross-section (a, c, e) and along the river (b, d, f). Dune height is predicted with equation 2 in main manuscript. The RMSE between the predicted and measured dune height is indicated as numbers in the sub-figures. Bias correction is performed to reduce the RMSE and compare the patterns of predicted and measured dune height. In parenthesis the amount of bias correction is shown.

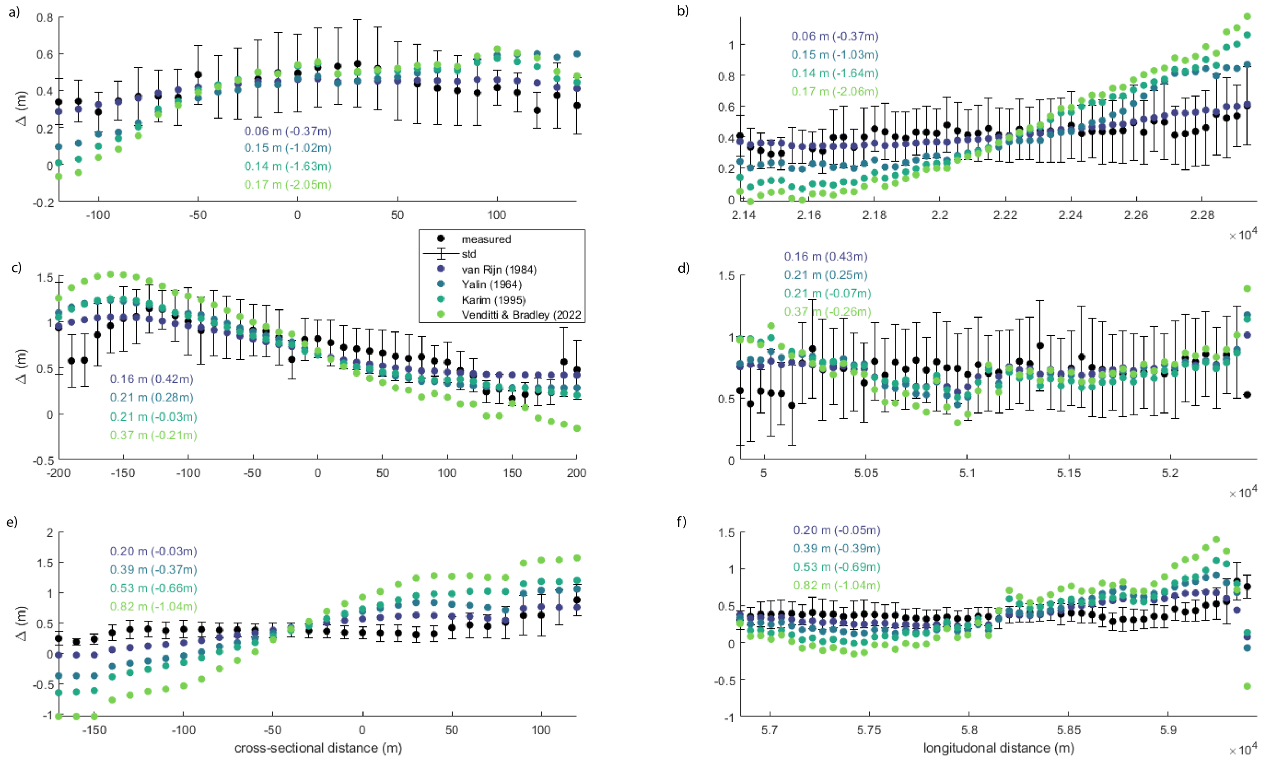

Figure S6. Predicted dune height compared to the measured dune height over the cross-section (a, c, e) and along the river (b, d, f). Dune height is predicted with equation 2, 9, 10 and 12, all in the main manuscript. The RMSE between the bias-corrected predicted and measured dune height is indicated as numbers in the sub-figures. Bias correction is performed to reduce the RMSE and compare the patterns of predicted and measured dune height. In parenthesis the amount of bias correction is shown.

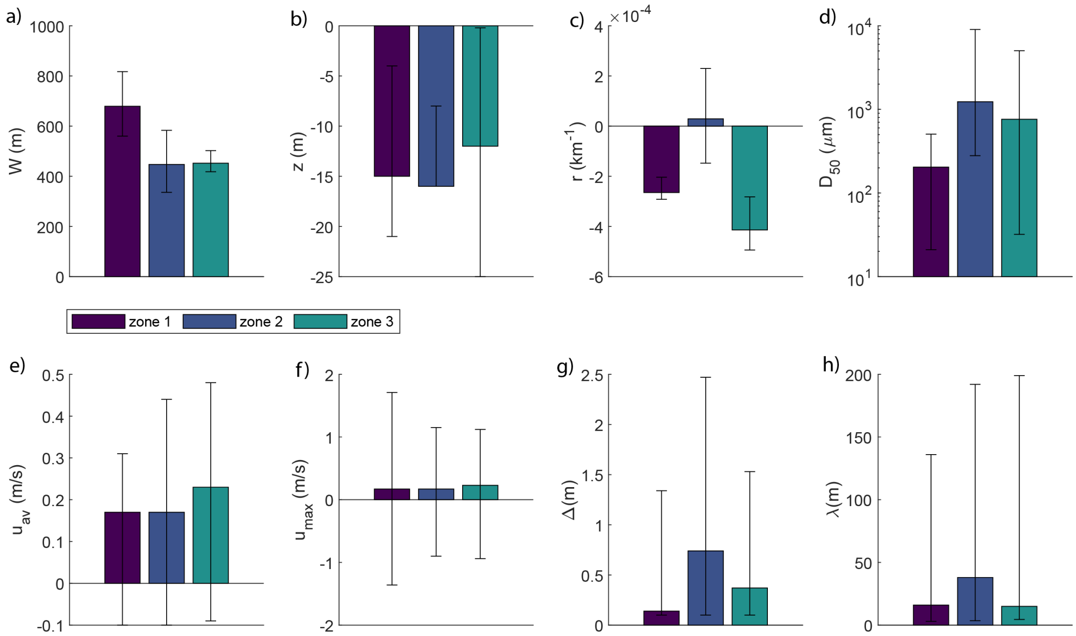

Figure S7. Characteristics of the focus areas. a) width (W), b) bed level (z), c) curvature (r), d) median grain size (D_{50}), e) tidally-averaged flow velocity (u_{av}), f) maximum flow velocity (u_{max}), g) dune height (Δ), h) dune length (λ).

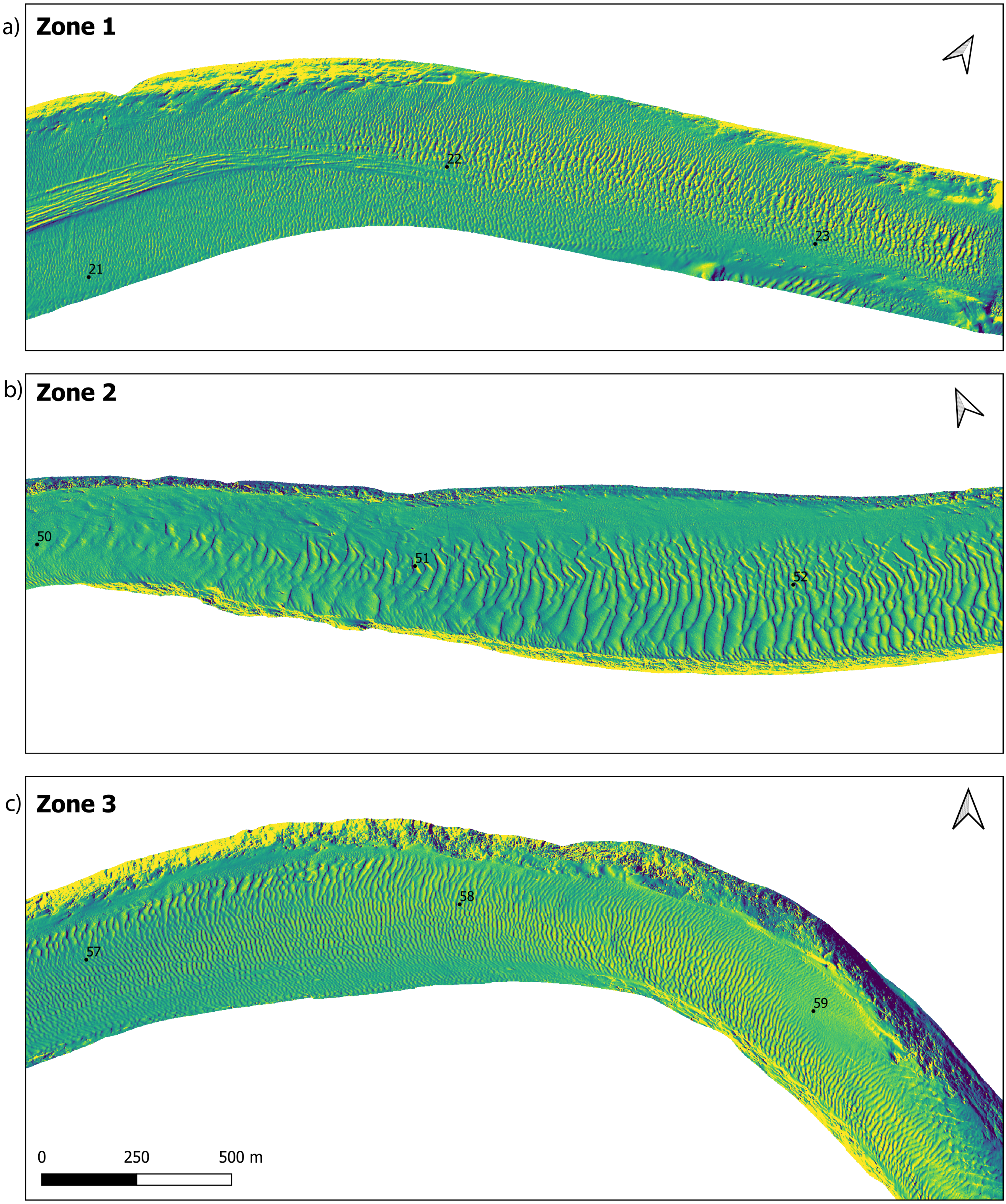

Figure S8. Dune fields in focus areas.

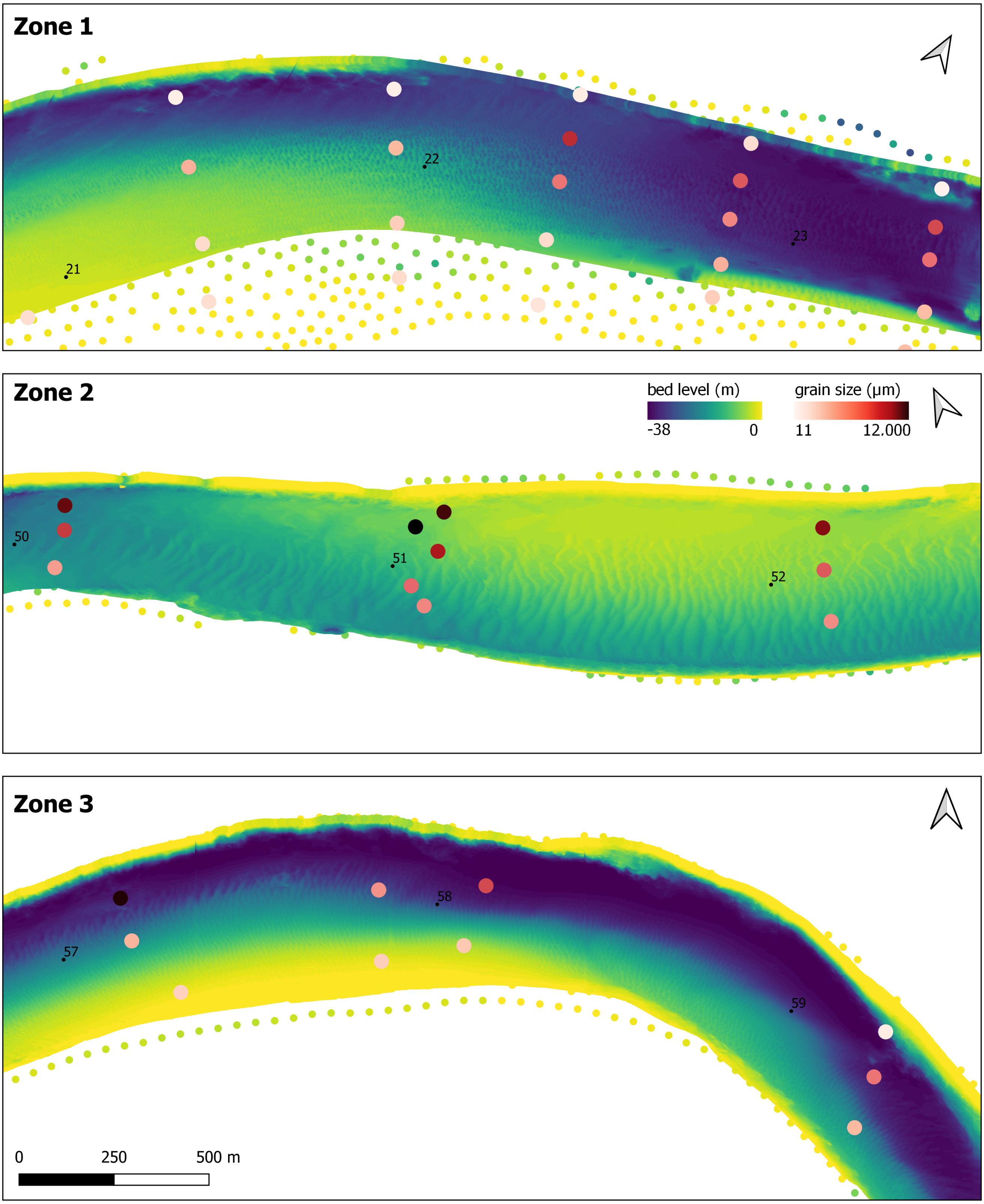

Figure S9. Bed level and grain size (D_{50}) in focus areas.

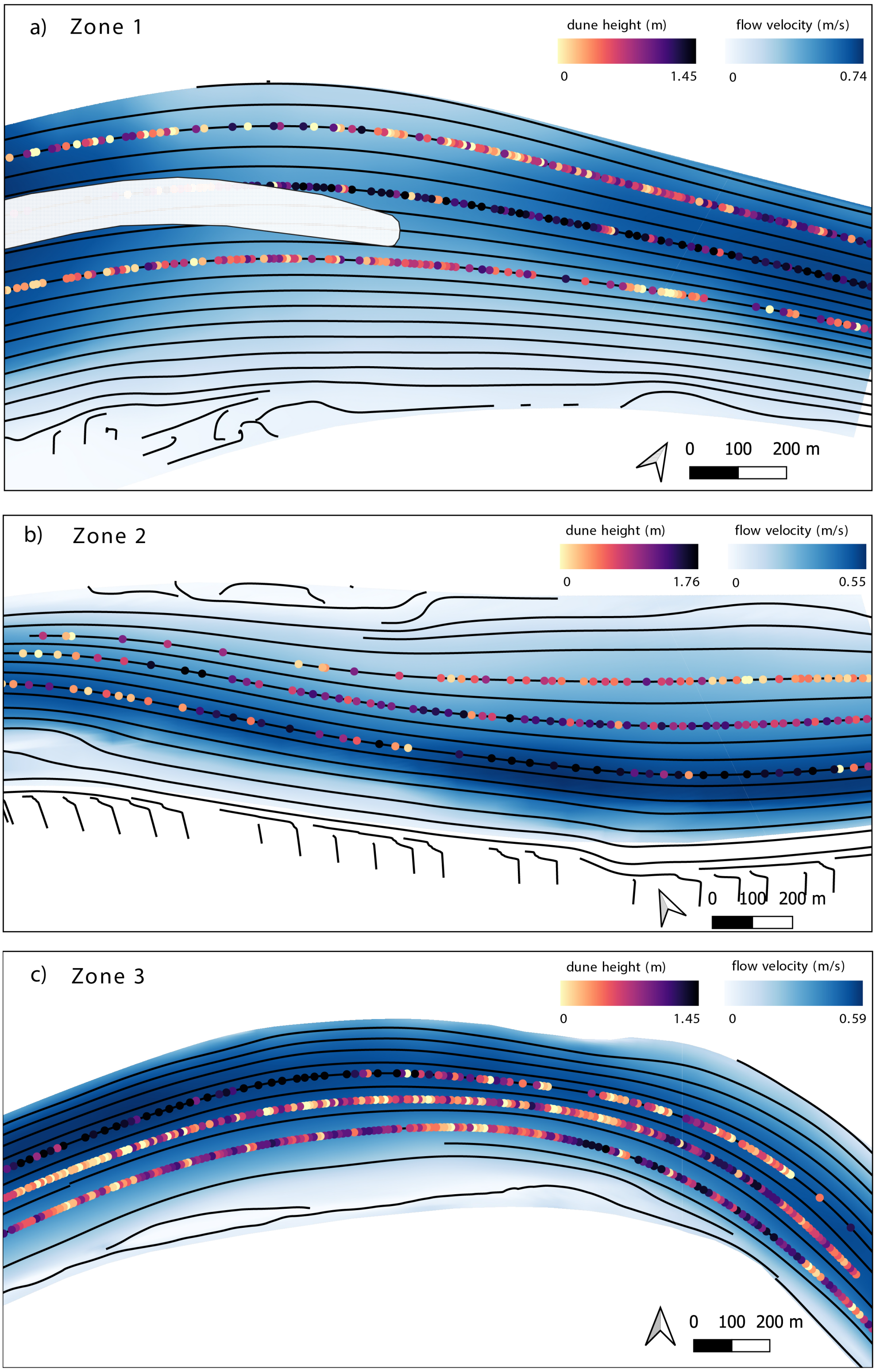

Figure S10. Tidally-averaged flow velocity (blue) in focus areas. Stream lines are indicated in black. Dune height along three the steam lines is shown.

Figure S11. Intertidal areas between Steveston Harbour and Deas Island Tunnel (a), and New Westminster and Port Mann Pumping Station (b). Intertidal areas are shaded in blue.